FHWA-NJ-2023-003

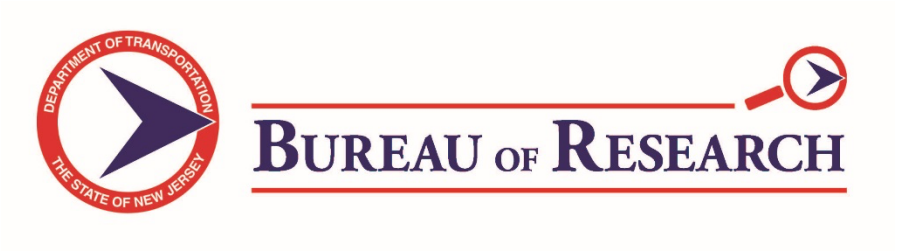

Advanced Reinforced Concrete Materials for Transportation Infrastructure
FINAL REPORT

March 2023

Submitted by

Matthew J. Bandelt, Ph.D.
Associate Professor
NJIT

Matthew P. Adams, Ph.D.
Associate Professor
NJIT

Hao Wang, Ph.D.
Associate Professor
Rutgers University

Husam Najm, Ph.D.
Professor
Rutgers University

Andrew Bechtel
Associate Professor
TCNJ

Seyed Masoud Shirkhorshidi
Graduate Research Assistant
NJIT

Jin Fan
Graduate Research Assistant
NJIT

NJDOT Research Project Manager
Giri Venkiteela, PhD

In cooperation with

New Jersey
Department of Transportation
Bureau of Research
And
U. S. Department of Transportation
Federal Highway Administration

DISCLAIMER STATEMENT

“The contents of this report reflect the views of the author(s) who is (are) responsible for the facts and the accuracy of the data presented herein. The contents do not necessarily reflect the official views or policies of the New Jersey Department of Transportation or the Federal Highway Administration. This report does not constitute a standard, specification, or regulation. “

TECHNICAL REPORT DOCUMENTATION PAGE

1. Report No. FHWA NJ-2023-003	**2. Government Accession No.**	**3. Recipient's Catalog No.**
4. Title and Subtitle **FINAL REPORT** Advanced Reinforced Concrete Materials for Transportation Infrastructure: Final Report		**5. Report Date** March 2023 **6. Performing Organization Code** NJIT
7. Author(s) Matthew J. Bandelt, Ph.D., P.E., Matthew P. Adams, Ph.D., F.ACI, Hao Wang, Ph.D., Husam Najm, Ph.D., S.E., P.E., Andrew Bechtel, Ph.D., Seyed Masoud Shirkorshidi, Jin Fan		**8. Performing Organization Report No.**
9. Performing Organization Name and Address New Jersey Institute of Technology University Heights, Newark, NJ 07102		**10. Work Unit No.** **11. Contract or Grant No.** NJDOT Contract ID Number
12. Sponsoring Agency Name and Address Federal Highway Administration (SPR) 1200 New Jersey Avenue, SE Washington, DC 20590 New Jersey Department of Transportation (SPR) 1035 Parkway Avenue, P.O. Box 600 Trenton, NJ 08625.0600		**13. Type of Report and Period Covered** Final Report, May 2019 – December 2022 **14. Sponsoring Agency Code** FHWA, NJDOT

15. Supplementary Notes
Conducted in cooperation with the U.S. Department of Transportation, Federal Highway Administration.

16. Abstract
Transportation infrastructure systems must resist conditioning from the natural environment and physical demands from service loading to meet the needs of users across the state. Reinforced concrete, which is widely used in bridge decks, pavements, super- and substructures, and other systems, deteriorates under environmental conditioning due to electro-chemical processes that cause expansive mechanics stresses at various length scales (e.g., reinforcement corrosion, freeze-thaw, etc.), leading to costly and timely durability and maintenance challenges. This report provides a background on the state-of-the-art of advanced reinforced concrete materials that are being investigated to improve reinforced concrete transportation infrastructure. A series of experimental and numerical research activities were then carried out to assess the mechanical properties and long-term durability of these systems. Results show benefits across a range of metrics and have the potential to substantially improve the in-service behavior of reinforced concrete transportation infrastructure.

17. Key Words Ductile concrete materials, alternative reinforcement, numerical modeling, experimental testing, corrosion, freeze-thaw, HPFRCC, UHPC	**18. Distribution Statement** No restrictions.		
19. Security Classif. (of this report) Unclassified	**20. Security Classif. (of this page)** Unclassified	**21. No. of Pages** 107	**22. Price**

Form DOT F 1700.7 (8-72) Reproduction of completed page authorized

ACKNOWLEDGEMENTS

The author(s) wish to acknowledge the NJDOT Bureau of Materials, especially Yong Zeng, Emmanuel Bassey, and Nehemie Jasmin, as well as NJDOT Research Project Manager, Dr. Giri Venkiteela, without whom this project would not have been possible.

TABLE OF CONTENTS

LIST OF FIGURES

LIST OF TABLES

EXECUTIVE SUMMARY

A range of highly ductile concrete materials have been developed in recent years that can improve the mechanical and durability performance at the material level, resulting in potential benefits at the structural component or system level. Additionally, advances in material science have led to new reinforcing steels used in reinforced concrete structures to improve the durability of reinforced concrete infrastructure. These concrete and reinforcing materials are often evaluated in isolation and not compared using consistent test methods, making it difficult to compare performance across material systems.

This research program evaluated the mechanical and durability performance of three highly ductile concrete materials and compared their response to two standard NJDOT mixtures. Durability performance in terms of salt-scaling, corrosion, freeze-thaw, shrinkage, and chloride ingress were evaluated. A range of alternative reinforcing systems were also evaluated as part of the corrosion testing program. The mechanical behavior of the highly ductile concrete materials restrained crack widths, which is believed to have blocked corrosion product formation or resulted in self-healing of cracks. High corrosion activity was observed early in the testing program in galvanized reinforcement due to the high reactivity of the zinc; however, the long-term response remained stable. Two of the highly ductile concrete materials had freeze-thaw and salt-scaling performance that exceeded the behavior of the standard concrete mixtures. The two best performing materials had a mortar matrix, without coarse aggregate. Test procedures showed that the inclusion of fibers in the highly ductile concrete materials required slight modifications to standard testing procedures, which need to be considered when evaluating durability performance in novel materials.

The in-service performance of highly ductile concrete materials was evaluated through numerical modeling techniques and life-cycle costs are reported. Reinforced bridge deck specimens were designed and analyzed under the combined effects of mechanical loading and environmental conditioning. Bridge decks with highly ductile concrete materials exhibited improved resistance to chloride penetration and corrosion propagation according to the numerical simulations. Structural deterioration occurred at a significantly slower rate in the highly ductile concrete bridge deck systems compared to that of reinforced normal strength concrete systems. Life-cycle cost analysis showed that bridge decks made with highly ductile concrete materials show high economic potential, although the life-cycle cost varies significantly depending on construction cost.

The results of this research can be used to guide best practices for decision making around deploying novel concrete materials to improve the service life of reinforced concrete infrastructure. Additional recommendations for future research and implementation are described at the end of this report.

BACKGROUND

Transportation infrastructure systems must resist conditioning from the natural environment and physical demands from service loading to meet the needs of users within a geographic environment. Reinforced concrete, which is widely used in bridge decks, pavements, super- and substructures, and other transportation systems, deteriorates under environmental conditioning due to electro-chemical processes that cause expansive mechanics stresses at various length scales (e.g., reinforcement corrosion, freeze-thaw, etc.), leading to costly and timely durability and maintenance challenges.

Advances in material science have created a range of new concrete and reinforcing materials that have the potential to drastically increase the service-life of transportation infrastructure. Such materials include highly ductile concrete systems, which use short, randomly oriented fibers to bridge crack openings and limit the ingress of chlorides and other harmful substances that can lead to deterioration in reinforced concrete. Additional advances in terms of reinforcing steel include the use of alloyed, stainless, and other steel systems that slow the rate of corrosion.

While numerous materials have been developed, there is a relatively little understanding as to how the materials behave under the same durability metrics. Part of this knowledge gap is due to the fact that many standard test methods that have been developed for ordinary concrete materials and require adjustments to evaluate the behavior of novel systems, such as ductile concrete systems. Additionally, many of the materials have been developed by individual research groups and have not been tested under the same testing protocols, making results difficult to interpret.

In addition to some of the obstacles in characterizing material performance, there are also challenges in conveying the potential economic benefits to the end users of these new materials. Since deterioration of transportation infrastructure is caused by the combined effects of mechanical loading, temperature effects, environmental conditioning, and other mechanisms, research is needed to understand how these combined effects influence the life-cycle performance of novel reinforced concrete systems.

The research activities presented in the proceeding sections aim to further understand the challenges to understand the behavior of these advanced reinforced concrete materials. An experimental and computational research program is then used to overcome knowledge gaps that exist in the literature.

OBJECTIVES

The overall objective of this project is to understand how advanced materials can be used to improve the durability of reinforced concrete transportation infrastructure in the State of New Jersey. A primary focus of the research program was on highly ductile concrete materials, often referred to as high-performance fiber-reinforced cementitious composites (HPFRCCs). A range of these materials were studied within this research program. Additionally, several alternative reinforcing systems were also investigated. To achieve this overall objective, the following specific research tasks were carried out:

1. Identify novel materials that can be deployed to improve the service life of New Jersey's reinforced concrete transportation infrastructure. The materials selected as part of this task should be significantly documented in the engineering literature such that their behavior has been characterized and evaluated in numerous experimental and/or computational research settings.

2. Select cost-effective and structurally feasible materials for evaluation using a variety of research methods to benchmark constructability, deterioration behavior, and in-service performance. Experimental and computational approaches will be used to characterize response across a range of durability metrics.

3. Compare the life-cycle impacts of different advanced materials across durability mechanisms and structural loading through in-service modeling. Using the simulated response, assess the life-cycle costs of the advanced reinforced concrete materials studied in this research program.

4. Develop guidelines for testing, modeling, and selecting advanced concrete and cementitious materials for transportation infrastructure applications.

INTRODUCTION

The approach taken to address the previously outlined research tasks involved completing a detailed literature review, experimental testing, computational simulations, and life-cycle cost modeling. These are described in detailed in the proceeding sections; however, a summary is provided herein.

The literature review involved completing a search on advanced materials for reinforced concrete infrastructure. This review includes a summary of ductile fiber-reinforced concrete materials for use in transportation infrastructure. The mechanical properties and mixture constituents are discussed, and their corrosion performance is summarized.

The experimental testing program involved a series of mechanical testing, corrosion testing, testing in freezing environments, and shrinkage testing. An overview of the materials studied in this report including material constituents, representative mechanical properties, and mixture design is provided. The individual mechanical properties obtain from each subset of experiments are covered in their associated sections. Corrosion testing of ductile and normal concrete systems using a chloride ponding test method is then reported. Specimens across a range of cementitious materials were cast and exposed to chloride ponding for over one year. Various steel reinforcing bars were studied, and systems were tested in uncracked and pre-cracked conditions. The performance of ductile and normal concrete systems in freezing environments is then reported. Specifically, freeze-thaw testing and salt-scaling experimental activities were conducted, and results are presented. Drying shrinkage behavior of the ductile and normal concrete systems investigated throughout this report are then reported.

A numerical modeling approach for simulating the corrosion behavior of ductile concrete systems is provided. This approach is used to understand the long-term chloride ingress and corrosion performance of ductile and non-ductile concrete systems in service applications. A study on the in-service and life-cycle behavior of a reinforced concrete bridge deck using reinforced ultra-high performance concrete and traditional reinforced concrete materials is then provided. Results are compared in terms of chloride content, cracking behavior, and a delamination rating.

Life-cycle cost modeling is then reported to assess the life-cycle costs of a representative bridge-deck made with normal reinforced concrete and a highly ductile concrete system. Results include annualized costs of various systems, considering the observed benefits in deterioration performance.

SUMMARY OF THE LITERATURE REVIEW

Overview of Ductile Concrete Systems

Ordinary cement concrete is one of the most popular materials in civil engineering with many desirable properties. However, it also has deficiencies such as low tensile and flexural strengths, poor durability, high porosity, and vulnerability to aggressive environments [1]. Due to normal concrete deficiencies, numerous research studies have been conducted to propose new materials and mixture designs that can improve the weaknesses of ordinary concrete materials. The result of such studies has yielded new materials such as fiber-reinforced polymers, high performance, and high strength concrete, and fiber-reinforced concrete. These materials could be used as alternatives to conventional concretes due to their advantages in terms of mechanical properties, strength, toughness, stiffness, ductility, cracking pattern, early age properties, corrosion resistance, and durability.

This section of the report provides background information about the development and specification of three ductile concrete materials (ultra-high performance concrete, hybrid fiber reinforced concrete and engineered cementitious composites) as alternatives for conventional concrete. A detailed review of these ductile concrete systems in regards to corrosion behavior is provided to assist in identifying potential gaps and needs for more investigation on their corrosion performance.

Design Theories and Mechanical Properties of Ductile Concretes

Ductile concretes such as ultra-high performance concrete (UHPC), hybrid fiber reinforced concrete (HyFRC) and engineered cementitious composites (ECC) have improvements in mechanical properties compared to ordinary concrete. The most important and common feature among ductile concretes is the higher tensile strain capacity and ductility which can lead to enhance durability properties. The focus on designing UHPC is to provide high compressive and tensile strength, while ECC materials are designed for high strain capacity. HyFRC provides both strength and ductility but at a lower level compared to UHPC and ECC. The proceeding sections explain the theories and concepts in designing of each ductile concrete and provides some information on the mechanical properties of these materials.

Overview of Ductile Concrete Materials

Figure 1**Error! Reference source not found.** shows representative mechanical behavior of normal and ductile concrete systems in compression and tension. The ductile concrete systems shown in Figure 1. are described in more detail in the proceeding sections; however, the systems shown in this figure refer to ultra-high-performance concrete (UHPC), hybrid fiber-reinforced concrete (HyFRC), and engineered cementitious composites (ECC). As can be seen, ductile concrete systems generally have high strain capacity in tension and compression. More strain capacity results in material toughness, ductility, and energy absorption capacity in ductile concrete systems. Also, ductile systems have greater flexural strength and crack resistance. Ductile concrete systems show different cracking behavior compared to

normal concrete and allow multiple cracks to form before localization.

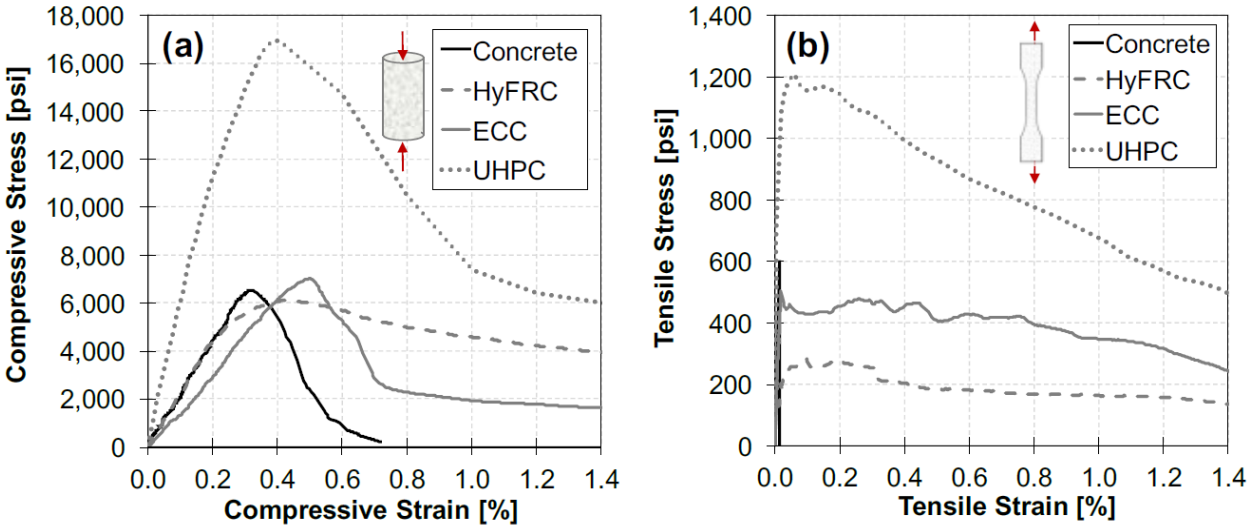

Figure 1. a) Compressive behavior of ductile and normal systems, b) Tensile behavior of ductile and normal systems [2–4]

The ductility described in Figure 1 is achieved through short, randomly oriented fibers that restrain crack openings and allow for the system to have a cracking response in which multiple cracks form as will be formed. Among ductile concrete systems, the mixture design and fiber selection can result in different durability and mechanical responses. UHPC has a denser microstructure than ECC and HyFRC, and has a higher tensile and compressive strength compared to other ductile systems. ECC consists of only fine particles, has a dense microstructure, and the fiber-matrix interaction is designed to achieve the highest level of tensile ductility. Since HyFRC generally contains coarse aggregate, it often has a microstructure similar to that of normal concrete. These changes in microstructure and mechanical response of ductile concrete systems affects the durability response of each system.

Ultra-high Performance Concrete (UHPC)

Ultra-high-performance concrete (UHPC) is a type of concrete with a compressive strength greater than 150 MPa and tensile strength of more than 7 MPa [5–12]. UHPC shows a ductile behavior in tension [13–18]. Some of the key parameters in a UHPC design include a low water-to-cement (w/cm) ratio, replacement of coarse aggregates with well-graded fine sand generally ranging between 150 to 600 µm and ground quartz with a particle size of 0.1 to 100 µm, using a large amount of pozzolans such as silica fume and fly ash, and a high dosage of high range water reducer admixtures [9,13,15,17,19–21]. The enhanced homogeneity provided by replacing coarse aggregates with very fine sands results in low porosity and improved mechanical behavior and durability [20]. Using very fine aggregates and silica fume decreases porosity, and fibers are added to the UHPC to increase ductility [20]. The fibers can be effective in arresting crack propagation. According to the literature, two percent by volume is the mostly used amount of fibers in

many research and toughness improves [7]. Using hybridization of fibers (i.e., a combination of different types or sizes of fibers) can improve the mechanical properties of UHPC systems [19].

The main deficiencies in UHPC systems include brittle post-cracking behavior because of the high amount of binder and micro-cracking due to autogenous shrinkage [5]. High strength, low permeability, high toughness and durability, high abrasion resistance, high freezing and thawing resistance, and increased load-carrying capacity are the most important benefits of UHPC [5,17,22–26]. Due to UHPC's beneficial properties, it has several applications in high-rise buildings, long-span bridges, rehabilitation, offshore oil platforms, and blast-resistant structures [6,13,20,22,27]. It is also used for joints, precast pre-stressed girders, and bridge decks [7,28,29]. Using UHPC has been proposed to reduce or eliminate reinforcing bars in structural elements and decreases the self-weight by more than 70% with substantial reductions in crack widths [28]. Also, the resistance of UHPC to chloride penetration makes it a good choice for using in chloride exposed environments such as marine structures to prevent reinforcement corrosion [30–32].

Hybrid Fiber Reinforced Concrete (HyFRC)

Hybridization is a technique of using different types of fibers for maximizing the advantages of various fiber properties [33]. Hybrid fiber-reinforced concrete (HyFRC) uses multiple types of fibers to take advantage of their properties. There are different types of hybridization including:

- Hybridization of fiber mechanical response: The fiber stiffness is the main variable in this form of hybridization. Fibers made of steel or Kevlar with high modulus of elasticity can effectively bridge microcracks, while some fibers with low modulus of elasticity, such as polypropylene, could be used at larger crack widths [33–36].

- Hybridization of fiber size and anchorage: In this category, fibers are divided into microfibers (less than 15mm in length) and macrofibers (greater than 15mm in length) [37]. Microfibers are effective at bridging cracks at an early age that yields increased strength and macrofibers are used to increase post-cracking toughness [33–36].

- Hybridization of fiber function: Fibers that are used to enhance early age properties like drying shrinkage and workability (usually polypropylene) and fibers are used to improve the mechanical properties (usually steel fibers) [33–36,38].

Using hybrid fiber systems has numerous advantages. Strong and stiff fibers can improve the stress at first cracking and ultimate strength, and flexible fibers can enhance the post-cracking strain capacity. Small microfibers bridge microcracks, which lead to higher tensile strength, and large nacrifibers can arrest the propagation of macrocracks and improve the toughness. Hybridization of different lengths of a specific type of fiber can help bridge microcracks and prevent propagation of macrocracks; hybridization of different types of fibers improves the strength and ductility of concrete. Also, durable fibers can increase the strength and/or toughness in aged concrete [35,36].

Fibers also can be divided into metallic (e.g., steel) and nonmetallic (e.g., polymeric) fibers. Metallic fibers improve the energy absorption and control macrocracks due to the high modulus of elasticity and length of steel fibers [39,40]. High amounts of steel fibers can decrease concrete slump significantly [40,41]. Different types of nonmetallic fibers including polyvinyl alcohol (PVA), polyethylene (PE), polypropylene (PP), and polyolefin (PO) fibers have been used in HyFRC. Nonmetallic fibers delay microcrack formation and prevent early age and shrinkage cracks [39,40]. Nonmetallic fibers have good dispersion in concrete and usually there are fewer workability concerns for nonmetallic fibers [41]. Using HyFRC can enhance flexural strength and toughness, ductile performance, matrix stiffness, crack resistance, energy absorption, durability, serviceability, ultimate limit state performance, post cracking stiffness, crack tortuosity, and permeability [33,34,38,42–44].

Engineered Cementitious Composites (ECC)

Engineered cementitious composites (ECC) are an ultra-ductile micro-mechanically designed cementitious composite that were developed in the early 1990s. A typical mixture design of ECC contains a high cement content (~1000 kg/m^3), fine sand (finer than 200 μm), fly ash, water, admixtures and short, randomly oriented polymeric fibers (e.g. polyethylene, polyvinyl alcohol) typically between 1.5 to 2% by volume [45–47]. Using hybridization of fibers can improve the mechanical properties and corrosion resistance of ECC [48,49]. The ultimate tensile strain of ECC is between 3 and 7 percent according to the coupon tensile specimens which is 350 to 500 times greater than that of ordinary concrete [45,46,50–56]. The ultimate tensile strain range of ECC can change when the tensile specimen size changes [57,58]. The compressive strain capacity of ECC is 0.4 to 0.65 percent, approximately two times greater than fiber reinforced concrete [54,56,59]. The high tensile strain capacity of ECC is due to the macroscopic strain-hardening phenomenon after first cracking accompanied by multiple micro-cracking [45,50,60]. With increasing load, crack widths steadily increase to approximately 60 μm at around 1% strain. After this strain, crack widths tend to remain constant while the number of cracks increases until a dominant crack forms which induces softening of the material [45,47,50].

The strain hardening behavior of ECC is dependent on the fibers, matrix, and interface as composite material constituents. Researchers used micromechanics-based theories to design mixtures that provide bridging action of fibers. Using steady-state crack analysis, steady-state propagation of microcracks, strain hardening behavior, and consequently composite tensile ductility of ECC can be achieved. Due to the unique behavior of ECC, it is expected that the use of ECC can have a direct impact on infrastructure safety, durability, and productivity in the construction industry. Higher energy absorption and a more stable hysteresis loop can be observed in ECC specimens under cyclic loading. According to Li (2003) at a high level of drift, ECC showed no spalling while normal concrete specimens experienced spalling and loss of concrete cover [50]. These results show the high deformation capacity of ECC compared to normal concrete despite the elimination of stirrups [50].

ECC has beneficial properties such as the ability to reduce or eliminate shear reinforcement, compatible deformation with reinforcement, synergic interaction with fiber

reinforced polymer (FRP) reinforcement, good durability, high ductility, high damage tolerance, and tight crack width control [50,60–62]. Considering these properties, ECC has the potential to be used in structures requiring durability under severe loading conditions and harsh environments, and can enhance construction productivity. ECC has been used in bridge decks, pavements, as repairing material and infrastructure exposed to harsh environmental conditions [45,51,63–67].

Mechanisms Controlling the Corrosion Behavior of Reinforced Concrete Systems

Concrete is a barrier against chemical agents that can cause corrosion in reinforcement. The high PH of concrete, which ranges between 12.5 and 13.5 [68] provides a favorable environment for forming a passive layer that shields the reinforcement surface from corrosion start. Corrosive substances such carbon dioxide from the atmosphere, chlorides from seawater, and deicing salts can eventually penetrate concrete and reach the reinforcing surface [68]. The passive coating that shields the reinforcement can be destroyed and corrosion can start if chlorides build up to a critical threshold level at the reinforcement surface [69–73]. Anodic and cathodic regions of the reinforcement experience corrosion reactions, which can be summed up as follows:

$$Anodic\ Reaction: 2Fe \rightarrow 2Fe^{2+} + 4e^{-} \quad (1)$$

$$Cathodic\ Reaction: O_2 + 2H_2O + 4e^{-} \rightarrow 4OH^{-} \quad (2)$$

$$Total\ Reaction: 2Fe + 2H_2O + O_2 \rightarrow 2Fe(OH)_2 \quad (3)$$

The oxygen availability, temperature, pore water PH, and moisture content are some of the factors that influence how quickly corrosion reactions occur in concrete systems. The amount of corrosion products is three to four times more than that of steel due to their expansive nature [74]. More corrosion products are produced close to the reinforcing surface as corrosion spreads, placing expanding stress on the concrete and causing cracking. In addition to increasing the pace at which harmful substances enter a structure, cracking brought on by expansive corrosion products can also cause spalling, delamination, and, in severe circumstances, partial or complete structural collapse [74].

The following sections discuss the corrosion performance and other durability of ductile concrete systems compared to other mixtures provided by the New Jersey Department of Transportation.

SUMMARY OF THE WORK PERFORMED

Materials Investigated in this Report

Overview

Five different types of concrete systems are investigated in the remaining sections of this report, including high-performance concrete (HPC), self-consolidating concrete (SCC), hybrid fiber reinforced concrete (HyFRC), Engineered cementitious concrete (ECC), and ultra-high-performance concrete. A wide range of materials were used in this study, as described in the following subsections.

Aggregates

Two coarse aggregates were used with a nominal maximum size of 19 mm for HPC and SCC and 9.5 mm for HyFRC. Regular sand with a fineness modulus of 2.75 was used in HPC, SCC, and HyFRC. Very fine sand with a nominal maximum size of 300 μm (#50) was used in the ECC mixture. The sieve analysis of sands used in this study is shown in Figure 2.

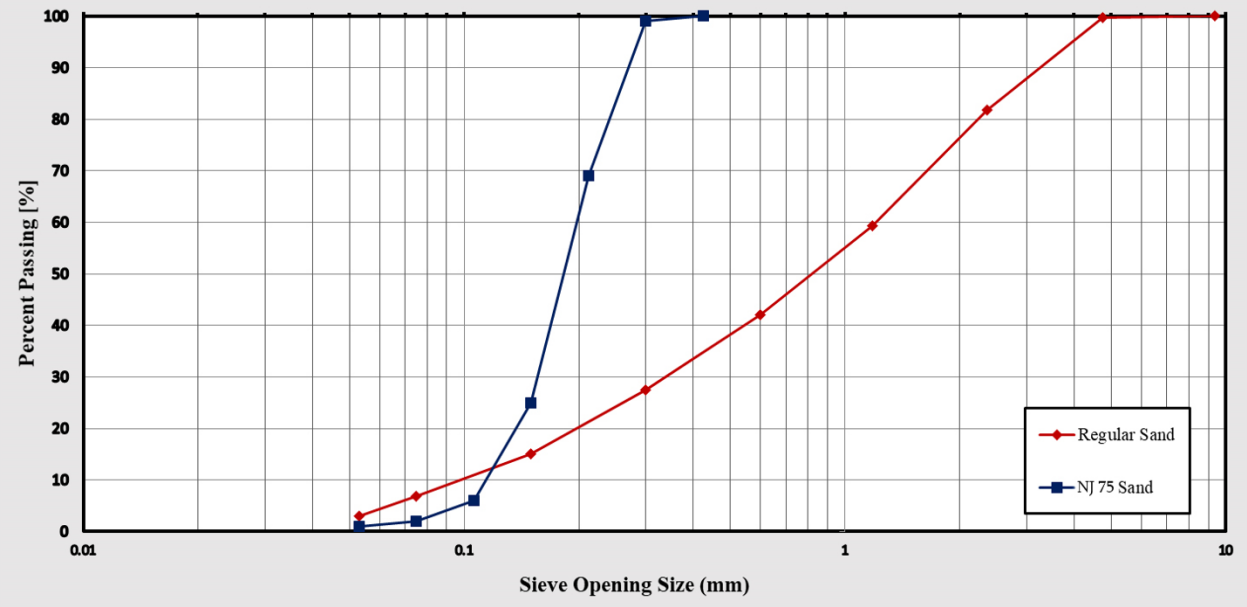

Figure 2. Sands sieve analysis

Cement and Supplementary Cementitious Materials

Type I portland cement was used in all systems. Different types of SCMs based on mixture designs were used in each system. Slag and micro-silica were used in the HPC mixture design. Fly ash class F was the SCM used in ECC and HyFRC, and slag was used in the SCC mixture. Detailed information about the content of each material in different mixtures will be provided in the next section.

Admixtures

Four types of high-range water reducers, two types of air entertaining agents, and two types of viscosity modifying agents were used. Glennium 7710, Viscocrete 6100, Glennium 3030NS, and ADVA 190 were used in HPC, SCC, HyFRC, and ECC mixtures, respectively, in calibrated dosages. Master Air AE 90 and Sika Air were the air-entraining agents in HPC and SCC mixtures. Rheomac VMA 362 and VMAR-3 were used as viscosity-modifying agents in HyFRC and ECC. A Premia 150 admixture (High range water reducer and accelerator) was used based on the recommended dosage of the supplier for pre-bagged UHPC.

Fibers

This project used two types of steel fibers and one type of PVA fibers. RECS 15 PVA fibers with a length of 8 mm, aspect ratio of 200, and tensile strength of 1600 MPa were used in ECC and HyFRC mixtures. A hooked Dramix© 3D 55/30BG steel fiber with a length of 30 mm, aspect ratio of 55, and tensile strength of 1100 MPa was used in HyFRC. The steel fibers used in UHPC were straight fibers with a length of 13 mm, an aspect ratio of 65, and tensile strength of more than 2000 MPa. Figure 3 shows the different fibers used in this project. The fiber dosage in each concrete system is summarized in the next section.

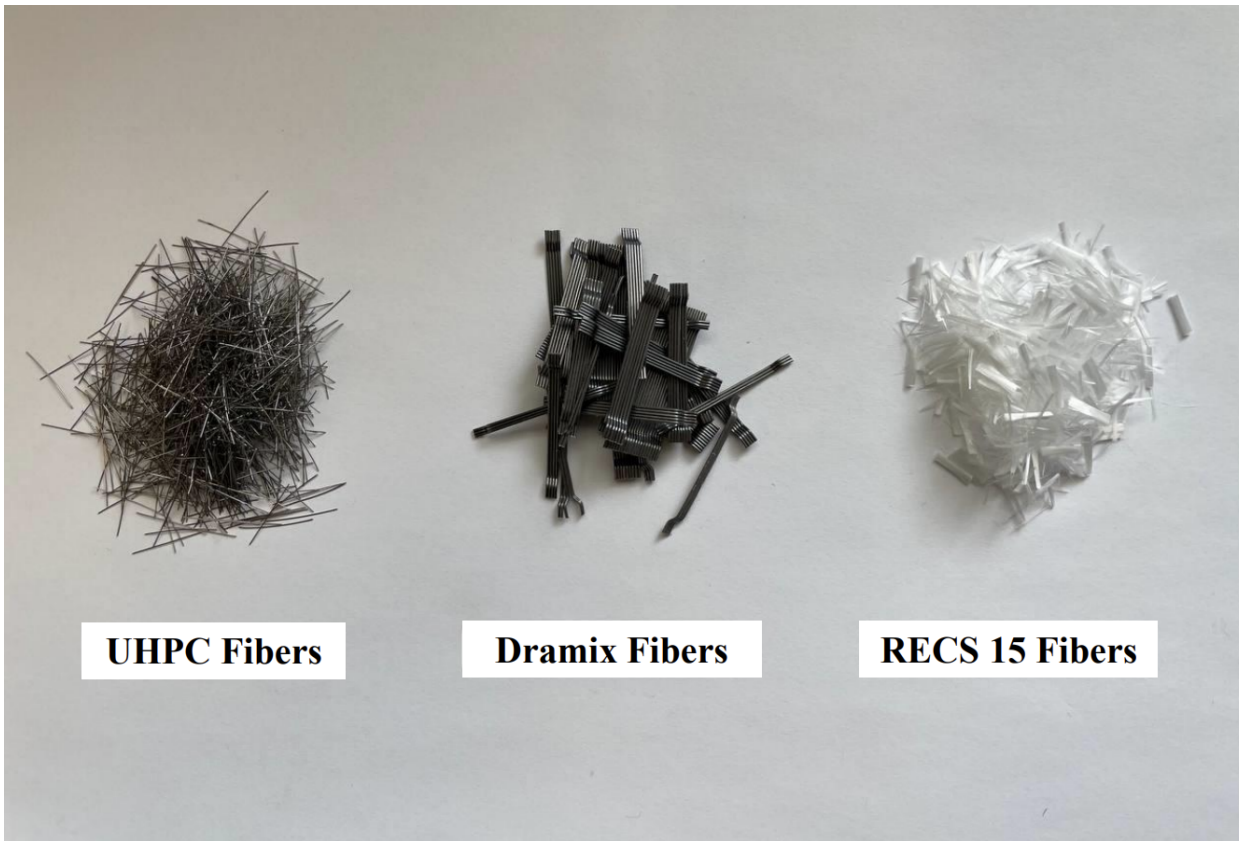

Figure 3. Steel and PVA fibers

Bars

Five different types of reinforcement were used in corrosion tests. Based on the ASTM G109 test method described in later sections for corrosion testing, number four bars were used in this study. Black bar according to ASTM A615 Gr 420/60, epoxy coated bar (ECR) Gr 420/60 in compliance with ASTM A775 and A1078, ChromX_4000 according to ASTM A1035 grade 100, continuous hot-dip galvanized bar according to ASTM 1094 Gr 420/60, and stainless steel S316 bars according to ASTM A955 Gr 75 were used as the reinforcement in G109 beams for corrosion evaluation. Figure 4 shows galvanized, black, ChromX, and epoxy-coated bars used in this study.

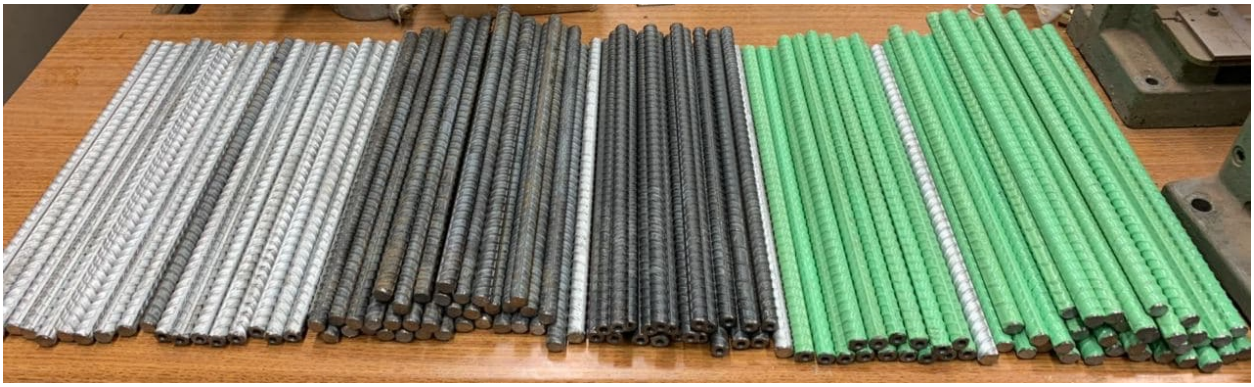

Figure 4. Galvanized, black, ChromX and epoxy-coated bars

Mixture Designs

Two non-ductile concrete mixtures, including a self-consolidating concrete with a compressive strength of 7000 psi and a high-performance concrete mixture (HPC) with compressive strength of more than 8000 psi, as well as three ductile concrete systems including a self-consolidating HyFRC (SC-HyFRC), an engineered cementitious composite and a pre-bagged UHPC (JS 1000 from Ductal Lafarge including two percent of steel fibers) were used in this study. Based on the literature a typical Ductal UHPC mixture includes portland cement, silica fume, quartz sand, ground quartz, water, high range water reducer, accelerator, and steel fibers [21]. The materials and mixture design of each concrete system can be seen in Table 1.

Table 1. Concrete systems mixture design

ECC (/Cement Ratio)		SC-HyFRC (Kg/Cu.m)		HPC (lbs./Cu.Yard)		SCC P (lbs./Cu.Yard)	
Cement	1	Cement	397	Cement	435	Cement	473
Fly Ash	1.2	Fly Ash	131	Slag	240	Fly Ash	157
ECC Sand	0.8	Coarse Agg (3/8")	418	Microsilica	25	Sand	1330
Water (W/cm)	0.68(0.31)	Sand	1044	Sand	1253	Coarse Agg. (3/4")	1707
HRWR	0.007	Water	237	Coarse Agg (3/4")	1834	Water	252
VMA	0.018	HRWR (ml/100 kg binder)	880	Water	250	HRWR	as needed
PVA Fiber Volume %	2	VMA (ml/100 kg binder)	2200	HRWR	as needed	Air Entraining	as needed
		Steel Fibers	1.3	Air Entraining	as needed		
		PVA Fibers	0.2				

A series of trial castings were done to calibrate each mixture's admixtures content and quality control. Also, compressive testing was performed on each mixture according to ASTM C39 to validate each mixture compressive strength [75]. These mixtures were used to be tested in different experiments in this study. Mechanical properties for each mixture will be reported along with the other experimental results.

Chloride Ponding Behavior of Ductile Concrete Systems

Introduction

The most significant limitations of conventional concrete include low tensile and flexural strength, poor ductility, low energy absorption capacity, large porosity, poor durability against corrosion, low freeze-thaw resistance, and sensitivity to acidic conditions [1,76–78]. Numerous studies have been done to increase ductility to enhance ordinary concrete's properties. With regard to this, several solutions have been proposed, including the employment of various kinds of fibers and the addition of supplementary cementitious materials. Ductile concrete systems that utilize these combination designs are known as high-performance fiber-reinforced cementitious composites (HPFRCC).

In reinforced concrete structures, corrosion is a serious durability issue that can lead to early deterioration [72,79,80]. One of the primary reasons for corrosion initiation is the ingress of chlorides into concrete to the surface of steel reinforcement [81]. Chlorides can destroy the passive coating that protects reinforcement and start corrosion if they accumulate to a critical threshold level at the surface of the reinforcement [69–73]. The rate of chloride penetration and corrosion performance of reinforced concrete components can be affected by a number of variables, including concrete quality, permeability, and cracking [73]. More porosity and cracks can speed up the penetration of chlorides, oxygen and the start of corrosion, whereas a denser microstructure can slow chloride penetration and restrict oxygen access [81–83]. Compared to ordinary concrete systems, ductile concrete systems are thought to have superior corrosion resistance because of their tight microstructure and enhanced cracking behavior. However, other parameters, such as cracking and durability problems, can affect the corrosion performance of ductile concrete systems. This section investigates the corrosion performance of both

cracked and uncracked beams. Also, different types of reinforcement were tested to compare the corrosion performance of ductile concrete systems and alternative reinforcement. A series of hybrid beams were tested to investigate the improvement in corrosion resistance using a ductile concrete system and alternative reinforcement.

Experimental Program

Two sets of experiments were used to investigate the chloride ponding behavior of concrete systems. First, the corrosion behavior of different systems was evaluated using a long-term corrosion test to compare the corrosion behavior of different concrete systems and reinforcement. Second, ponded specimens were profiled to measure the chlorides content in different depths of concrete to investigate the chlorides penetration resistance of different concrete systems. The following sections discuss the corrosion test and chloride profiling of specimens thoroughly.

Corrosion Test

Corrosion tests were performed according to the ASTM G109 test method [84]. ASTM G109 is an accelerated corrosion test method that uses three percent NaCl for the salt solution and bi-weekly wetting and drying cycles to accelerate the corrosion. Figure 5 shows a schematic of these beams. Two layers of bars were placed in a 280 × 150 × 115 mm (11 × 6 × 4.5 in.) beam. A 38 mm (1.5-inch) cover was used for the bars to ensure the minimum cover depth considering the maximum aggregates size in different mixtures. To investigate the effect of cracking behavior on the corrosion performance of ductile concrete systems, corrosion beams were tested in cracked and uncracked stages. For cracking, beams were loaded in three-point bending up to 80 percent of the beam capacity based on the concrete mixture. Specimens were ponded with the salt solution at the top, and two layers of bars were connected using a resistor to measure the corrosion current. The top bar was considered the anode, and the two bars at the bottom were considered the cathode. The results were reported based on corrosion current density for different systems.

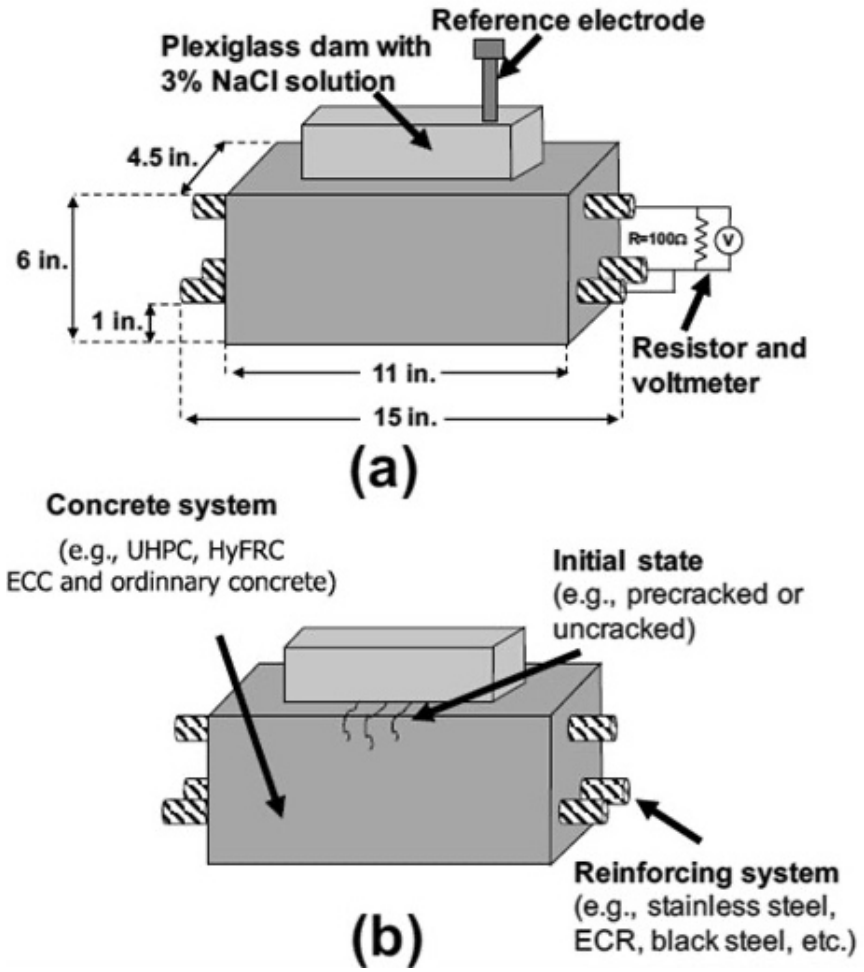

Figure 5. Corrosion beams in ASTM G109 test method a) Uncraceked beam b) Cracked beam

Five types of concrete systems, including two mixtures provided by the New Jersey Department of Transportation (HPC and SCC P) and three ductile concrete systems (UHPC, ECC, and HyFRC), and five different types of reinforcement, including black bar, epoxy coated bar, ChromX, galvanized, and stainless steel bars were investigated in this study. Epoxy-coated bars were tested in both damaged and undamaged states to evaluate the effect of defects in the epoxy coating due to transportation and concrete casting in the field. A combination of different concrete systems and reinforcement was considered for corrosion testing to derive the most outcomes of this research. Table 2 shows the testing plan for different concrete systems and reinforcement in corrosion testing. Three specimens for each test were cast, and a total of 102 beams were cast for corrosion testing.

Table 2. Corrosion testing plan

Concrete / Rebar	NJ DOT HPC	NJ DOT SCC P	UHPC	HyFRC	ECC
Black	✓ ✓	✓	✓ ✓	✓ ✓	✓ ✓
ECR	✓ ✓	✓	✓ ✓	✓ ✓	✓
ECR-Damaged	✓ ✓	✓	✓	✓	✓
ChromX	✓	✓	✓ ✓	✓ ✓	-
Galvanized	✓ ✓	✓	-	-	-
Stainless Steel	✓	✓	-	-	-

✓: Uncracked ✓: Cracked

Rebar Preparation

The rebar was prepared according to the ASTM G109. First, the rebar was cut in 15 inches pieces, and the edges were smoothed using a grinder. One end of each bar was drilled and tapped. Metallic bars were soaked in hexane, and both ends were taped with an electroplater tape and covered with a neoprene tube. A screw and two beads were used for the wire connection of the bars. The end of the neoprene tube was filled with epoxy to seal both ends of the bars. Figure 6 shows black bars in different stages of preparation. Instead of soaking in hexane, epoxy-coated bars were washed using soap and hot water. Also, a series of bars were damaged using a four-flute drill bit in a CNC machine to consider the effect of damage on the epoxy coating in transportation and concrete casting. Six holes with a diameter of 3.2 mm were made at the two sides of the bar to damage the epoxy cover on the bars, representing around 0.58 percent of the bar surface. Figure 7 represents the damaged epoxy bars.

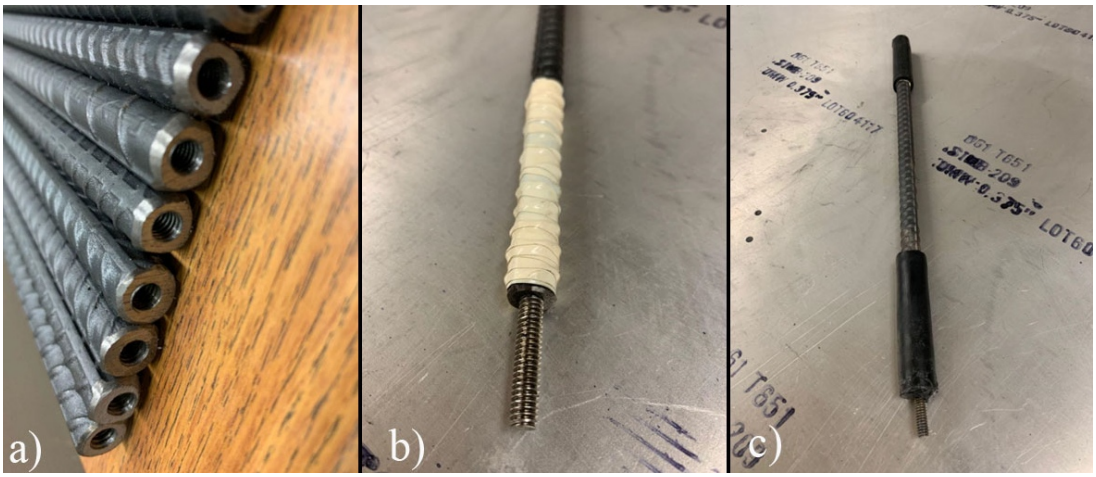

Figure 6. Rebar after a) drilling and tapping, b) electroplater taping, c) covered with neoprene tube and filled with epoxy

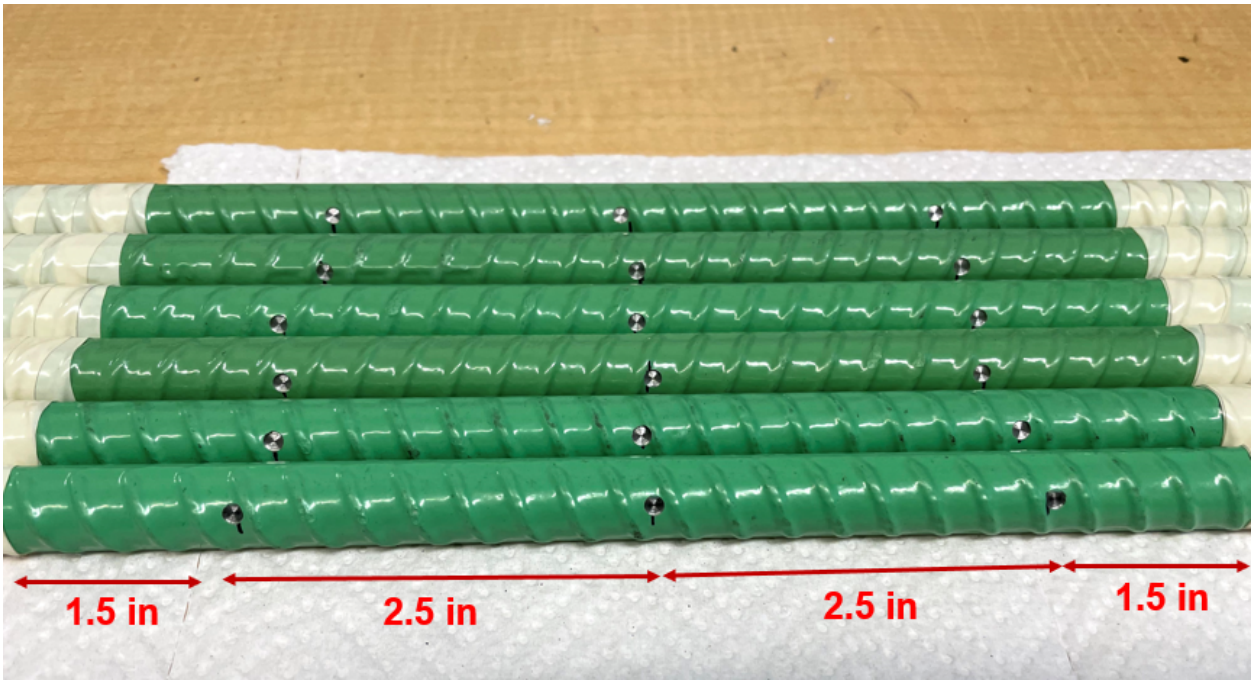

Figure 7. Damaged epoxy-coated bars

Concrete Casting, Cracking, and Corrosion Testing

PVA molds were prepared in 4.5 by 6 by 11 inches according to ASTM G109. Bars were placed in the molds so that the center of the bar was in the same line as the middle of the molds. Self-compacting systems, including SCC P, HyFRC, and UHPC, were cast in one layer, and the surface was finished. HPC and ECC systems were cast in two layers, and each layer was compacted using hitting and vibrating the molds. Figure 8 shows a series of G109 beams while finishing the surfaces. Specimens were

covered with wet burlap and plastic sheets and left in the lab for 24 hours before demolding. UHPC specimens were demolded after 48 hours due to the manufacturer's recommendation. Then, specimens were moved for 28 days in the 100 percent moisture room, followed by 28 days in the 50 percent moisture room prior to corrosion testing. A dam with 3 by 3 by 6 inches was placed on the top of the sample, and specimens were covered with special epoxy to seal all around the specimens other than the bottom surface.

Figure 8. G109 Beam after Casting

All of the cracked specimens were cracked in three-point bending before placing the dam and epoxy coating. All cracked beams were loaded up to 80 percent of their capacity, considering the used concrete and reinforcement. The beam's capacity was found using simulation and trial beam testing. The results of beam cracking are summarized in the section 4.3.

Chloride Profiling

At the end of corrosion testing, chloride profiling on the beams was done according to ASTM C1152 [85]. Also, the corrosion testing was stopped on a series of selected beams at 365 days for chloride profiling to compare the chloride penetration of concrete systems at the same age. Specimens were ground in different depths according to the ASTM C1556 [86]. Table 3 shows the recommended grinding depths for chloride profiling

based on different water to cement ratios. Figure 9 shows a specimen after gridning in different depths from the top view. The collected powder was then used in the chemical analysis for chloride content according to ASTM C1152.

Table 3. Recommended grinding depths for chloride profiling in mm

w/cm	0.25	0.3	0.35	0.4	0.5
Depth 1	0-1	0-1	0-1	0-1	0-1
Depth 2	1-2	1-2	1-2	1-3	1-3
Depth 3	2-3	2-3	2-3	3-5	3-5
Depth 4	3-4	3-4	3-5	5-7	5-8
Depth 5	4-5	4-6	5-7	7-10	8-12
Depth 6	5-6	6-8	7-9	10-13	12-16
Depth 7	6-8	8-10	9-12	13-16	16-20
Depth 8	8-10	10-12	12-16	16-20	20-25

Figure 9. Ground specimens in different depths

Results and Discussion

Mechanical Testing Results

Table 4 summarizes the compressive strength and unit weight of all systems. All concrete systems met the criteria for the mixture designs provided by the New Jersey Department of Transportation and ductile concrete systems extracted from the literature.

Table 4. Compressive strength and unit weight results

Concrete Type	28 Days Compressive Strength (Psi)	Unit Weight (lbs/Cu.ft)
HPC	8240	153.3
SCC P	6960	150.1
SC-HyFRC	5460	135.2
ECC	6065	120.6
UHPC	20855	155

Specimens were cracked in three-point bending after compressive strength verification. Based on numerical simulation and trial beam results, 80 percent of flexural capacity was applied on the selected beams to crack the specimens. Figure 10 shows one of the trial beams tested in three-point bending to verify the beam's capacity. As can be seen, beams were placed upside down in the testing machine in order to crack the upper side of specimens that will be ponded.

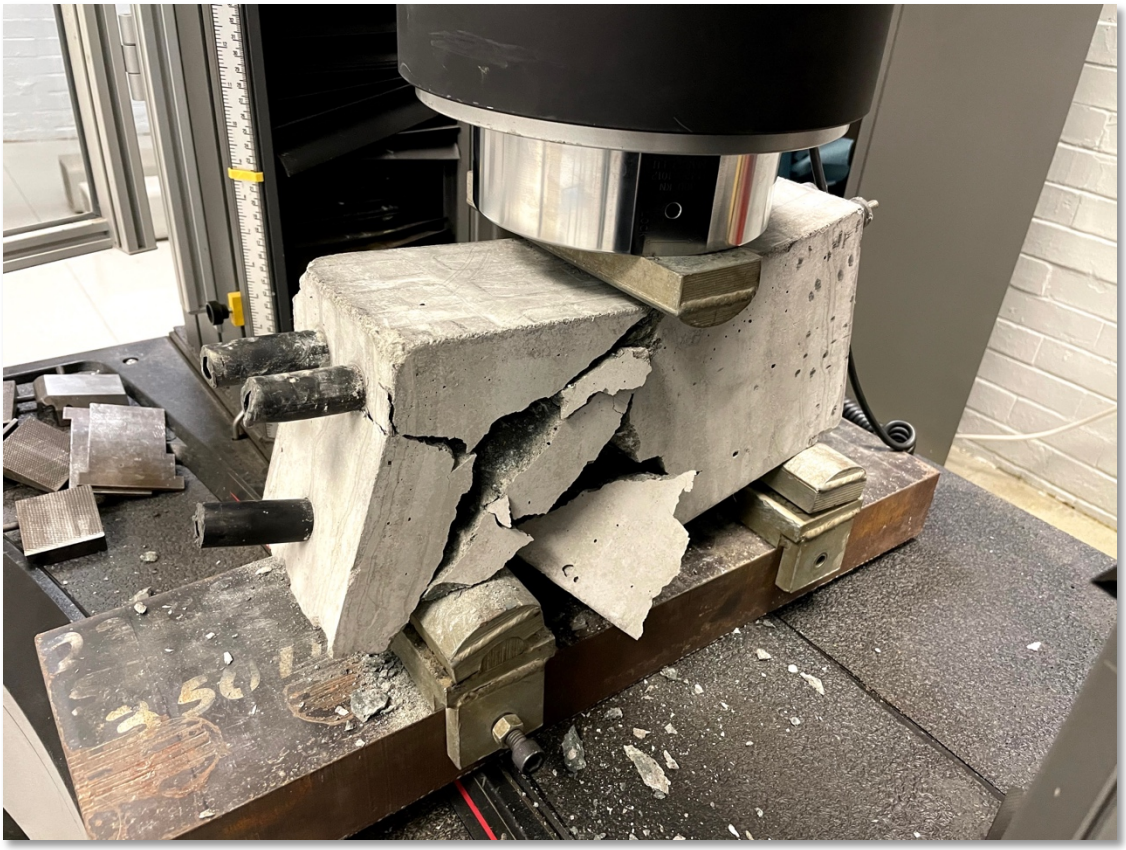

Figure 10. Finding the flexural capacity of a trial beam

The pre-cracking results are summarized in Table 5 to Table 8. HPC specimens were loaded in 72 to 75 Kn for precracking. Table 5 shows the loads used to crack the specimens and the resulting crack widths. In all HPC specimens, the crack was located

approximately in the middle of the beam. Figure 11 shows the crack in the middle of the HPC beam after cracking.

Table 5. Cracking results of HPC beams

Specimen	Load (Kn)	Crack Width (mm)
HPC-Black-1	72	0.15
HPC-Black-2	72	0.1
HPC-Black-3	75	0.15
HPC-ECR-1	75	0.15
HPC-ECR-2	72	0.2
HPC-ECR-3	72	0.15
HPC-Galv-1	72	0.1
HPC-Galv-2	72	0.1
HPC-Galv-3	72	0.25

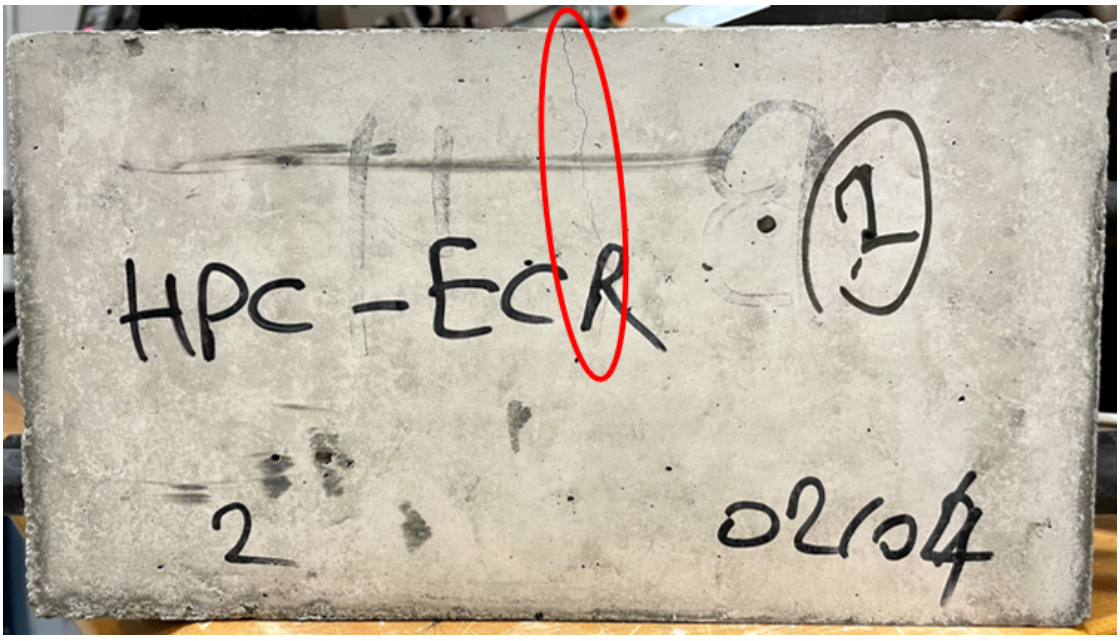

Figure 11. HPC beam after cracking.

Table 6 summarizes the cracking results of ECC. The first specimen failed due to overloading. A large diagonally oriented shear crack was created in the first specimen. Figure 12. Large shear crack in the failed ECC specimen. The next specimens were adjusted to account for this failure mechanism. Multiple macrocracks were observed in the ECC beams after loading. Figure 13 shows multiple microcracks in the ECC beam. However, no crack widths passed 0.1 mm in the loaded ECC specimens up to 80 percent of load capacity.

Table 6. ECC cracking results

Specimen	Load (Kn)	Max Crack Width (mm)
ECC-Black-1	96	-
ECC-Black-2	75	0.06
ECC-Black-3	75	0.04

Figure 12. Large shear crack in the failed ECC specimen

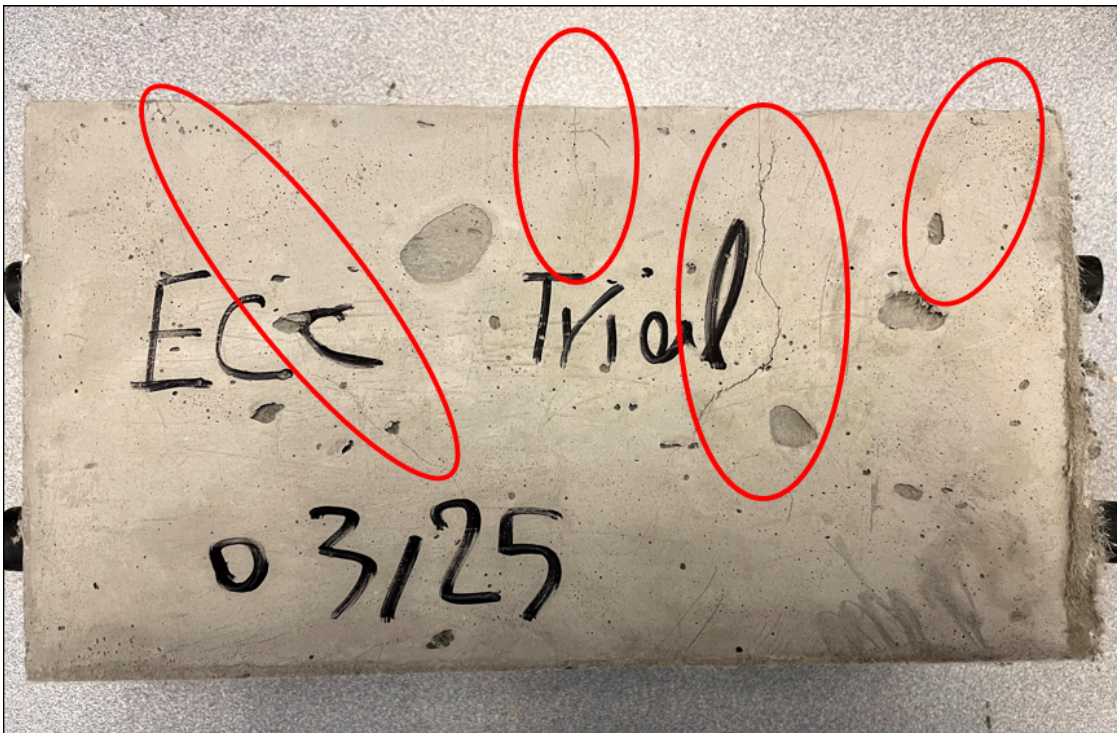

Figure 13. Microcracks in ECC specimen

No cracks were observed in UHPC specimens after applying 80 percent of the beam's capacity (168 kN). Therefore, the loading continued until a visible crack was observed in the specimens. Table 7 summarizes the crack width and cracks location of UHPC beams after loading. Multicracking behavior was observed in the UHPC beams, and no cracks larger than 0.1 mm were observed in the beams. Figure 14 shows the microcracks in UHPC beams after loading

Table 7. Cracking report of UHPC beams

Specimen	Load	Crack Width (mm)	Crack Location	Crack Width (mm)	Crack Location
UHPC-Black-1	209	0.03	Center	-	-
UHPC-Black-2	189	0.1	Center	0.06	Edge
UHPC-Black-3	169	0.03	Center	0.1	Edge
UHPC-ECR-1	226	0.1	Center	-	-
UHPC-ECR-2	196	0.06	Center	-	-
UHPC-ECR-3	178	0.08	Center	-	-
UHPC-ChromX-1	197	0.04	Center	-	-
UHPC-ChromX-2	188	0.08	Center	0.2	Edge
UHPC-ChromX-3	208	0.05	Center	0.05	Edge
UHPC-Trial	210	Failed	-	-	-

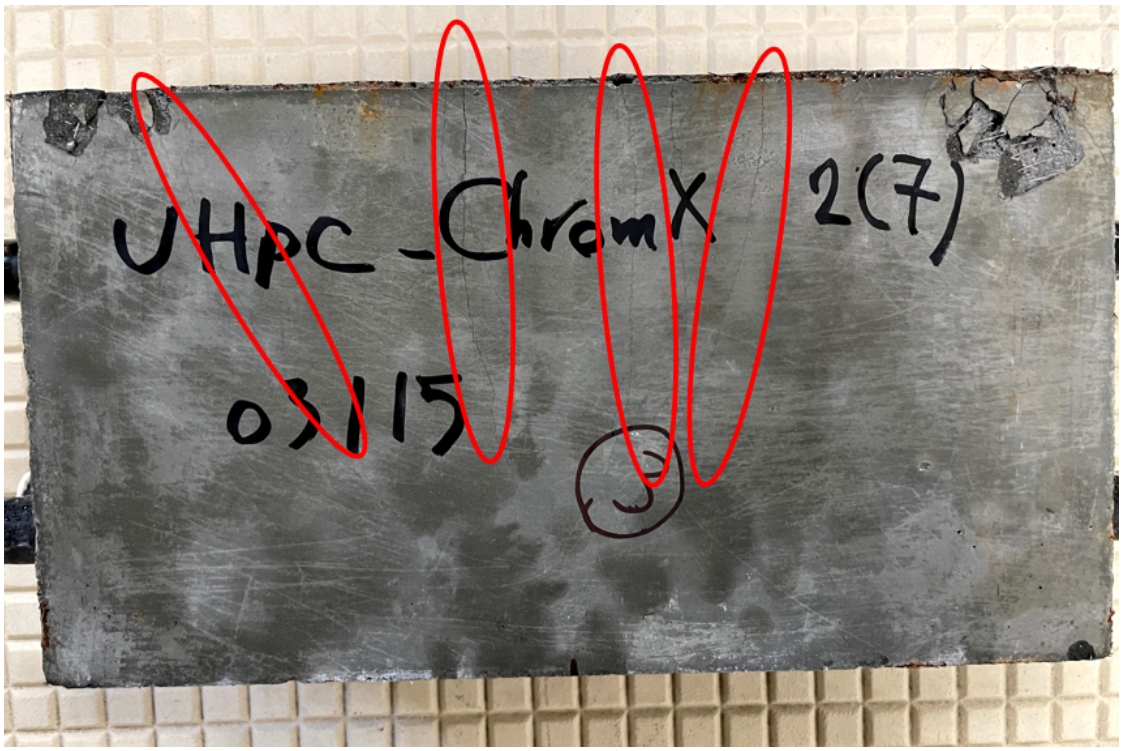

Figure 14. Microcracks in UHPC beams

All HyFRC specimens were loaded up to 88 Kn, which is 80 percent of the HyFRC beam capacity. HyFRC had lower compressive strength than other concrete systems but more flexural strength than HPC and ECC. Hybrid fibers improved the flexural strength of HyFRC. However, a larger crack width was observed in HyFRC specimens after loading. Table 8 shows the cracking results of HyFRC specimens. Cracks were created in different locations in the beams. Figure 15 shows the cracking in the HyFRC beam with ordinary black reinforcement.

Table 8. HyFRC cracking results

Specimen	Load (Kn)	Location 1	Crack Width (mm)	Location 2	Crack Width (mm)
HyFRC-Black-1	88	Center	0.1	Center	0.08
HyFRC-Black-2	88	Center	0.15	Center	0.2
HyFRC-Black-3	88	Center	0.2	Center	0.15
HyFRC-ECR-1	88	Center	0.15	Center	-
HyFRC-ECR-2	88	Center	0.25	Center	-
HyFRC-ECR-3	88	Center	0.2	Center	-
HyFRC-ChromX-1	88	Center	0.2	Center	-
HyFRC-ChromX-2	88	Center	0.12	Center	0.08 (Longitudinal)
HyFRC-ChromX-3	88	Center	0.04	Center	-

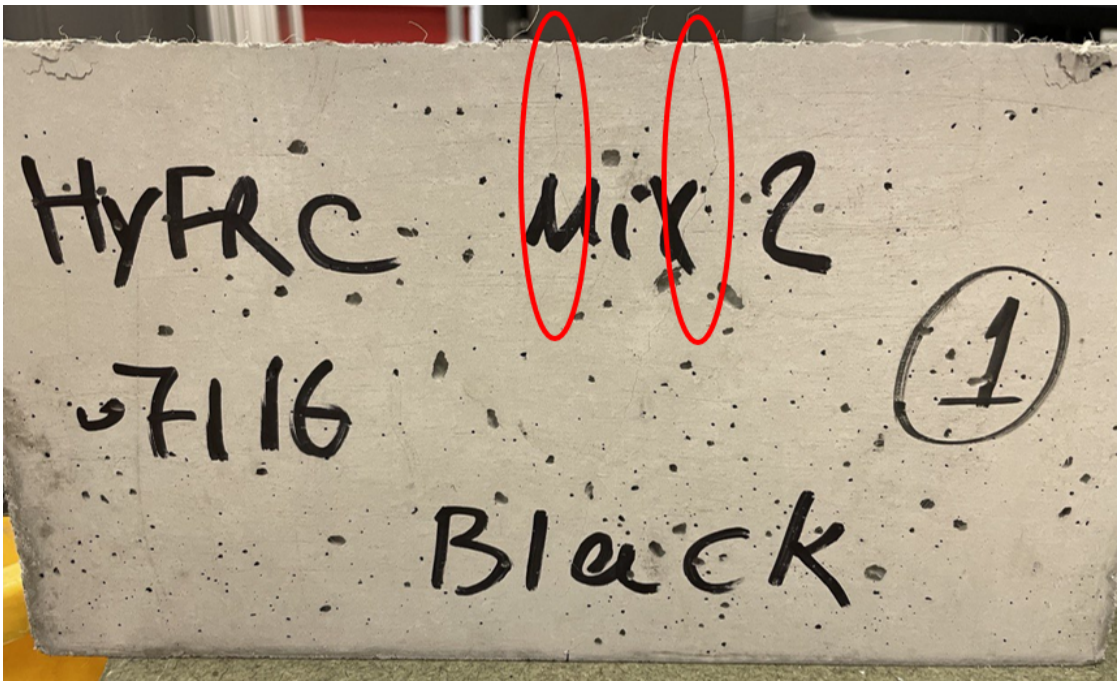

Figure 15. Cracked HyFRC specimen after loading.

Corrosion Test Results

Corrosion results are reported in two main parts for cracked and uncracked beams. Cracked beams should have less corrosion initiation time because cracks provide a path for chlorides to reach the reinforcement surface. Generally, if cracked samples have no sign of corrosion, there would be no corrosion sign in uncracked specimens with the same materials at the same age. The cracked beams results will be presented and discussed first, and uncracked beam corrosion results will be discussed next. Figure 16 to Figure 19 show the corrosion current density in different concrete systems with black bars. The threshold current density is 0.2 $\mu A/cm^2$. If the current density passes this number, there will be a high probability of corrosion initiation in the system. Figure 16 shows the corrosion current density in the HPC beam with black bars. There were fluctuations in the current density during the first weeks of ponding, but it never passed the threshold, and with passing time, it was constantly zero to the date of writing this report. For corrosion initiation, the beams need more time to pass the critical chloride threshold level at the reinforcement surface.

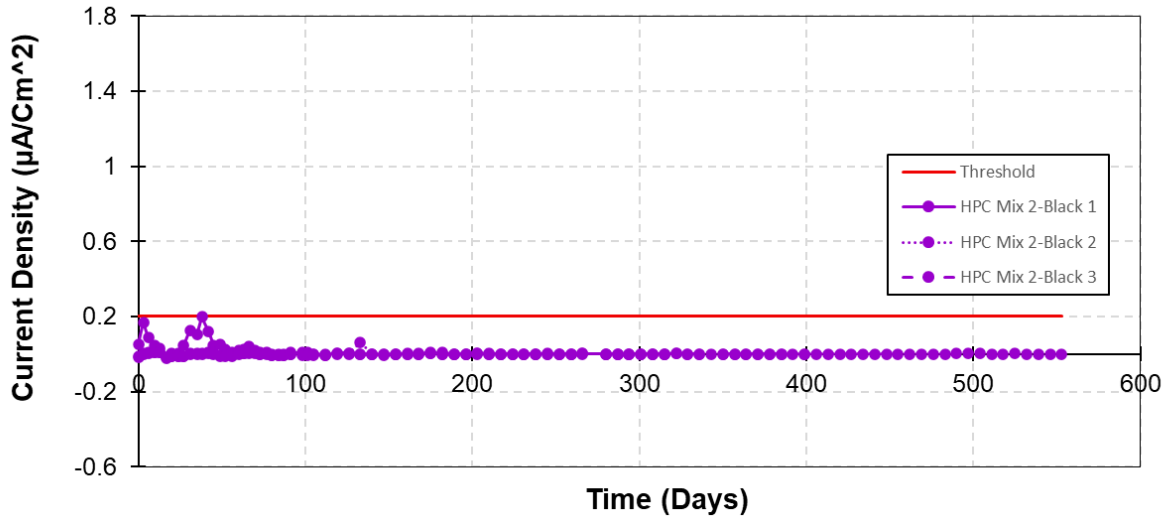

Figure 16. Corrosion current density in HPC beam with black bars

Figure 16 represents the corrosion result in ECC beams with black reinforcement. As can be seen, there were signs of corrosion during the first few weeks of starting the test; however, the current merged to zero gradually. A significant fluctuation was observed in the first ECC beam with a large shear crack. This beam was not used in comparison diagrams and discussion because of failure in shear. The two other ECC beams with black reinforcement represented the ECC beams with black reinforcement.

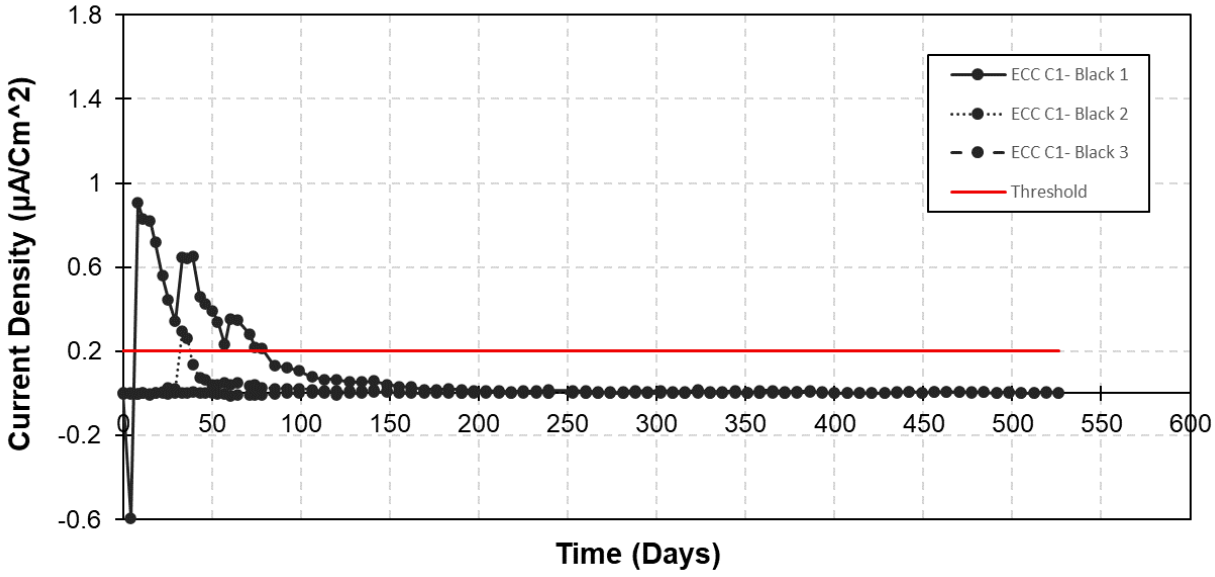

Figure 16. ECC with black reinforcement corrosion result

Figure 17 shows the results for UHPC beams with black reinforcement. Since starting the test, there was no sign of corrosion current in UHPC beams. UHPC beams were

expected to have more corrosion resistance compared to other systems because of the material's dense microstructure.

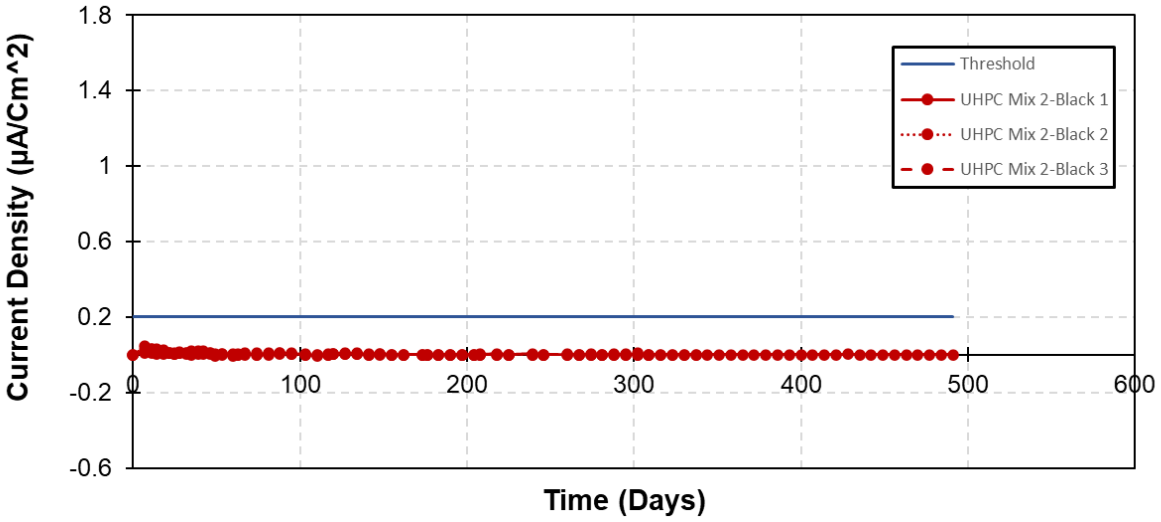

Figure 17. Corrosion result in UHPC beams with black reinforcement

Figure 19 represents the corrosion current density results in HyFRC beams. Corrosion was initiated in cracked HyFRC beams since the first day of ponding. The large crack width in cracked HyFRC beams compared to the other concrete systems caused corrosion initiation right after ponding. However, the results show that the current density approached the corrosion current density threshold with passing time.

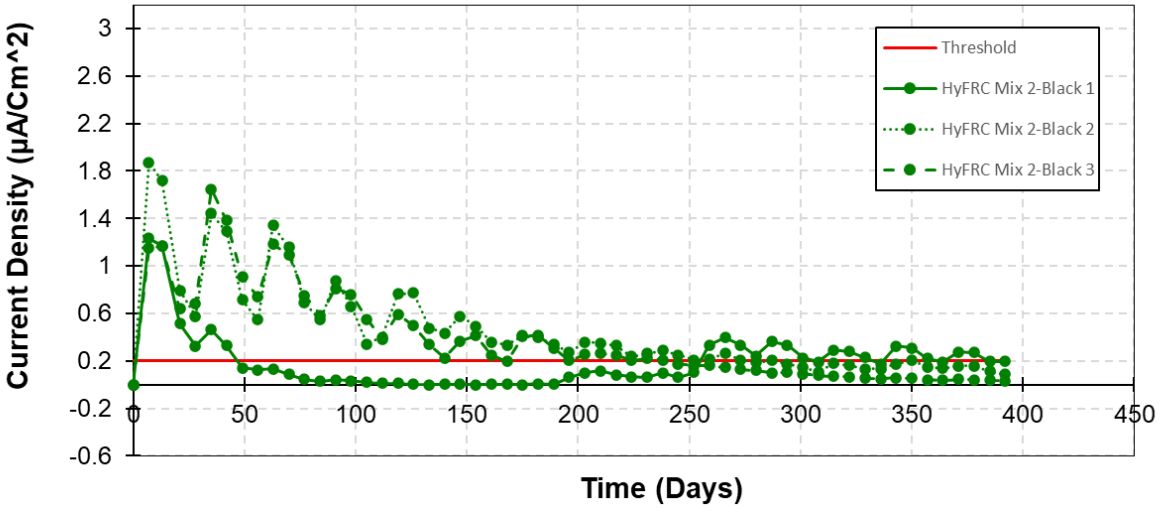

Figure 19. Corrosion current density in cracked HyFRC beams with black reinforcement

Figure 19 shows the result for the corrosion current density of cracked HPC beams with galvanized reinforcement. Due to the high reactivity of the zinc coating on the

galvanized bars, a high current was recorded during the first few months of ponding. However, all samples merged to zero with passing time which was expected based on the corrosion behavior of galvanized bars in environments with chlorides.

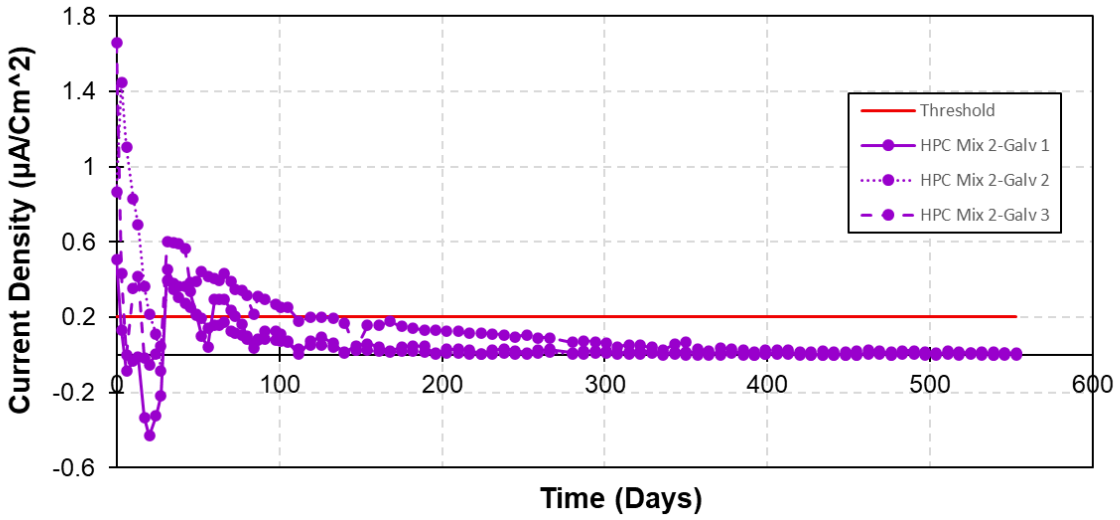

Figure 19. Corrosion result of cracked HPC beams with galvanized reinforcement

Figure 20 and Figure 21 show the corrosion current density results in cracked UHPC and HyFRC beams with ChromX reinforcement. ChromX bars are supposed to have a higher corrosion resistance compared to black bars. There was no sign of corrosion in UHPC beams with ChromX reinforcement. Cracked HyFRC beams with ChromX reinforcement showed signs of high corrosion current after the first day of ponding, like black bars. However, in the first beam, there was no sign of corrosion at all. The tight crack width in this beam after precracking was the main reason for the no signs of corrosion.

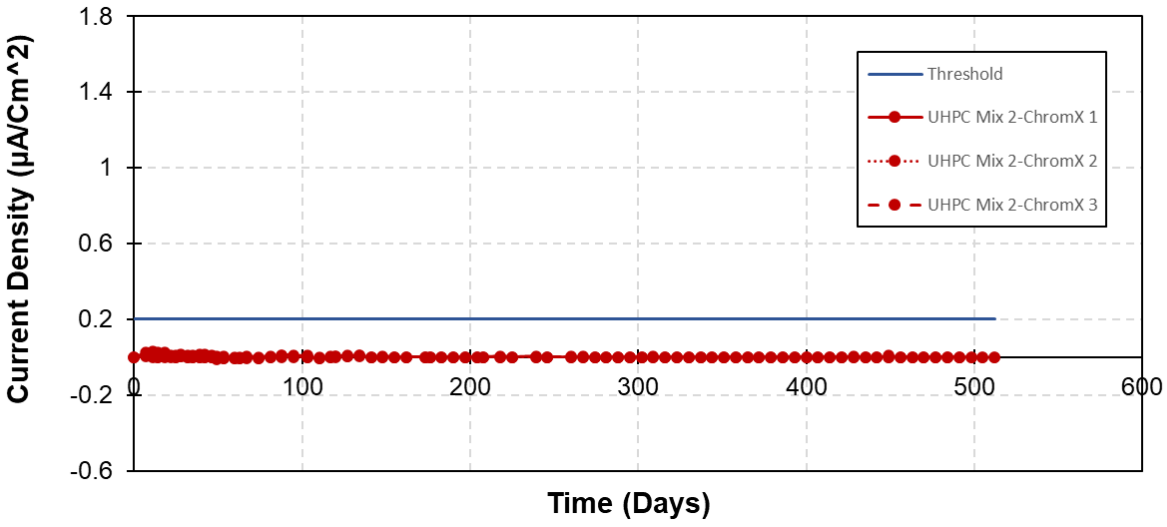

Figure 20. Cracked UHPC beams with ChromX reinforcement

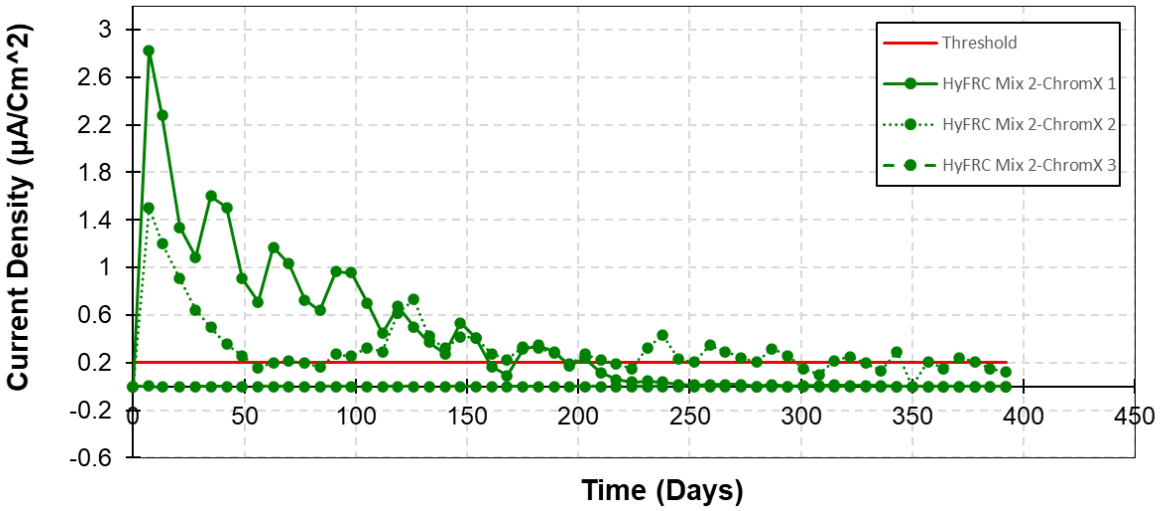

Figure 21. Cracked HyFRC beams with ChromX reinforcement

Figure 22 to Figure 24 shows all cracked beams with ECR. No sign of corrosion was observed in the beams with ECR. The coating prevents chloride from reaching the steel surface and needs more time for corrosion initiation.

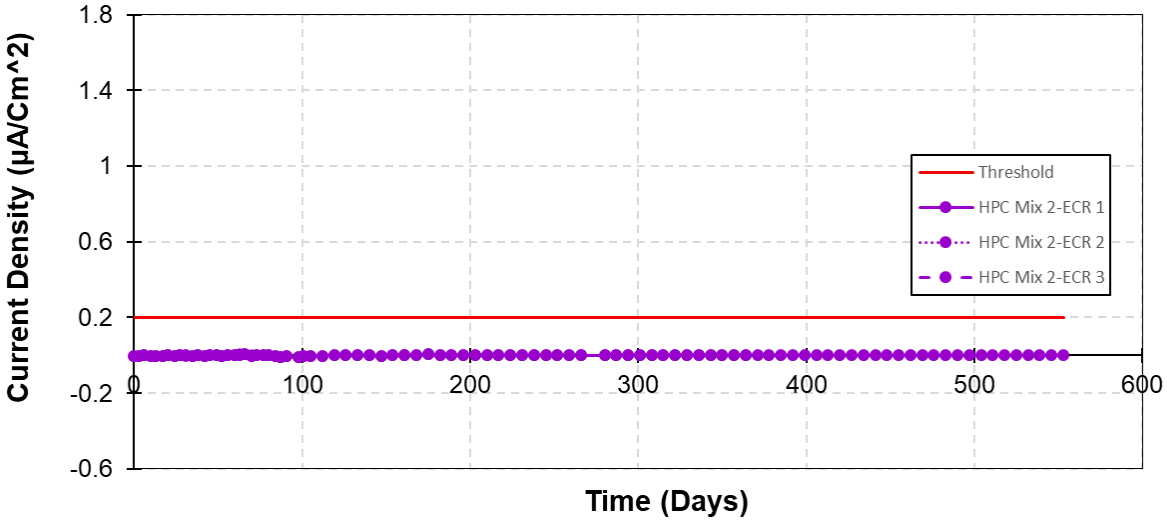

Figure 22. Corrosion current in cracked HPC beams with ECR

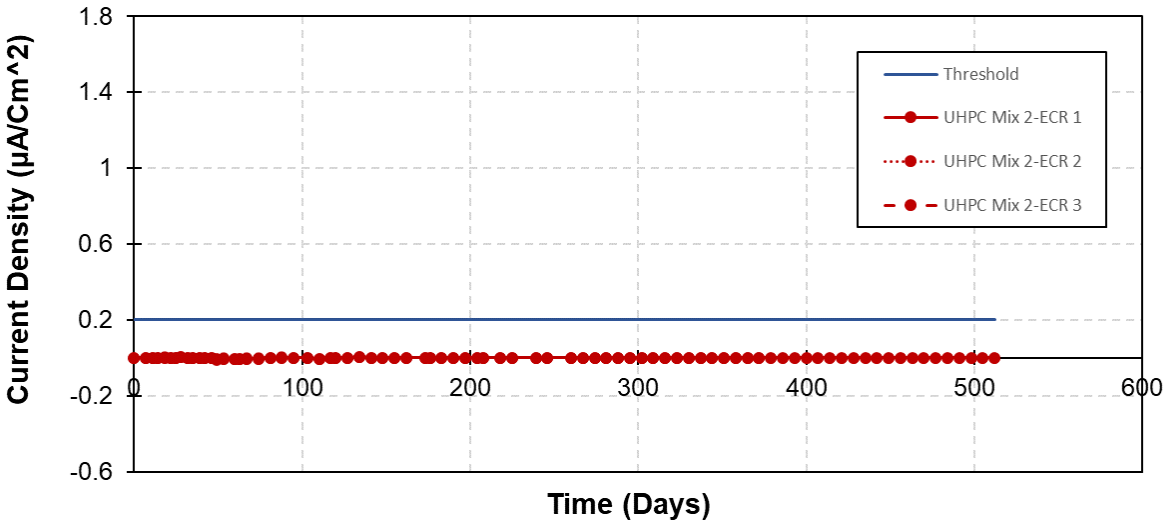

Figure 23. Corrosion current in cracked UHPC beams with ECR

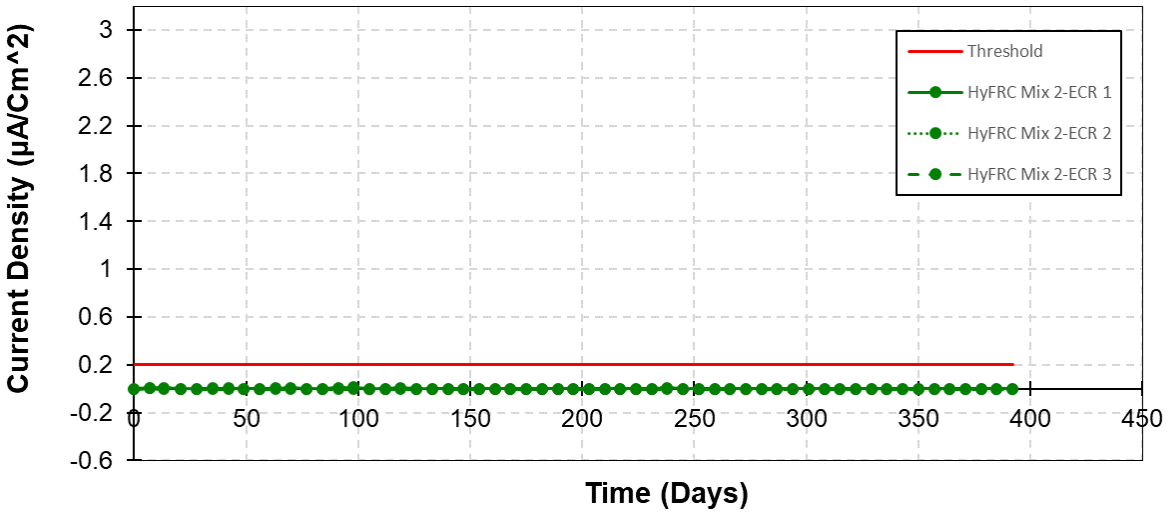

Figure 24. Corrosion current in cracked HyFRC beams with ECR

Figure 25 to Figure 29 show the corrosion current density in uncracked beams with black reinforcement. There was no sign of corrosion in uncracked beams. More time was needed for corrosion initiation in uncracked beams. The results will be updated after corrosion initiation in uncracked beams and reported to NJDOT in a supplement.

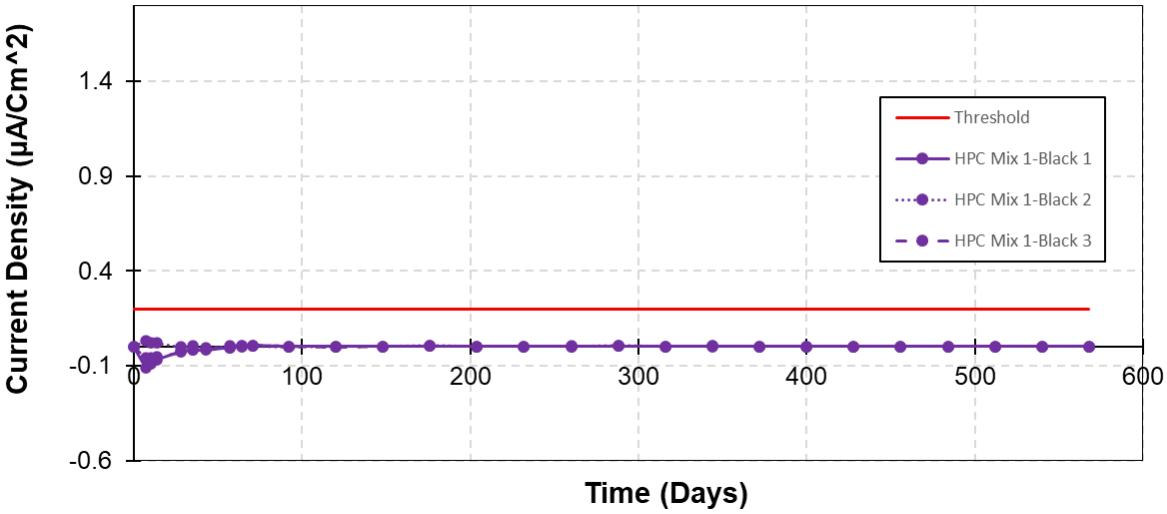

Figure 25. Corrosion current density in uncracked HPC beams with black reinforcement

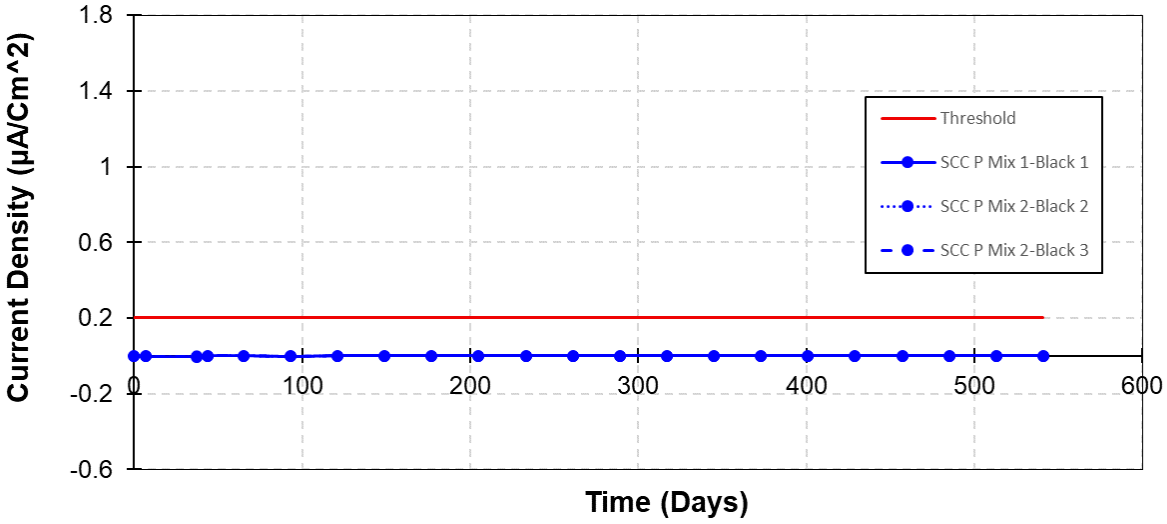

Figure 26. Corrosion current density in uncracked SCC P beams with black reinforcement

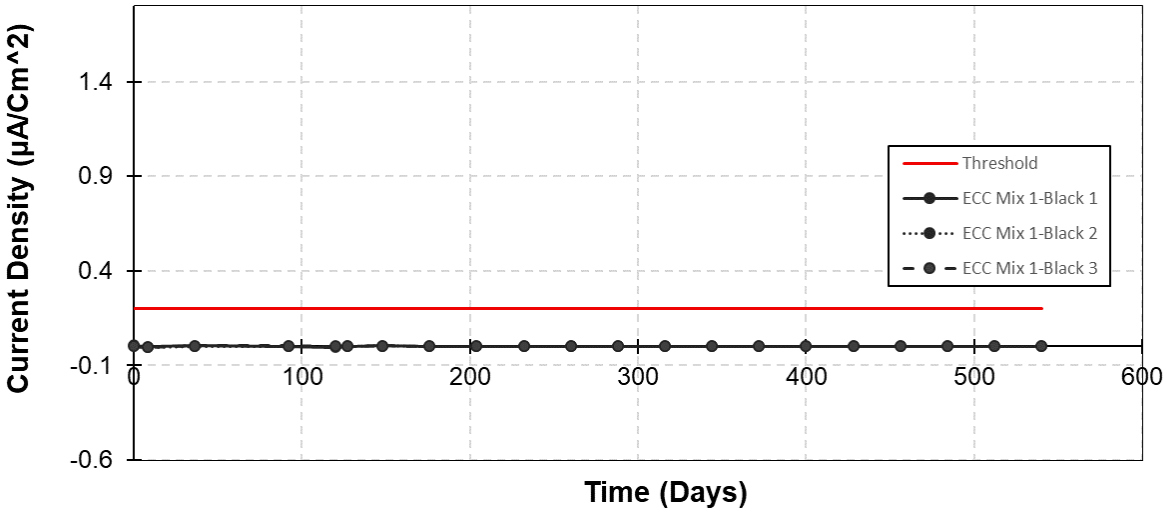

Figure 27. Corrosion current density in uncracked ECC beams with black reinforcement

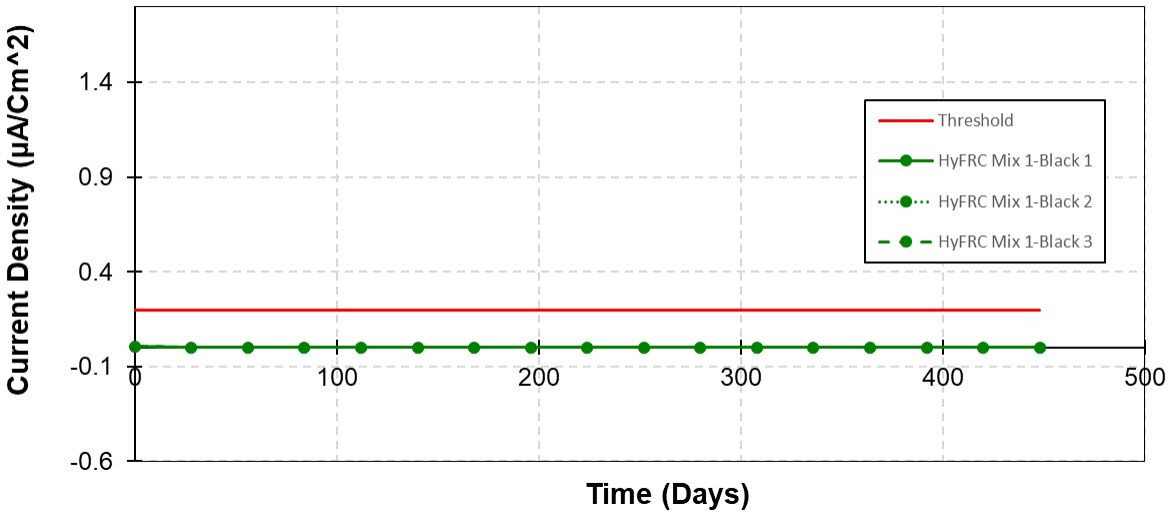

Figure 28. Corrosion current density in uncracked HyFRC beams with black reinforcement

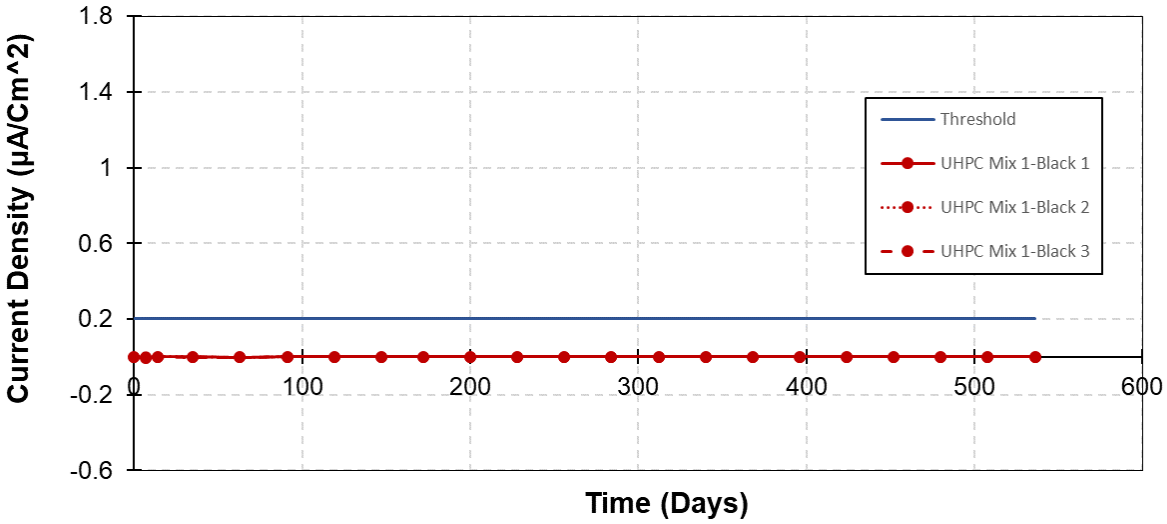

Figure 29. Corrosion current density in uncracked UHPC beams with black reinforcement

The results for uncracked beams with ECR, ChromX, and stainless steel reinforcement are not shown here as it is expected to have no corrosion in beams with ECR, Chromx, and stainless steel reinforcement. These types of reinforcement provide superior corrosion resistance compared to black reinforcement.

Figure 30 summarizes the corrosion current density for all cracked beams with black reinforcement. As can be seen, there is no sign of corrosion in all systems other than HyFRC. HyFRC beams had more crack width compared to other systems. The results in the beams show that there is a direct relationship between corrosion intensity and

cracked width in cracked beams. Signs of corrosion were not observed in cracked beams with a crack width of 0.1 mm or less. Small crack widths can be easily blocked by corrosion products and salts and hinder access to chlorides and oxygen. Moreover, the self-healing effect in systems with specific supplementary cementitious materials is the other reason that prevents access to chlorides and oxygen.

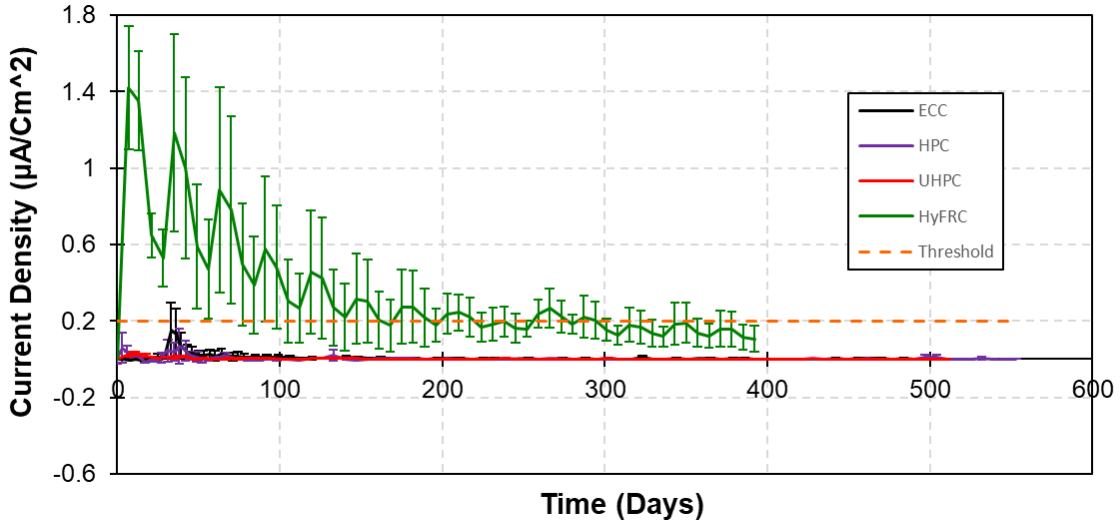

Figure 30. Corrosion current density in all cracked specimens with black reinforcement

Conclusions

According to ASTM G109, corrosion testing is a long-term test method that could take years to complete. An attempt was made to speed up this process through pre-cracking; however, the excellent crack control of the HPFRCC systems slowed down the ingress of chlorides. The summarized conclusions are based on the results of conducted tests to the date of writing the report. More conclusions can be derived from the test results after the test completion. The conclusions can be summarized as follows:

- There was no sign of corrosion in uncracked beams at the time of writing this report. Uncracked beams need more time for corrosion initiation
- High corrosion activity was observed in the galvanized bars due to the zinc coating. The corrosion current density decreased significantly over time.
- Ductile concrete systems and alternative reinforcement need more time for corrosion initiation. The complete conclusions on the corrosion performance of ductile concrete systems and alternative reinforcement will be updated later with getting the full results.
- Corrosion in cracked beams is highly dependent on the crack widths. Small cracks (Less than 0.1 mm) have minor or no effect on corrosion performance and can be blocked by corrosion products or self-healing.

Effect of Freezing Temperatures on the Durability of Ductile Concrete Systems

Introduction

Freezing temperatures can cause serious durability problems for concrete structures. Freezing and thawing is a main reason for concrete failure in cold areas [87–89]. Using de-icing salts on the roadways and walkways used in areas with cold climates causes salt scaling. Salt scaling is the other major durability issue in cold climates. According to the literature, using supplementary cementitious materials and fibers improves concrete's freeze-thaw and salt scaling resistance [90].

Ductile concrete systems, including ultra-high-performance concrete (UHPC), hybrid fiber-reinforced concrete (HyFRC), and engineered cementitious composites (ECC), are one solution that can improve the durability of concrete systems. Due to using fibers and supplementary cementitious materials in their mixture designs, it is expected that they can provide better durability. Among ductile concrete systems, the mixture design and fiber selection can result in different durability and mechanical responses. UHPC has a denser microstructure than ECC and HyFRC and a higher tensile and compressive strength than other ductile systems. ECC consists of only fine particles. It has a dense microstructure, and the fiber-matrix interaction is designed to achieve the highest level of tensile ductility. Since HyFRC generally contains coarse aggregate, it often has a microstructure similar to that of normal concrete. These changes in microstructure and mechanical response of ductile concrete systems affect each system's durability.

There are several ways to evaluate the performance of ductile concrete systems in freezing temperatures. Most of these studies focus on the freeze and thaw resistance of ductile concrete systems, and there is limited information on the salt scaling resistance of these systems [91–95]. The only available data that may apply to some ductile concrete systems in the literature is the result of investigations on high-performance concrete with W/C less than 0.3. According to the literature, concrete systems with W/C less than 0.30 do not require air entraining to resist salt scaling [96–98]. This result can apply to UHPC and ECC. Several studies investigated the freeze-thaw resistance of UHPC. According to these studies, the relative dynamic modulus of elasticity of UHPC did not degrade or changed slightly after 300 cycles [91–94]. Studies conducted by Gu et al., 2018 and Lepech and Li, 2005 on the ECC freeze-thaw resistance showed no degradation in the relative modulus of elasticity after 300 cycles [93,95]. However, according to Nam et al., 2016 the relative modulus of elasticity dropped between 70 to 95 percent of the original value for different ECC mixtures after 300 cycles [99]. Wang et al., 2021 investigated the freeze-thaw resistance of HyFRC, and the relative modulus of elasticity dropped between 82 to 96 after 100 cycles [100]. However, there is no study to compare the performance of various types of ductile concrete systems in freezing temperatures including freeze-thaw resistance and salt-scaling.

This section investigates the performance of ductile concrete systems, including UHPC, HyFRC, and ECC, as well as high-performance concrete (HPC) and self-consolidating concrete (SCC P) provided by the New Jersey Department of Transportation in freezing

temperatures. The freeze-thaw and salt scaling tests were used to study the behavior of concrete systems in freezing temperatures.

Methods

Freeze-thaw Test

The freeze-thaw tests were done according to the ASTM C666 [101]. Based on the standard, Procedure A, rapid freezing and thawing in water was used. The normal procedure for freezing and thawing cycles was lowering the temperature from 40 to 0 °F [4 to -18 °C] and increasing from 0 to 40 °F [-18 to 4 °C]. This cycle was completed in less than two hours and not more than 5 hours. At least 25% of the time was used for the thawing. Concrete prisms with dimensions of 3 by 4 by 14 inches were used. Specimens were cast and cured for 14 days in saturated lime water at 73.4 ± 3 °F [23.0 ± 2.0°C] prior to testing. Before testing, specimens were brought to a temperature within -2 °F and +4 °F [-1 °C and +2 °C] of the target thaw temperature and mass, and the dimensions of specimens were measured. The test was started by putting specimens in the freeze-thaw machine containers filled with water at the thawing water. The test was stopped every 36 cycles, and specimens were removed from the freeze-thaw machine for fundamental transverse frequency tests and mass measurements. Figure 31 shows the specimens in the freeze-thaw machine containers before testing.

Figure 31. Specimens in the freeze-thaw machine

The relative dynamic modulus of elasticity and durability factor was calculated for each specimen as follows:

$$P_c = \left(\frac{{n_1}^2}{n^2}\right) \times 100 \tag{4}$$

Where P_c is the relative dynamic modulus of elasticity after *c* cycles, n is the fundamental transverse frequency at 0 cycles, and n_1 is fundamental transverse frequency after *c* cycles.

$$DF = PN/M \tag{5}$$

Where *DF* is the durability factor, *P* is the relative dynamic modulus of elasticity at *N* cycles, *N* is the number of cycles that *P* reaches the minimum amount or number of cycles that the test is supposed to be terminated, and *M* is the number of cycles that the test is considered to be terminated. In this project, the test was continued until 300 cycles or until the relative dynamic modulus of elasticity reached 60% of the initial number, whichever occurred first.

Salt Scaling Test

Salt scaling tests were performed according to ASTM C672 [102]. Specimens were cast in 10 by 10 by 4 inches molds, and the top surface was finished three times with sawing motions with a wood trowel and brushed according to the instructions in the ASTM standard. Specimens were cured for 14 days in a moist room and stored for 14 days at 23.0 ± 2.0°C [73.5 ± 3.5°F] and 45 to 55% relative humidity prior to testing. A dike made of PVC sheets with a thickness of one inch was used along the perimeter of the top surface and sealed using silicon caulk resistant against freezing temperatures for ponding the top surface with brine. The top surface of the specimens was covered with approximately 6 mm of calcium chloride solution. Every 100 ml of solution had 4 g of anhydrous calcium chloride. Figure 32 shows the specimens before ponding.

Figure 32. Salt scaling specimens ready to be ponded

The ponded specimens were placed into a freezer for 16 to 18 hours and then placed in laboratory air at 23 ± 2.0°C [73.5 ± 3.5°F] and relative humidity of 45 to 55 % for 6 to 8 h. This cycle was repeated daily for five days. After every five cycles, the the water standing on surface of the specimens was emptied, a visual evaluation was done, and photos were taken. After visual evaluation, the solution was replaced, and daily cycles continued. The visual examinations were performed every five cycles until 50 cycles

were completed. The surface evaluation of the specimen was according to the rubric in the ASTM C672 for the scaling rating, as shown in Table 9.

Table 9. Rating scale for the salt scaling visual examination

Rating	Condition of Surface
0	no scaling
1	very slight scaling (3 mm [1⁄8 in.] depth, max, no coarse aggregate visible)
2	slight to moderate scaling
3	moderate scaling (some coarse aggregate visible)
4	moderate to severe scaling
5	severe scaling (coarse aggregate visible over entire surface)

Results and Discussion

Compressive Strength

All concrete systems were tested at 28 days in compression for verification of concrete mechanical performance. Additionally, the unit weight was measured for each system to provide more information for comparing the results. Table 10 summarizes the compressive strength and unit weight of all systems. All concrete systems met the criteria for the mixture designs provided by the New Jersey Department of Transportation and ductile concrete systems extracted from the literature.

Table 10. Compressive strength and unit weight results

Concrete Type	28 Days Compressive Strength (Psi)	Unit Weight (lbs/Cu.ft)	Air Content (%)
HPC	7,773	153.3	3.5
SCC P	6,957	150.1	4
SC-HyFRC	5,459	135.2	7.5
ECC	6,063	120.6	5
UHPC	20,857	155	5

Freeze-thaw Results

The results of the freeze-thaw test are shown through figures Figure 33 to Figure 42. Figure 33 shows the relative dynamic modulus of elasticity for HPC after 180 cycles. According to ASTM C666, testing specimens with less than 60 percent of initial relative dynamic modulus of elasticity is not recommended. The test was continued beyond this threshold to ensure that the decreasing trend would continue. According to the results, the relative dynamic modulus of elasticity for HPC dropped below 60 percent between 108 and 144 cycles. Figure 34 shows the samples after 216 cycles. The result of sample three wasn't considered since it was out of the acceptable range for ASTM C666.

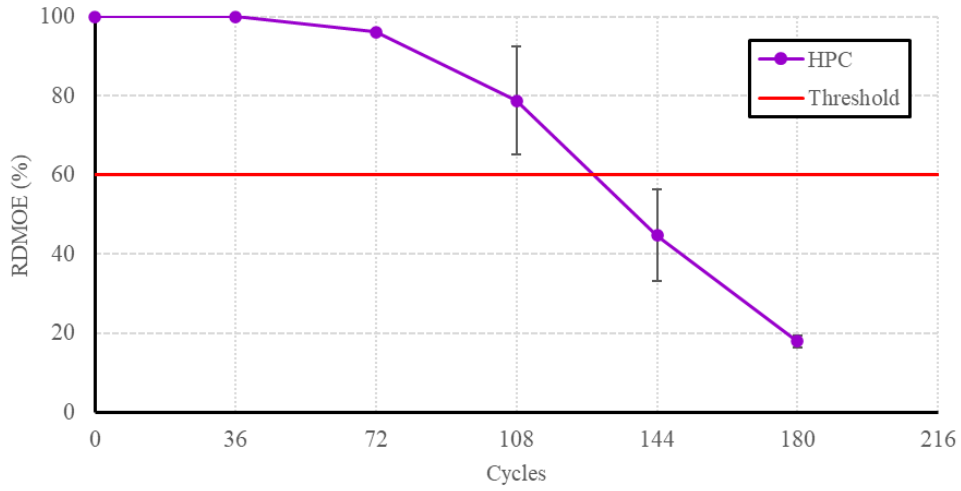

Figure 33. HPC freeze-thaw results

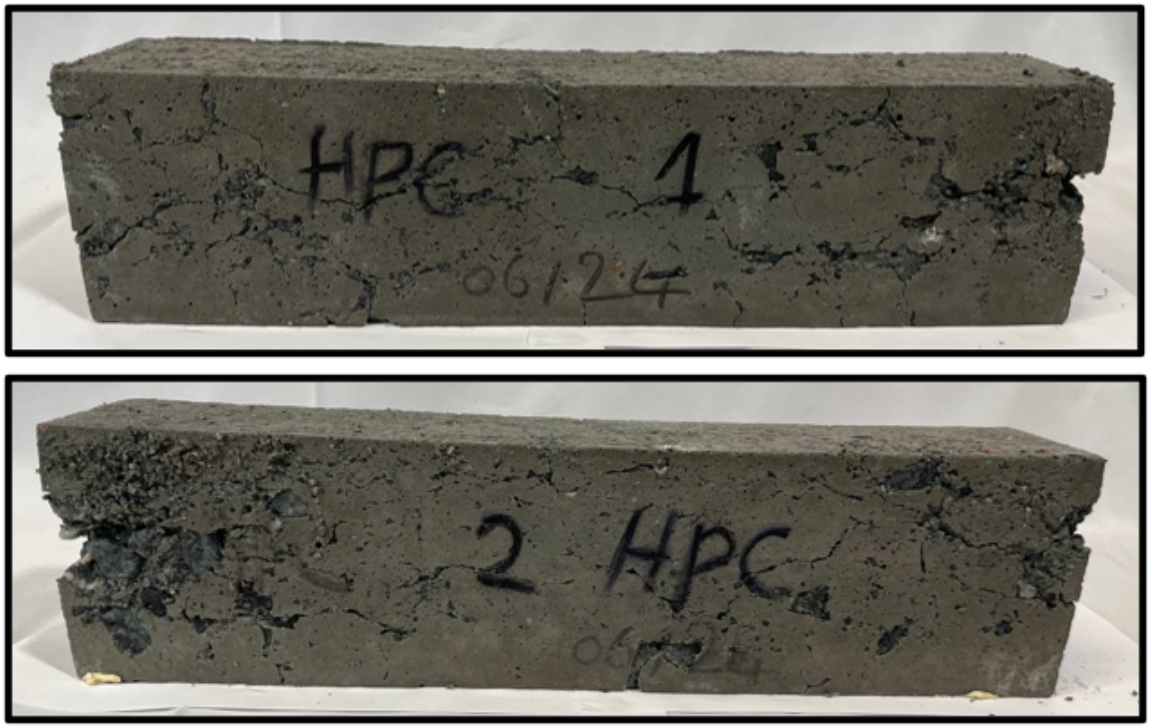

Figure 34. HPC samples after 216 cycles

Figure 35 shows the results of the SCC P mixture. The relative dynamic modulus of elasticity dropped below 60 percent with less than 36 cycles in the first series of freezing and thawing cycles. Figure 36 shows the SCC P samples at the end of 108 cycles. According to this figure, SCC P specimens were severely destroyed, and large pieces of the concrete fell apart.

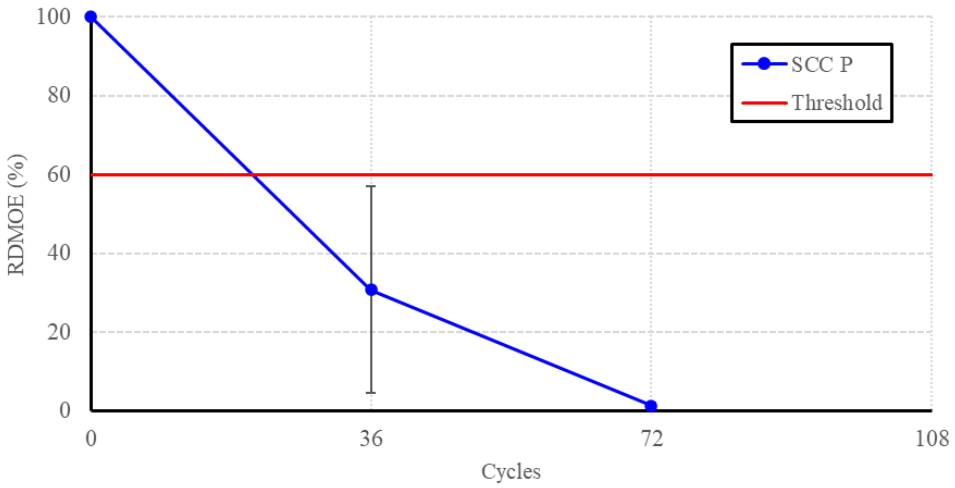

Figure 35. SCC P freeze-thaw result

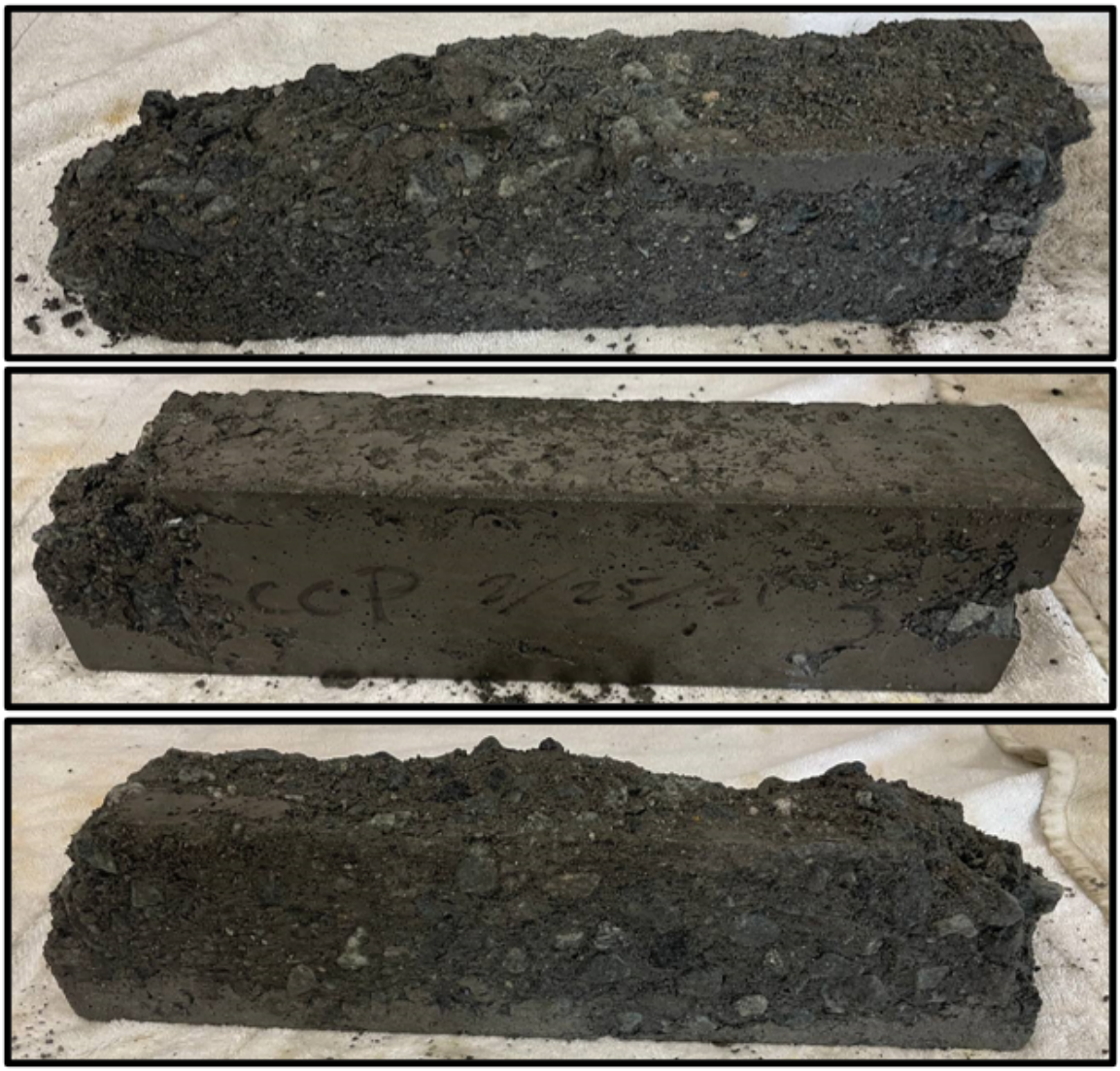

Figure 36. SCC P after 108 cycles

Figure 37 shows the results for the ECC mixture. Based on the results, the relative dynamic modulus of elasticity dropped to 76 percent with a standard deviation of 12 percent after 300 freezing and thawing cycles. The ECC mixture kept more than 90 percent of its relative dynamic modulus of elasticity after 180 cycles. After 180 cycles, it dropped to close to 80 percent and decreased gradually with every series of freezing and thawing cycles. Figure 38 shows ECC samples after being exposed to 300 cycles. ECC samples were still in good condition, some PVA fibers were exposed, and some signs of degradation could be observed on the surface.

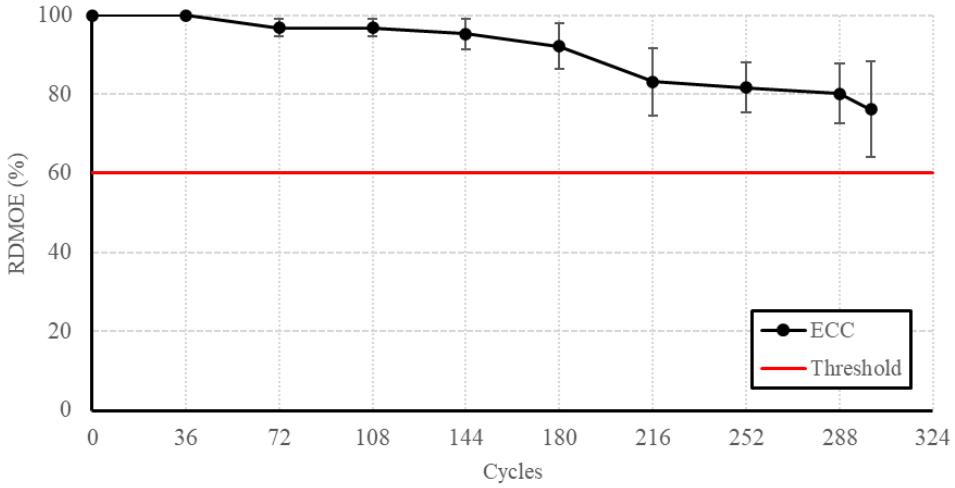

Figure 37. ECC freeze-thaw result

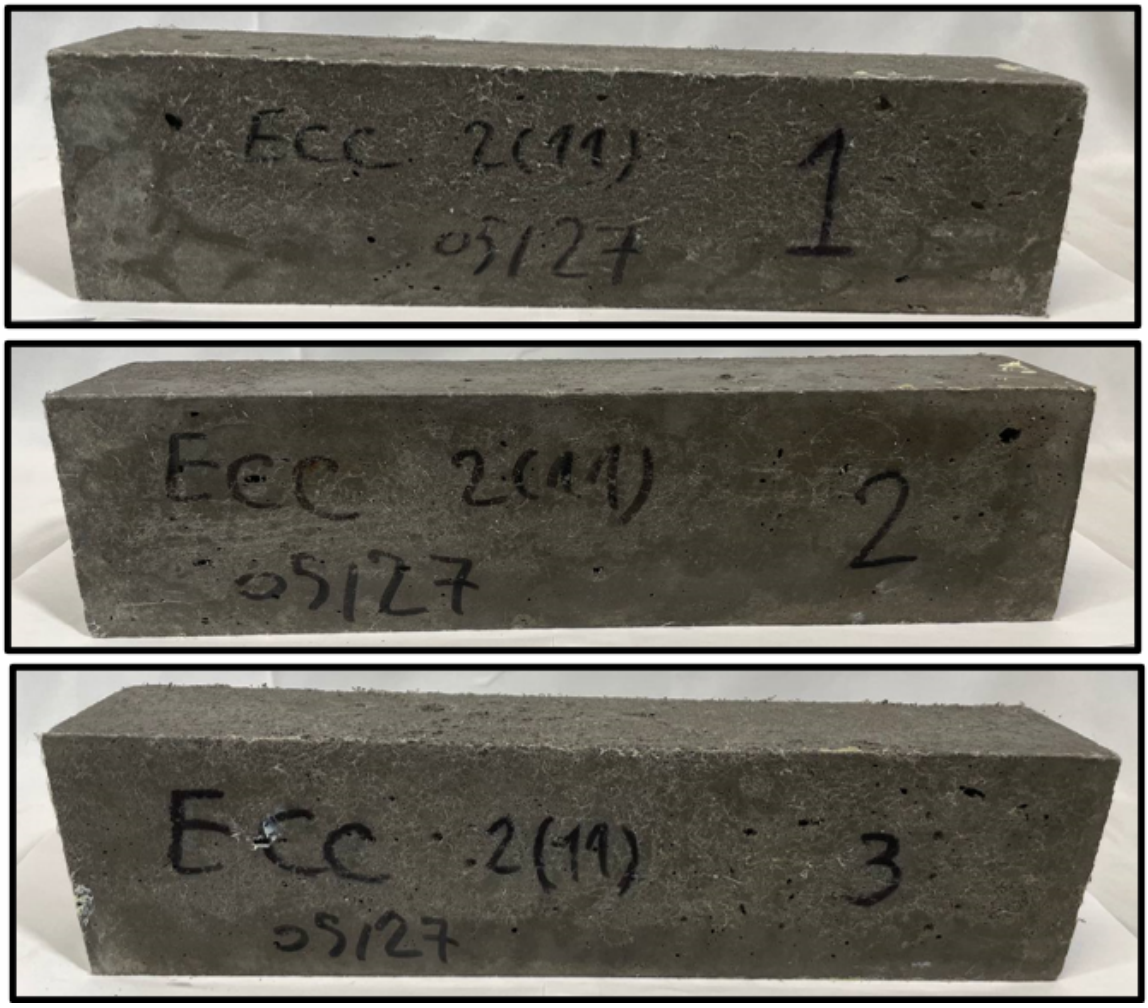

Figure 38. ECC samples after 300 cycles

Figure 39 shows the freeze-thaw results for the HyFRC mixture. All ductile concrete systems were tested for fundamental transverse frequency up to 300 cycles to compare the freeze-thaw resistance of these materials at the same age. The relative dynamic modulus of elasticity for HyFRC dropped below 60 percent between 108 and 144 cycles, similar to HPC. The decreasing trend in relative dynamic modulus of elasticity continued to 216 cycles, around 40 percent. However, the relative dynamic modulus of elasticity didn't change significantly after 216 cycles. Figure 40 shows HyFRC samples after 300 cycles. The samples were still in good shape with exposed PVA and steel fibers. However, the surface degradation of HyFRC was more compared to ECC samples.

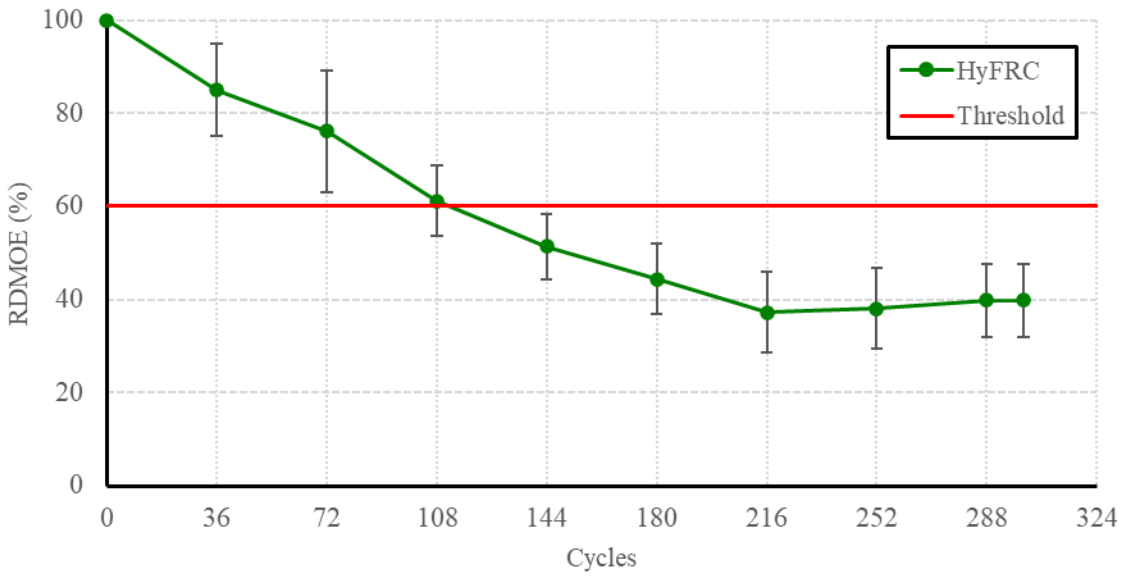

Figure 39. HyFRC freeze-thaw result

Figure 40. HyFRC samples after 300 cycles

Figure 41 shows UHPC freeze-thaw results after 300 cycles. The relative dynamic modulus of elasticity of UHPC didn't change after 100 cycles. Figure 42 shows UHPC specimens after 300 cycles. UHPC specimens remained almost intact after 300 cycles of freezing and thawing. The surface degradation of UHPC samples was negligible compared to other types of concrete systems used in this test.

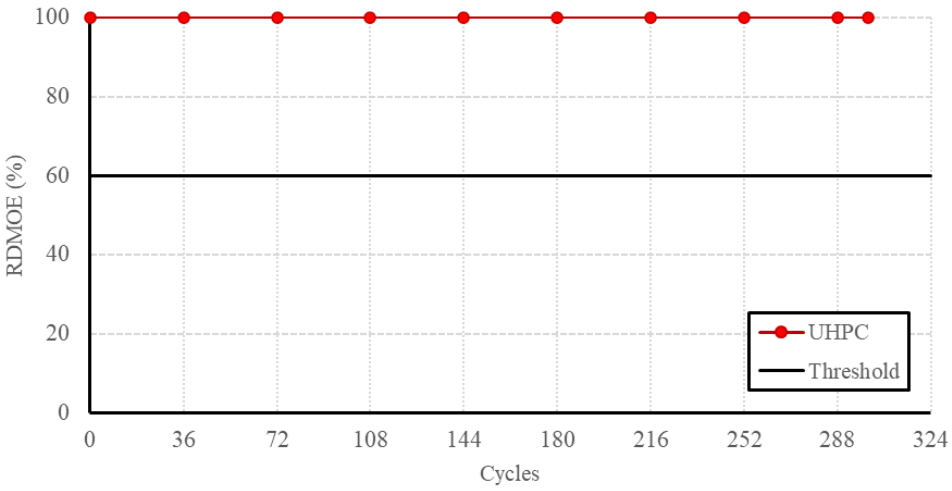

Figure 41. UHPC freeze-thaw results

Figure 42. UHPC specimens after 300 cycles

The relative dynamic modulus of elasticity for all concrete systems is shown in Figure

43.

Table 11 summarizes the durability factor of all concrete systems. UHPC and ECC showed superior freeze-thaw resistance compared to other concrete systems. The durability factor for UHPC and ECC was 100 and 76.3, respectively. HPC and HyFRC specimens failed between 108 and 144 cycles. The durability factor of HPC and HyFRC were 25.1 and 21.3, respectively. SCC P had the lowest freeze-thaw resistance between tested systems. SCC P specimens failed in less than 36 cycles with a durability factor of 3.7. Figure 44 shows the average mass change of all concrete systems every 36 cycles. The mass change of all systems other than SCC P was negligible during the test. SCC P was the only specimen that experienced relatively significant mass changes due to the concrete loss. However, it should be mentioned that SCC P samples didn't show any significant mass change up to 108 cycles, and the relative modulus of elasticity dropped below 70 percent after only 36 cycles.

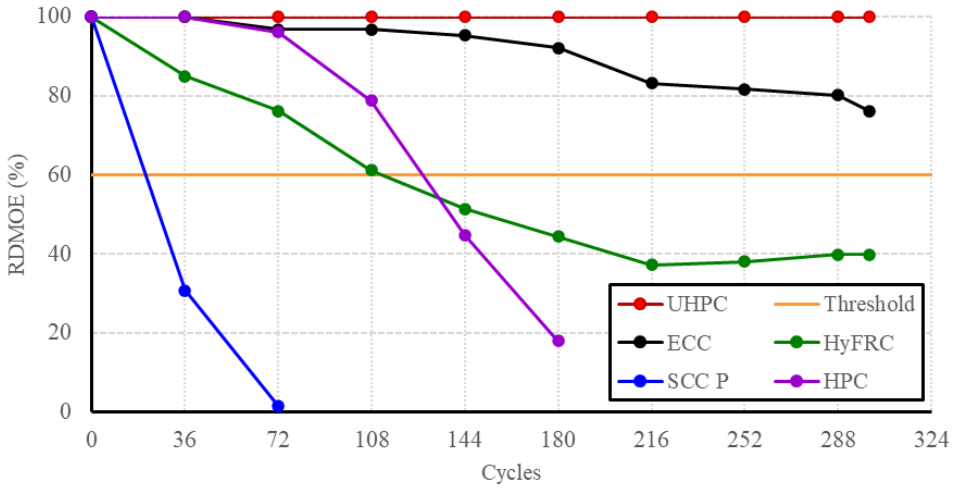

Figure 43: Relative dynamic modulus of elasticity results for all concrete systems

Table 11. Durability factor of concrete systems

Concrete Type	HPC	SCC P	HyFRC	ECC	UHPC
Durability Factor	25.1	3.7	21.3	76.3	100

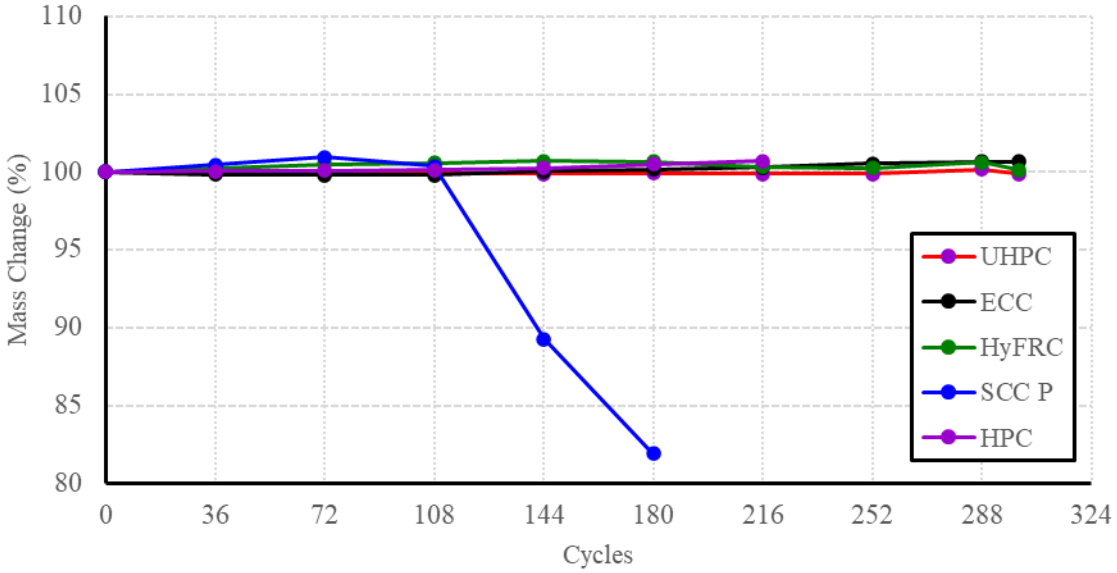

Figure 44. Average mass change of specimens in freeze-thaw test

Salt Scaling Results

The salt scaling ratings are reported in Table 12 after every five cycles. For HyFRC, two different numbers are reported for cycle 50. The number out of parentheses shows the surface evaluation before wire brushing the surface and the number in the parentheses shows the surface evaluation after a gentle wire brushing. Figure 45 to Figure 51 show the surface of concrete systems at zero and 50 cycles. Figure 45 shows the HPC surface at zero and 50 cycles. The scaling rating for HPC specimens one, two, and three were 1, 2, and 0, respectively, after 50 cycles. Specimen three showed no scaling after 50 cycles, while specimen two showed more scaling compared to specimen one. However, none of the specimens showed severe scaling on the scale of 0 to 5 after 50 cycles.

Table 12. Salt scaling ratings of concrete systems

Cycle	HPC			SCC P			HyFRC		
	1	2	3	1	2	3	1	2	3
5	0	0	0	1	1	2	0	0	1
10	0	0	0	2	2	2	1	1	1
15	0	1	0	2	2	2	1	1	1
20	0	1	0	2	2	2	1	1	2
25	0	1	0	2	2	2	2	1	2
30	0	1	0	2	2	2	2	1	2
35	0	1	0	2	3	3	2	1	2
40	0	1	0	2	3	3	2	1	3
45	0	1	0	2	3	3	2	1	3
50	1	2	0	3	3	3	2(3)	1(2)	3(4)

Cycle	ECC			UHPC		
	1	2	3	1	2	3
5	0	0	0	0	0	0
10	0	0	0	0	0	0
15	0	0	0	0	0	0
20	0	0	0	0	0	0
25	0	0	0	0	0	0
30	0	0	0	0	0	0
35	0	0	0	0	0	0
40	0	0	0	0	0	0
45	0	0	0	0	0	0
50	1	0	1	0	0	0

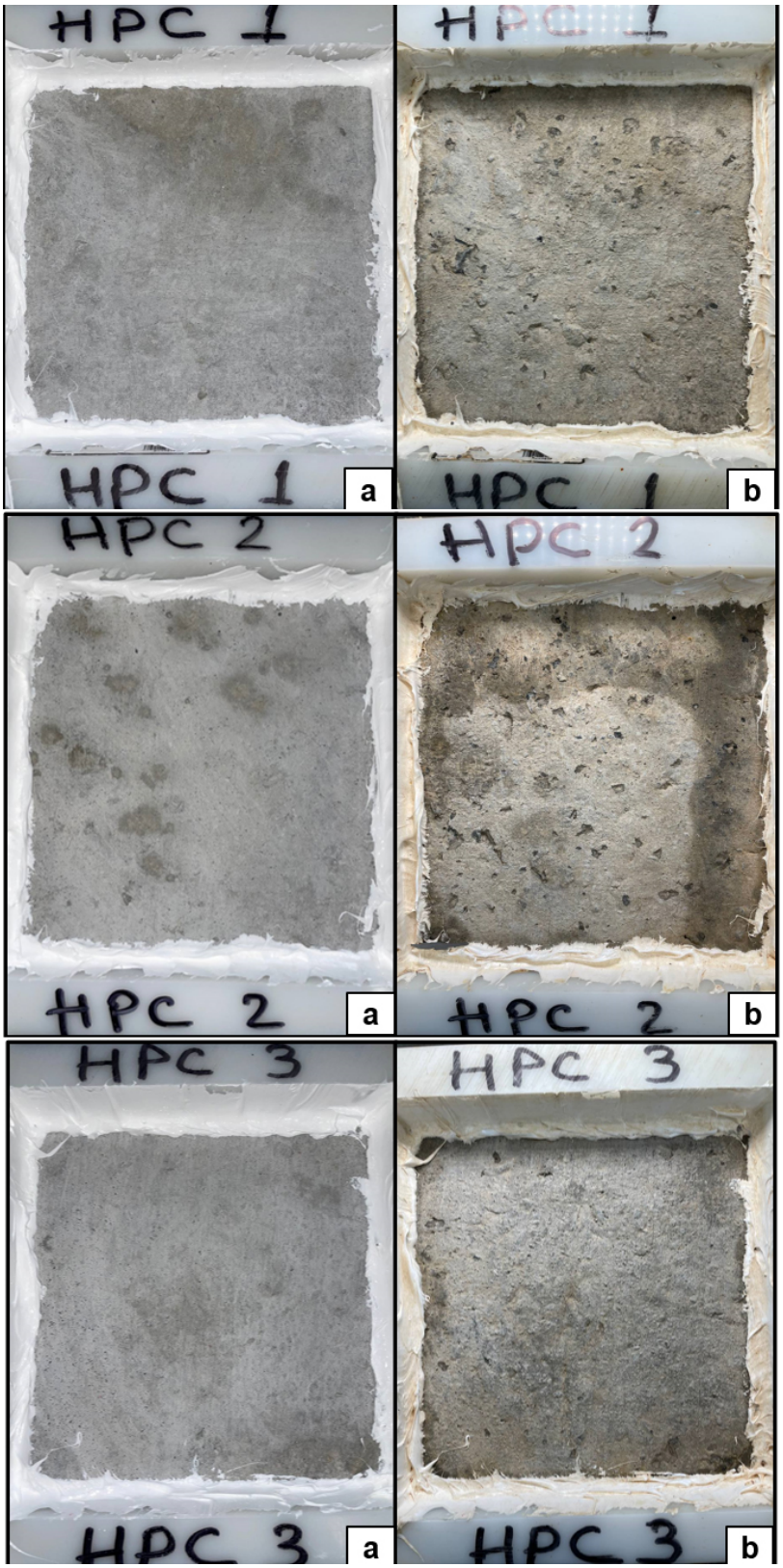

Figure 45. HPC surface at zero and 50 cycles

Photos of SCC P at zero cycles and after exposure to 50 cycles are shown in Figure 46. Based on the picture, all SCC P specimens experienced almost the same scaling level. The rating of scaling for SCC P samples was three. A significant part of the damage was observed during the first 5 to 15 cycles for SCC P. After 15 cycles, the extent of damage increased slightly, and some areas had minor scaling.

Figure 47 shows the HyFRC surface at zero and 50 cycles. The first evaluation was performed based on the dried surface of the specimens after 50 cycles. Based on these observations, the scaling rating for HyFRC samples one, two, and three were 2, 1, and 3, respectively. As seen in this figure, some loose materials are on the surface. The observations showed that these materials could be removed from the surface easily. Therefore, a wire brush was used to brush the surface and remove all the loose parts gently. Figure 48 shows the gentle wire-brushed surface of HyFRC specimens after 50 cycles. As seen, the extent of scaling is more than what it looked like before wire brushing. The scaling rating for HyFRC specimens one, two, and three were 3, 2, and 4, respectively, for the wire-brushed surfaces. The average rating for the HyFRC specimens was three. The smaller maximum size of aggregates and PVA and steel fibers in the HyFRC mixture changed the salt scaling structure compared to the normal concrete systems. The fibers kept the damaged and loose parts after scaling on the surface, while in practice, they can come off easily. Also, the smaller maximum size of aggregates caused smaller areas than the big chips of concrete in SCC P.

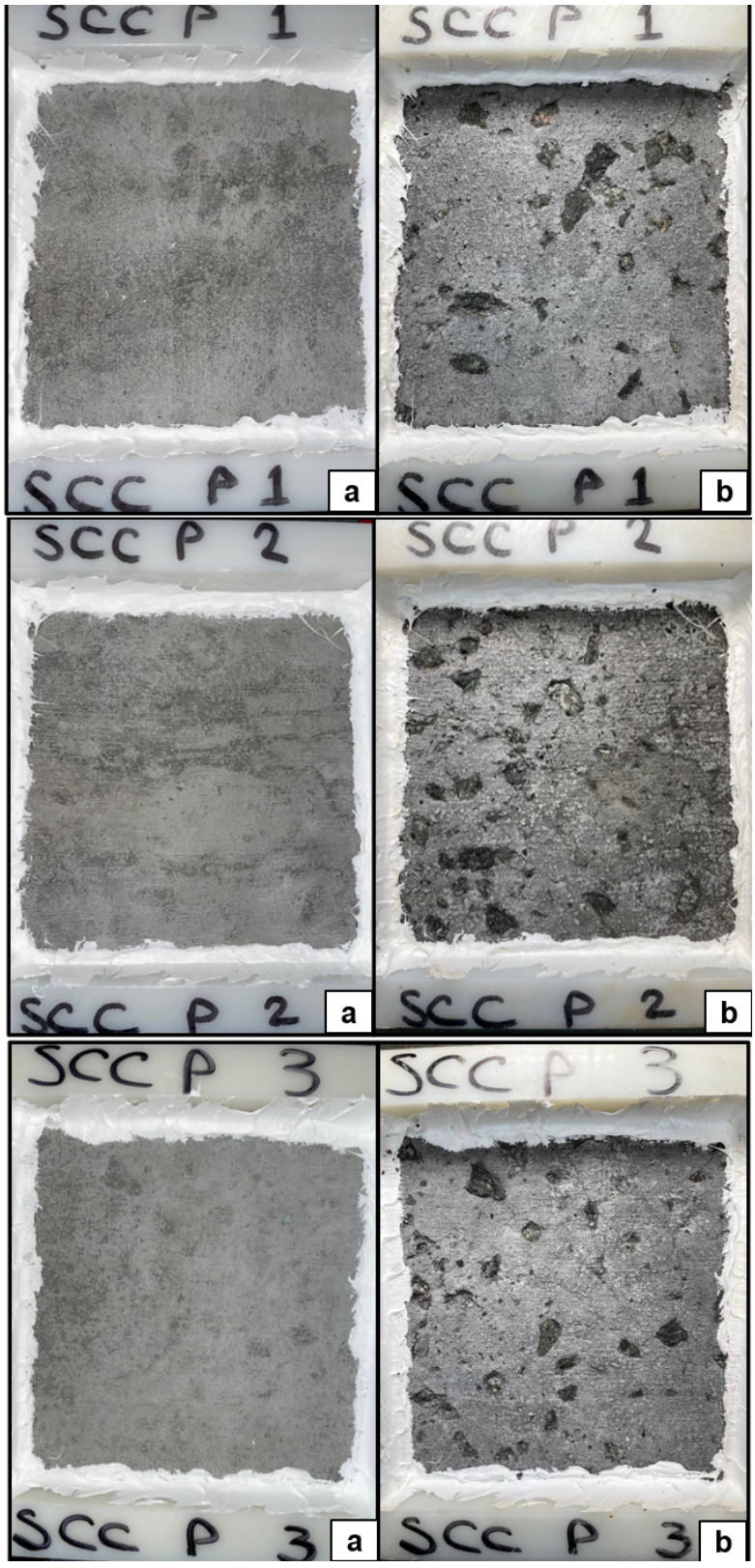

Figure 46. SCC P surface at zero and 50 cycles

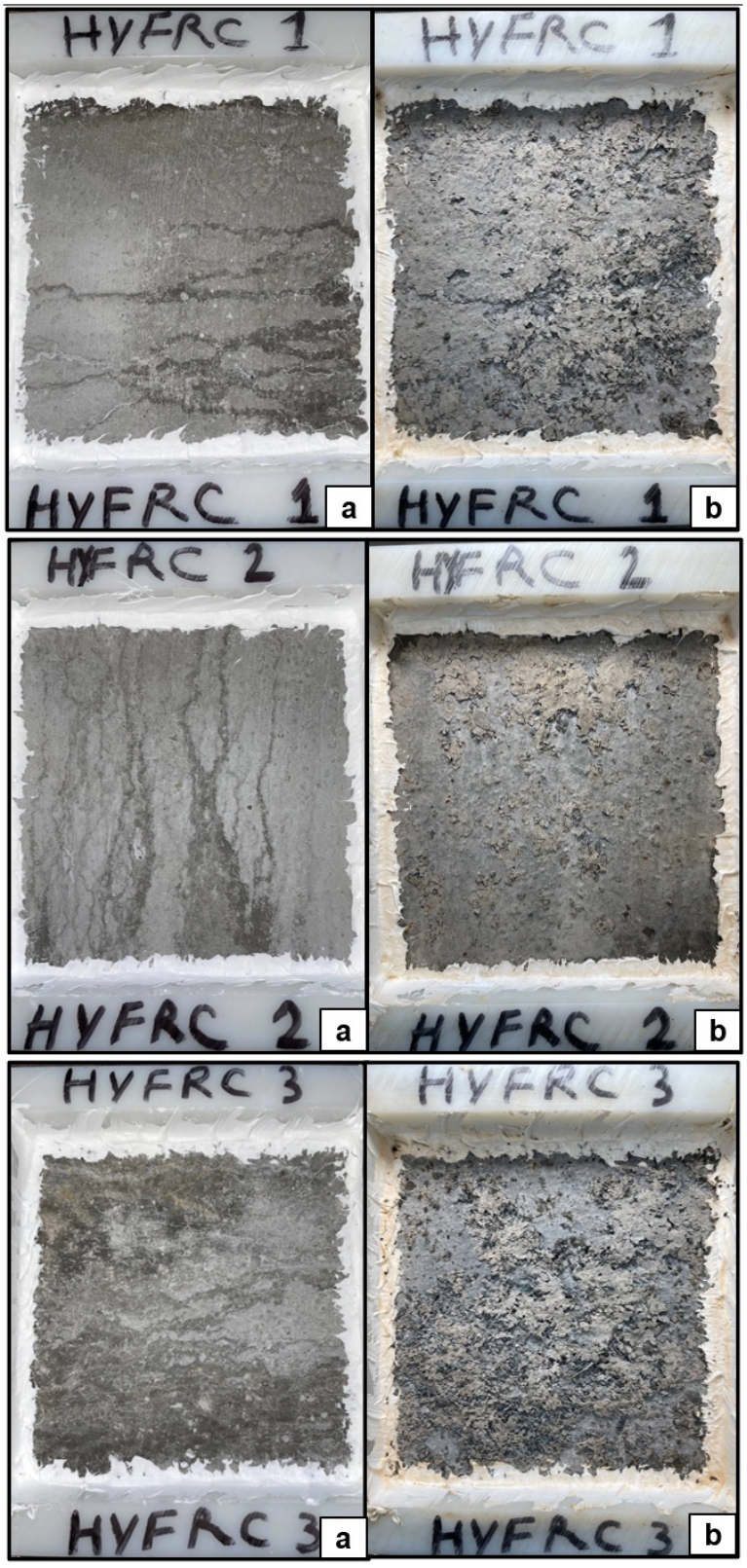

Figure 47. HyFRC surface at zero and 50 cycles

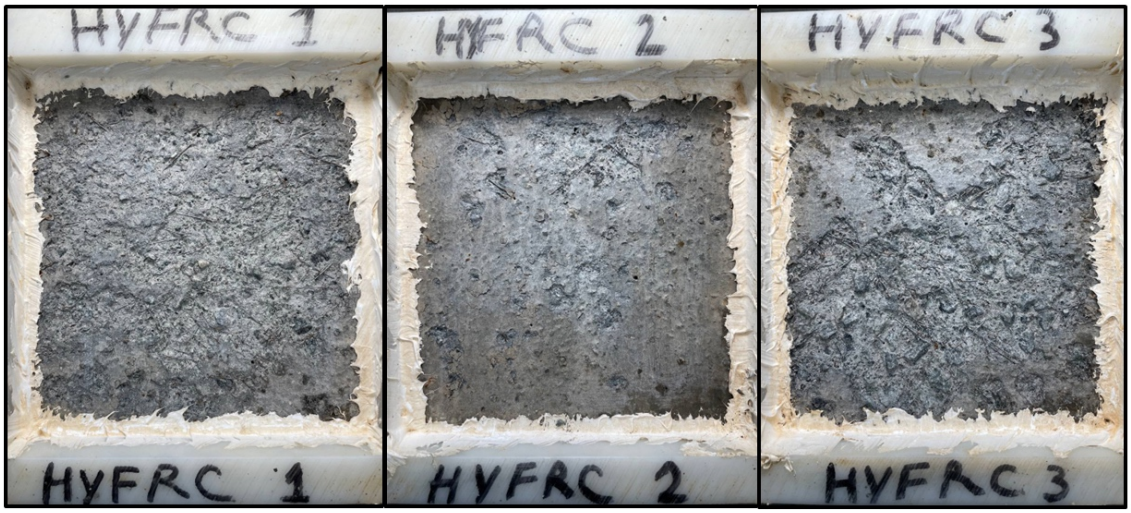

Figure 48. Wire brushed surface of HyFRC specimens after 50 cycles

Figure 49 shows the ECC specimens at zero and after 50 cycles. The scaling rating for ECC specimens one, two, and three were 1, 0, and 1, respectively. There was no coarse aggregate in the ECC mixture design, and only very fine graded sand and SCMs were used in the ECC mixture design. Additionally, two percent of PVA fibers were used. These materials cause a different scaling behavior in ECC compared to the other concrete systems. Signs of delamination were observed on the surface of specimens two and three, which is a different behavior than scaling in normal concrete systems. Figure 50 shows a closer view of the damage in ECC specimen number three. Due to different materials and using fibers in ductile concrete systems, it is difficult to rate the scaling extent in ductile concrete systems based on the criteria of normal concrete systems.

Figure 51 shows UHPC at zero and 50 cycles. No scaling was observed in UHPC samples after 50 cycles. UHPC has a very dense microstructure with low water to cement ratio that provides great resistance against salt scaling and freeze-thaw damage. There were small spots of rust on the surface due to the corrosion of the steel fibers at the top; however, it did not change the surface negatively through 50 cycles of testing. In practice, the finishing methods can be implemented so that no fibers remain exposed and decrease or eliminate the corrosion of steel fibers at the surface.

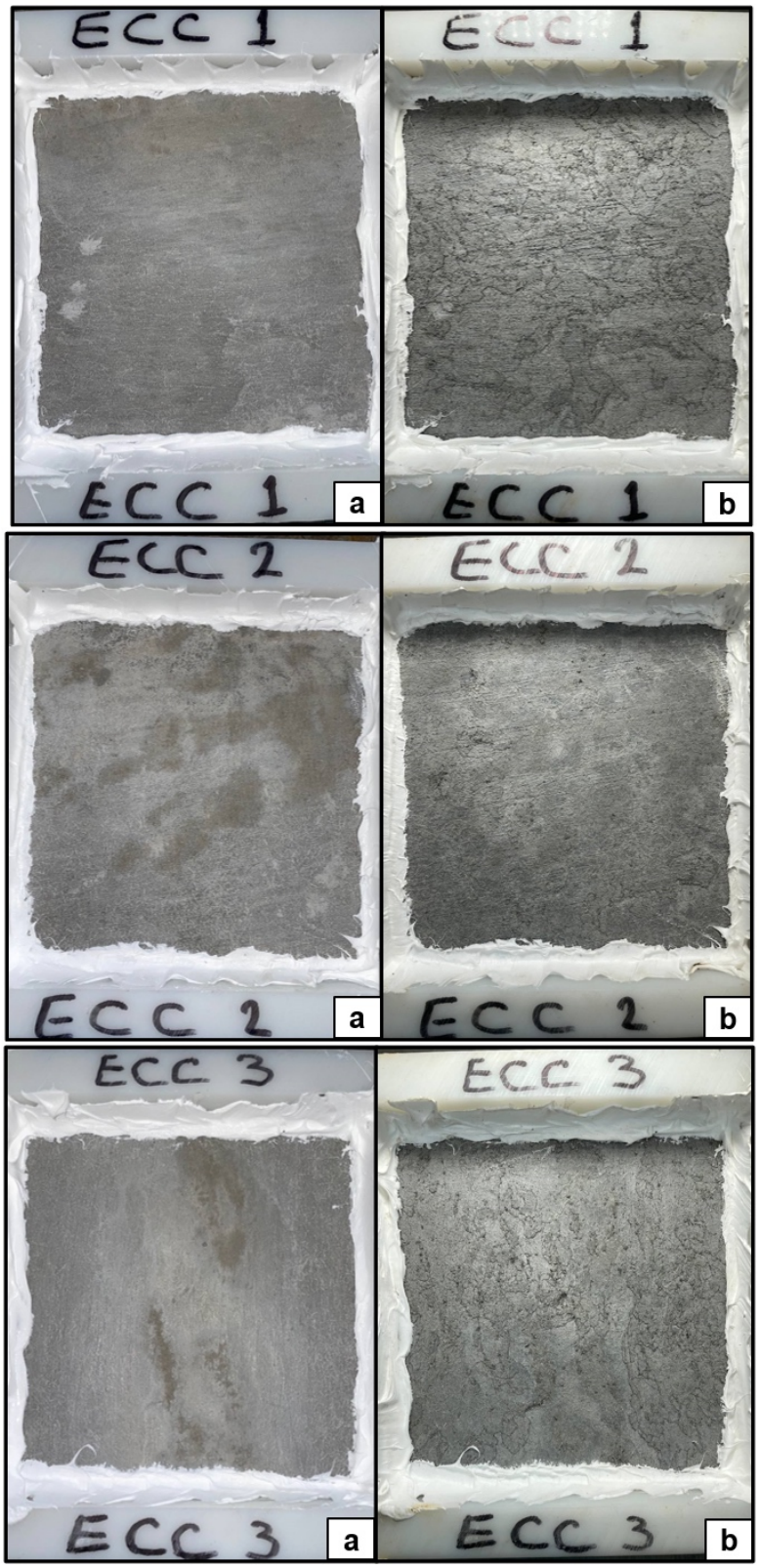

Figure 49. ECC specimens at zero and 50 cycles

Figure 50. Scaling damage in ECC sample three

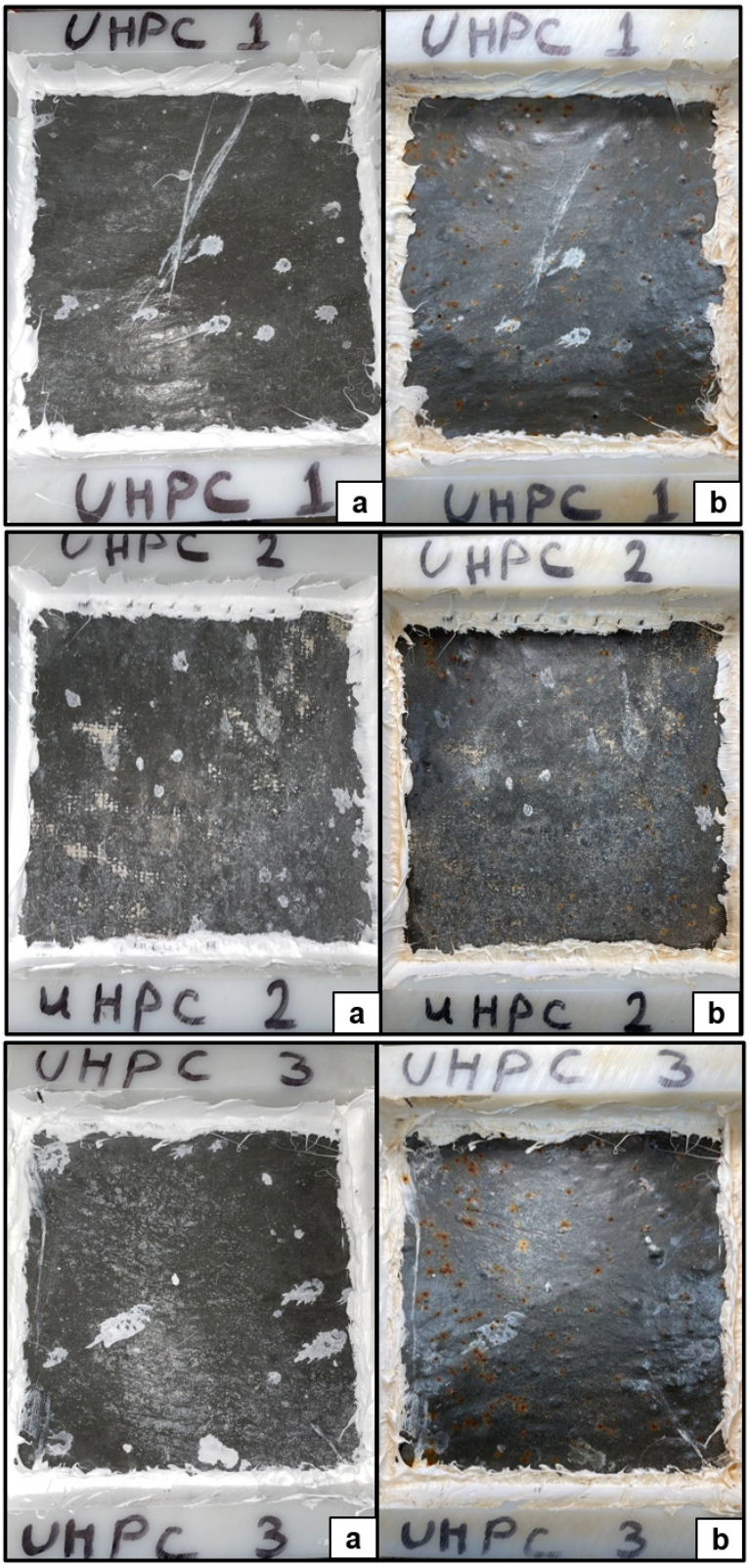

Figure 51. UHPC at zero and 50 cycles

Conclusions

This study investigated the performance of five different concrete systems, including ductile concrete systems, in freezing temperatures using freeze-thaw and salt scaling tests. Comparing the results of the tests, the following conclusions can be derived:

- UHPC performed the best in in salt scaling and freeze-thaw tests compared to the other systems. UHPC specimens showed no signs of degradation in the testing range used according to the ASTM.
- ECC performed better in the freeze-thaw test than HyFRC, HPC, and SCC P systems. The ECC durability factor in the freeze-thaw test was 76.3 compared to 21.3, 25.1, and 3.7 in HyFRC, HPC, and SCC P, respectively.
- ECC and HPC had better salt scaling resistance than HyFRC and SCC P. The average salt scaling rating for ECC and HPC was approximately one compared to the three in HyFRC and SCC P.
- HyFRC and SCC P had similar performance in the salt scaling test; however, HyFRC performed significantly better in the freeze-thaw test than SCC P. The results show how fibers can improve the freeze-thaw resistance of concrete systems.
- Different raw materials and fibers in ductile concrete systems cause different behavior in salt scaling. Rating the scaling in ductile concrete using ASTM C672 can be difficult as no coarse aggregates are used, and fibers help keep loose parts together. A different test method or modifications may be needed to properly rate the salt scaling in ductile concrete systems.

Drying Shrinkage of Ductile Concrete Systems

Introduction

There are several weaknesses in normal concrete, such as low tensile and flexural strengths, poor durability, and high porosity [78]. Many studies have been performed to improve normal concrete deficiencies. High-performance fiber-reinforced cementitious composites (HPFRCCs) are a category of developed materials using different types of supplementary cementitious materials and fibers to improve the microstructure, mechanical properties, and durability of reinforced concrete systems [103].

Drying shrinkage is one of the most critical issues in concrete structures. Concrete shrinkage significantly impacts structural members designed for their service limit state [104,105]. In addition, high shrinkage cause cracks in concrete structures. Cracks affect the performance of concrete and provide a path for the ingress of harmful substances into the concrete, such as chlorides [106]. Therefore, it is crucial to investigate the drying shrinkage of concrete systems to guarantee better durability performance. HPFRCCs are more prone to shrinkage for several reasons. In some HPFRCCs, the coarse aggregates are eliminated or limited to a smaller maximum size of aggregates in lower contents and have more cement compared to normal concrete, which results in more drying shrinkage [107].

Several studies have investigated the shrinkage in HPFRCCs. Hsie et al., 2008 recorded 515 to 595 microstrains at 40 days. The researchers used hybrid polypropylene fibers [108]. Yao et al., 2012 investigated drying shrinkage in ECC. They recorded a drying shrinkage between 1000 to 1300 for different ECC mixture designs [109]. Zhu et al., 2011 recorded 1100 to 1200 microstrain for ECC mixtures with 50 to 60 percent fly ash replacement [110].

This section investigates the drying shrinkage of three types of ductile concrete systems, including ultra-high-performance concrete (UHPC), engineered cementitious composites (ECC), and hybrid fiber-reinforced concrete, as well as two mixtures from the New Jersey Institute of Technology in the same testing conditions.

Methods

A series of compression tests were done on the cementitious mixtures to verify the minimum requirements of the New Jersey Department of Transportation and literature. In the next step, drying shrinkage tests were performed according to ASTM C157 [111]. Specimens were cast in 3 by 3 by 11 ¼ inches molds. Specimens were cured in lime-saturated water at 73 ± 3 °F [23 ± 2 °C] for 28 days. Then the specimens were kept in a room with 50 ± 4% relative humidity for drying shrinkage readings. The comparator readings were done at 4, 7, 14, and 28 days and after 8, 16, and 32 weeks. Figure 52 shows casting concrete in drying shrinkage molds.

Figure 52. Casting SCC P in drying shrinkage molds

The length change in different ages was calculated using the comparator reading number and initial reading as follows:

$$\Delta L_x = \frac{CRD - initial\ CRD}{G} \times 100 \quad (6)$$

Where ΔL_x Is the length change of the specimen at any age, %, *CRD* is the difference between the comparator reading of the specimen and the reference bar at any age, and *G* is the gage length (10 in. [250 mm]).

Results and Discussion

The results are divided into two main sections. The first section summarizes the compressive test results. The second section discussed drying shrinkage results in concrete systems.

Compressive Strength

In order to evaluate the quality of all concrete systems, tests were conducted after 28 days in compression. Also, the unit weight was measured for each system to provide more details for comparing the results. The compressive strength and unit weight of each system are listed in Table 13. The New Jersey Department of Transportation's mixture designs and ductile concrete systems extracted from the literature met the criteria for all concrete systems.

Table 13. Compressive strength and unite weight of all concrete systems

Concrete Type	28 Days Compressive Strength (Psi)	Unit Weight (lbs/Cu.ft)
HPC	8,240	153.3
SCC P	6,960	150.1
SC-HyFRC	5,460	135.2
ECC	6,065	120.6
UHPC	20,855	155

Drying Shrinkage

Figure 53 shows the drying shrinkage results after 32 weeks. According to the results, ECC showed the highest drying shrinkage, and UHPC showed the lowest drying shrinkage among all systems. Based on literature, ECC has a drying shrinkage between 1000 to 1300 mirostrain at 90 days. According to Koh et al., UHPC experiences a small drying shrinkage and high autogenious shrinkage[112]. HyFRC had the highest drying shrinkage after ECC. Based on the study of Hsie et al., 2008, HyFRC had a drying shrinkage of 515 to 595 microstrains at 40 days. However they used hybrid polypropylene fibers [108]. HPC and SCC P showed a higher drying shrinkage than UHPC but less than the other two ductile concrete systems. Generally, ductile concrete systems have more shrinkage than other concrete types. While water to cementitious materials ratio is not relatively low, the high amount of cementitious materials and very fine particles makes them more prone to shrinkage. The UHPC used in this study has a very low water to cement ratio, a dense microstructure, and a high volume of steel fibers that helps to improve the drying shrinkage.

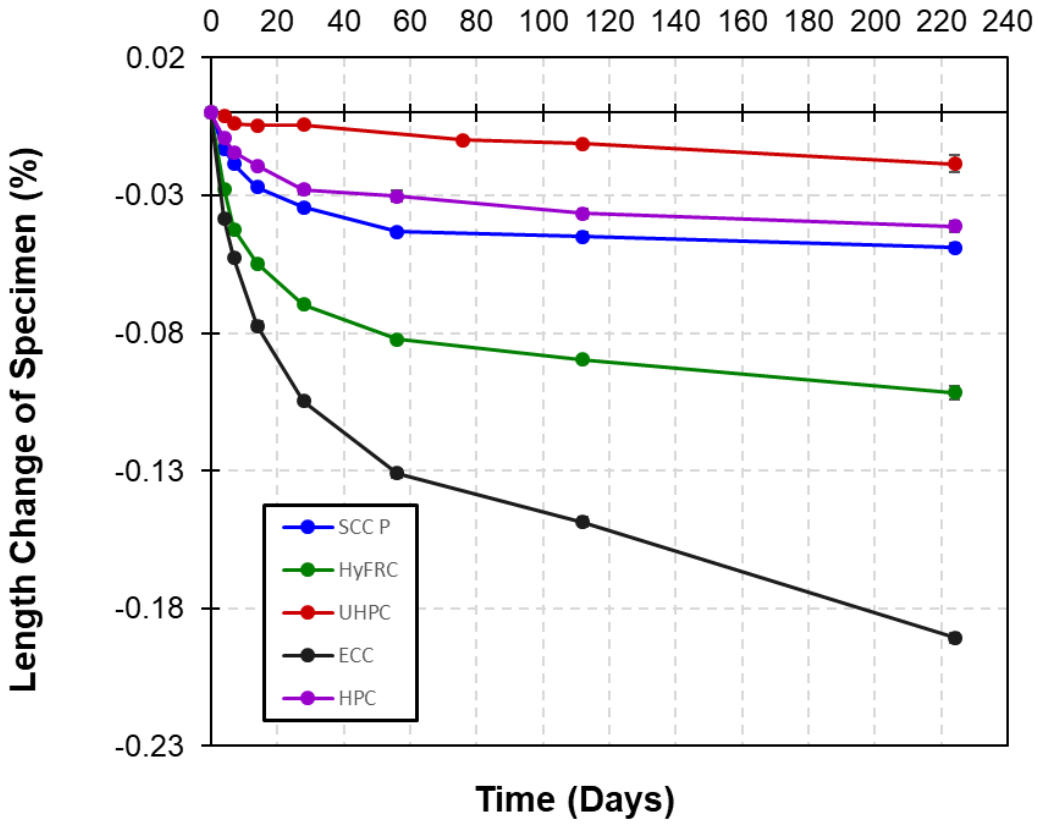

Figure 53. Drying shrinkage results after 32 weeks

Conclusions

The following conclusions can be drawn from the testing presented herein:

- UHPC Ductal has the lowest drying shrinkage compared to other systems due to the very low water to cement ratio
- SCC P and HPC mixtures from NJDOT have lower drying shrinkage compared to ECC and HyFRC
- High cement and fine particles and eliminated or limited content of coarse aggregates make ductile concrete systems more prone to drying shrinkage
- The results for ductile concrete systems are in the same range as the literature

In-Service Performance of UHPC Bridge Deck in Local Climates

Introduction

Ultra-high performance concrete (UHPC) is an advanced class of construction materials that has been one of the focuses as sustainable construction practices. The dense and improved homogeneity composition characteristic of UHPC resulted in ultra-high mechanical and durability performance, such as very high damage tolerance and improved harmful material penetration resistance [113,114]. Therefore, UHPC showed great potential for applications in structural infrastructures. Bridge decks in cold regions is one of the most easily deteriorated structural components since the deck is exposed to harsh environmental conditions as well as traffic loading.

Research has shown that UHPC specimens exhibited greater resistance to de-icing material induced corrosion compared to normal strength concrete specimens [115]. However, the initial damage condition- a critical factor that affects the durability behavior- varies on the structural type. As such, the durability performance of reinforced UHPC bridge deck may differ from the commonly studied reinforced UHPC beams. Furthermore, the regional environmental characteristics, such as periodically applied chloride material and local temperature fluctuations affects the corrosion performance [116]. A systematic study on reinforced UHPC bridge deck under realistic environmental conditions is needed to further investigate the superior durability characteristics and potential application in bridge construction.

This section focuses on examining and quantifying the long-term serviceability characteristics of reinforced normal strength concrete bridge deck and reinforced UHPC bridge deck. The reinforced UHPC deck has a reduced size by re-designing. The computational approach accounts for realistic regional environmental conditions such as seasonally applied de-icing material and temperature change throughout the service life of the bridge deck. Simulation results in terms of cracking patterns, chloride profiles, and structural deterioration after corrosion are explored to quantify the service life performance of reinforced UHPC and reinforced normal strength concrete bridge deck.

Theoretical Background

Concrete or UHPC acts as a barrier against de-icing materials that can cause corrosion in steel reinforcement. Corrosion initiates over time once a critical level concentration (Cl_{crit}) of such materials penetrated through the barrier and reached the steel surface. The chloride penetration process through concrete or UHPC cover can be numerically described as follows [117]:

$$\frac{\partial C_{Cl}}{\partial t} = \nabla \cdot (D_{Cl} \nabla C_{Cl}) \tag{7}$$

where C_{Cl} (% mass of cementitious materials) is the chloride concentration in concrete, D_{Cl} (m^2/s) denote the chloride diffusion coefficient, and t (seconds) is the diffusion time.

For normal strength reinforced concrete, Cl_{crit} is generally adopted as 0.06% of the concrete mass [118,119]. Due to insufficient available data, the critical chloride content of UHPC was assumed to be the same as concrete in this study. $D_{Cl} = D_{ref} \cdot f(T)$, where D_{ref} is the reference diffusion coefficient, $f(T)$ considers the influence of temperature [120]:

$$\mathrm{f(T)} = \exp\left[\frac{U}{R}\left(\frac{1}{T_{ref}} - \frac{1}{T}\right)\right] \tag{8}$$

where *U* is the activation energy (KJ/mol), R is the gas constant (J/mol), T_{ref} is the reference temperature of the measured diffusion coefficient (K), and T is the concrete/UHPC temperature.

Corrosion of the steel can be described as two electrochemical half-cell reactions [121,122]:

$$\mathrm{Fe} \rightarrow \mathrm{Fe^{2+}} + 2\mathrm{e^-} \tag{9}$$

$$\frac{1}{2}\mathrm{O_2} + \mathrm{H_2O} + 2\mathrm{e^-} \rightarrow 2\mathrm{OH^-} \tag{10}$$

As a result, the corrosion current density is [122]:

$$\mathrm{i_{corr}} = \mathrm{i_{Fe}^0}\exp\left(2.303\frac{\phi - \phi_{\mathrm{Fe}}^0}{\beta_{\mathrm{Fe}}}\right) \tag{11}$$

The steel reinforcement bar radius reduction can be calculated as [123]:

$$\sigma(\mathrm{t}) = \frac{\int_0^{\mathrm{t}} \mathrm{i_{corr}(t)dt} \cdot \mathrm{M_s}}{\mathrm{Z_{Fe}} \cdot \mathrm{F} \cdot \rho_{\mathrm{s}}} \tag{12}$$

where $\underline{t}$ is the corrosion duration time (seconds), M_s denote the atomic mass of the iron, Z_{Fe} indicates the valency of anodic reaction, and ρ_s is the steel density.

The corrosion product has greater volume than the original steel and may gradually fill the porous steel/concrete interfacial transition zone. The rust layer expansion thickness $u(t)$ around the reinforcing bar can be obtained as:

$$\mathrm{u(t)} = (\mathrm{n} - 1) \cdot \sigma(\mathrm{t}) \tag{13}$$

where n is rust to steel volume expansion ratio and is assumed to be 3 [124–126].

Methodology

In this study, multiple phenomena were simulated, such as mass (chloride ion) transport

in porous media (concrete or UHPC), electrochemical reaction of steel corrosion process, solid mechanics of structural response before and after corrosion. The bridge deck designs, and modeling set up are introduced in this section.

Bridge Deck Design

Figure 54 shows the cross-section details of a representative reinforced concrete bridge deck. The deck thickness was 250 mm. The top concrete cover was 63 mm while the bottom one was 25 mm. The transverse reinforcement bar diameter was 19 mm. The longitudinal reinforcement was not considered in this study. The reinforced UHPC bridge deck was assumed to have the same design details.

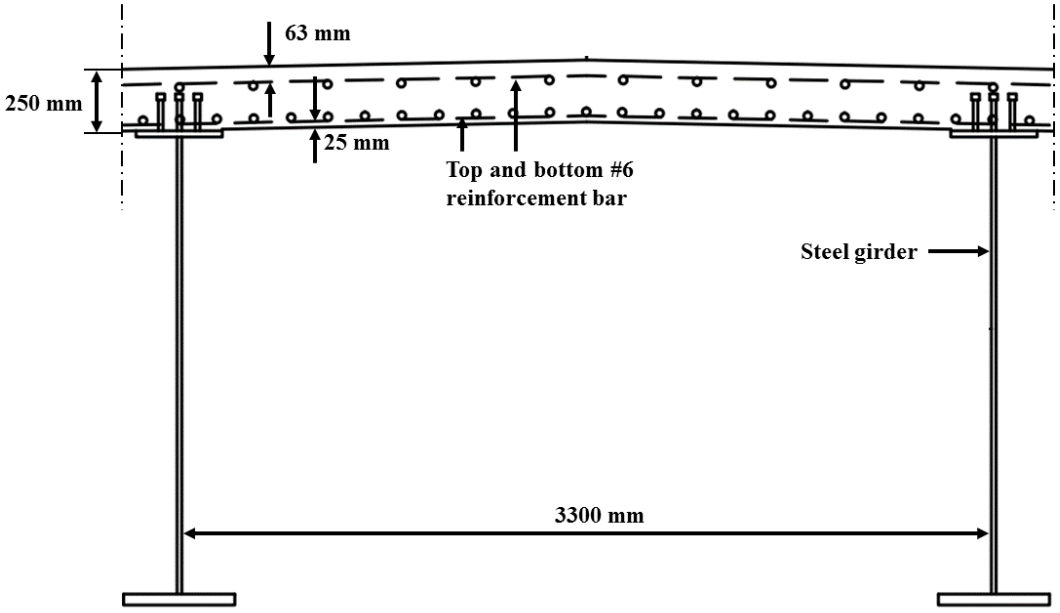

Figure 54. Cross section details of one span reinforced concrete bridge deck

Analysis Procedure

A mechanistic time-dependent modeling framework from the authors' previous work was adopted [126]. First, a simplified concentrated load was applied at the midspan of the bridge deck and then a structural analysis was conducted. The initial damage condition from the structural analysis was adopted and applied to the next step study- chloride penetration analysis. After that, the corrosion simulation was performed, and the corrosion product expansion thickness was calculated. Finally, the corrosion product expansion and traffic load was applied together to assess the structural response. The process was then repeated until the next time step. At each time step, the corrosion area of the steel reinforcement and the cracking status were updated. The time intervals for reinforced concrete and reinforced UHPC bridge deck were four months and five

years, respectively. A larger time step for reinforced UHPC specimen was adopted due to the slower chloride transport in UHPC.

Initial Damage Modeling Deck Design

As shown in Figure 55, half of the bridge deck was simulated due to symmetrical geometry. The nonlinear structural analysis finite element model was built in DIANA FEA Version 10.5 [127]. The reinforcement bar diameter was 19 mm. The plane stress elements had a mesh size of 12.5 mm × 12.5 mm. The horizontal deformation of the left side and vertical deformation of the left bottom corner was constrained. A loading plate was added in the model to avoid unrealistic load concentration at the bridge deck [128].

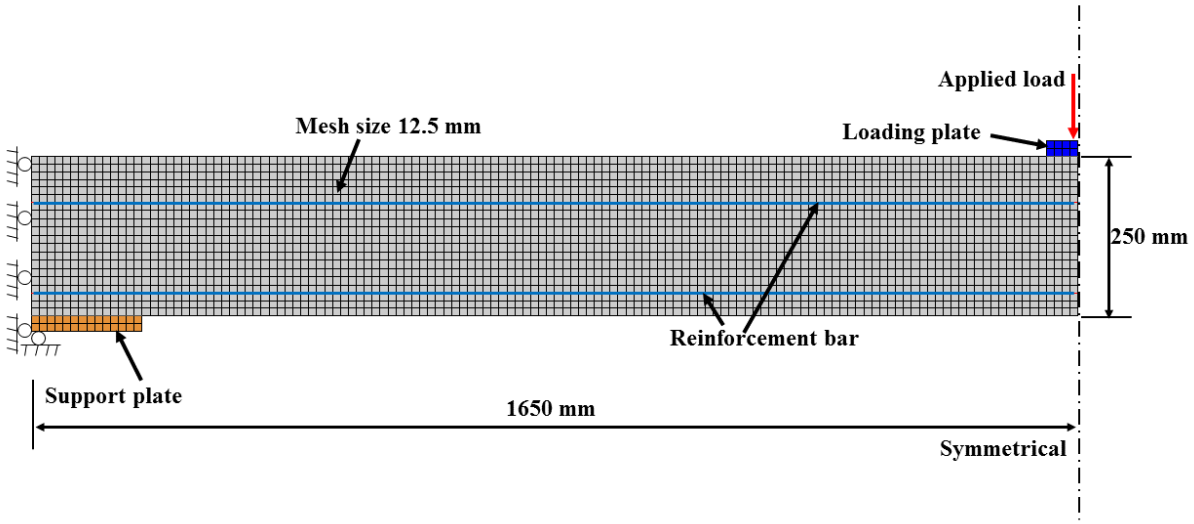

Figure 55. Structural modeling set up

Chloride Transport Modeling in Damaged Concrete and UHPC Materials

The computational platform COMSOL Multiphysics Version 5.4 was used to simulate chloride diffusion and steel corrosion process [129]. Oxygen was assumed to enter from the top and bottom surface of the bridge deck while chloride was assumed to penetrate only from the top surface, where de-icing material was applied. Diffusion coefficient of chloride in the cracked area of concrete was calculated from [130]:

$$D_{Cl\_concrete}(m^2/s)\begin{cases} = 2\times10^{-11}w - 4\times10^{-10}, 30\mu m \le w \le 80\mu m \\ \approx 14\times10^{-10}, w > 80\mu m \end{cases} \quad (14)$$

where w is the crack width (μm). A modified equation of diffusion coefficient in cracked area of UHPC was adopted according to Jin et al. [126]:

$$D_{Cl\_UHPC}(m^2/s)\begin{cases} = 4\times10^{-12}w - 3\times10^{-11}, 10\mu m \le w \le 80\mu m \\ \approx 3\times10^{-10}, w > 80\mu m \end{cases} \quad (15)$$

Boundary Conditions

For bridges in cold regions, the source chloride comes from de-icing materials in snowing seasons. As such, a steady high concentration of chloride ions (0.6% of concrete/UHPC mass) is assumed to be applied at the top surface of the bridge deck for four months in this study [116]. After the snow season, a lower residual surface chloride concentration of 0.2% of concrete/UHPC mass was assumed in the rest of the year [116]. The snowing seasons are normally from December to March in the studied region. Therefore, the month in Table 14 started from December. The temperature effect was considered using Equation (8). The reference temperature of chloride diffusion coefficients was 293 K. The source chloride concentrations and the average temperature of each month from 1999 to 2019 was summarized in Table 14.

Table 14. Source chloride concentrations and temperature

Source chloride (% concrete/UHPC mass)	**0.60**				**0.20**							
Time (month)	12	1	2	3	4	5	6	7	8	9	10	11
Average local temperature (K)	276	272	274	278	284	290	295	298	297	293	287	281

Material Properties and Input Parameters

Representative mechanical properties of UHPC and normal strength concrete such as tensile and compressive strength, modulus of elasticity, fracture energy, strain at crack initiation, strain at onset of softening and Poisson's ratio, were selected from available data in the literature and summarized in Table 15 [131]. Material properties of the reinforcement bar were listed in Table 15 [132].

Table 15. Mechanical properties of UHPC, concrete, and steel

Property	Unit	UHPC	Normal Concrete	Steel
Tensile Strength	MPa	10.5	3.1	-
Strain at crack initiation	%	0.019	0.01	-
Strain at onset of softening	%	0.2	0.01	-
Tensile fracture energy	MPa-mm	11.2	0.144	-
Compressive strength	MPa	180	41.9	-
Compressive fracture energy	MPa-mm	185.8	35.7	-
Young' modulus of elasticity	GPa	53.5	31.2	200
Poisson's ratio	mm/mm	0.2	0.2	0.3
Yield strength	MPa	-	-	455
Ultimate strength	MPa	-	-	675

Mass transport properties and electrochemical reaction parameters are summarized in Table 16. The reference chloride diffusion coefficient was $D_{Cl\_c} = 1.3 \times 10^{-11} m^2/s$, which was two order of magnitude bigger than that of UHPC ($D_{Cl\_UHPC} = 4.5 \times 10^{-13} m^2/s$) [133]. The concrete resistivity ρ was adopted as 159 $\Omega \cdot m$ [16], while ρ was adopted as 23067 $\Omega \cdot m$ for UHPC due to the dense material property of UHPC [133]. The anodic Tafel slopes (β_{Fe_c}, β_{Fe_UHPC}), cathodic Tafel slopes ($\beta_{O_2\_c}$, $\beta_{O_2\_UHPC}$), the equilibrium potentials and exchange current densities were adopted from literature [133]. Other parameters such as surface and initial oxygen contents, oxygen diffusion coefficients are listed in Table 16 [120,133,134].

Table 16. Diffusion and corrosion modeling input parameters.

Parameters	Unit	Values	Description
O_{2_surf}	mol/m3	0.268	Surface oxygen concentration
D_{Cl_c}	m2/s	1.3E-11	Chloride diffusion coefficient of concrete
$D_{O_2\_c}$	m2/s	3.02E-9	Oxygen diffusion coefficient of concrete
ρ_c	Ω·m	159	Electrolyte resistivity of concrete
Cl_{crit}	%	0.06	Critical chloride content of reinforcing bar
$O_{2\_init\_c}$	mol/m3	0.156	Initial oxygen concentration in concrete
D_{Cl_UHPC}	m2/s	4.5E-13	Reference chloride diffusion coefficient of UHPC
$D_{O_2\_UHPC}$	m2/s	4.2E-10	Oxygen diffusion coefficient of UHPC
ρ_{UHPC}	Ω·m	23067	Electrolyte resistivity of UHPC
$O_{2\_init\_UHPC}$	mol/m3	0.061	Initial oxygen concentration in UHPC
β_{Fe_c}	mV/dec	65	Tafel slope of iron oxidation in concrete
$\beta_{O_2\_c}$	mV/dec	-138.6	Tafel slope of oxygen reduction in concrete
β_{Fe_UHPC}	mV/dec	61	Tafel slope of iron oxidation in UHPC
$\beta_{O_2\_UHPC}$	mV/dec	-130.9	Tafel slope of oxygen reduction in UHPC
ϕ_{Fe}^0	mV	-600	Iron oxidation equilibrium potential
$\phi_{O_2}^0$	mV	200	Oxygen reduction equilibrium potential
i_{Fe}^0	A/m2	2.75E-4	Iron oxidation exchange current density
$i_{O_2}^0$	A/m2	6.00E-6	Oxygen reduction exchange current density
U	KJ/mol	44.6	Activation energy of chloride diffusion
R	J/mol	8.3	Gas constant
T_{ref}	K	293.2	Reference temperature

Results and Discussion

Initial Damage Status

The initial depth of the bridge deck was 250 mm, and the corresponding load capacity of the reinforced concrete bridge deck and reinforced UHPC deck were 142.3 kN and 498.1 kN, respectively. However, the excess capacity of the reinforced UHPC deck allowed for the use of less material to achieve the same strength. After re-design, the reinforced UHPC deck depth was reduced to 125 mm. The UHPC cover depth at the top surface was also reduced from 63 mm to 25 mm. The updated load capacity of reinforced UHPC deck became 145.1 kN, which was in the same level as the reinforced

concrete deck. The load deformation relationships of the new design are shown in Figure 56.

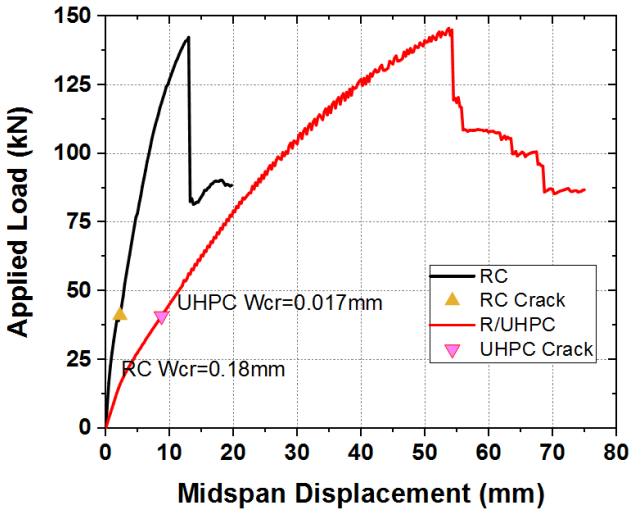

Figure 56. Load-deformation relationships before corrosion

According to ACI 224 R, the allowable crack width for the tensile face of reinforced concrete structure that exposed to de-icing chemical is 0.18 mm [135]. Therefore, the load in the service load range at which the crack width was 0.18 mm was selected as the initial condition for the reinforced concrete bridge deck. The initial crack width in the reinforced UHPC bridge deck at the same loading level was 0.017 mm, which was one order of magnitude smaller than that of reinforced concrete bridge deck.

Chloride Profiles

Figure 57 shows the chloride contour of reinforced concrete bridge deck and reinforced UHPC bridge deck after 30 years of chloride exposure. As shown in Figure 57, the reinforced concrete bridge deck experienced much faster chloride ingression at the same initial load condition. Moreover, 100% of the steel bar in the reinforced concrete bridge deck was corroded while only 13.3% of the steel bar in the reinforced UHPC bridge deck had corrosion even though the concrete cover was more than two times thicker than UHPC cover. Simulation results also show that the corrosion initiation of the reinforcing bar in the reinforced concrete and reinforced UHPC bridge deck occurred after 1 year and 25 years, respectively. The simulation results in terms of chloride profiles confirmed the excellent corrosion resistance of the UHPC material.

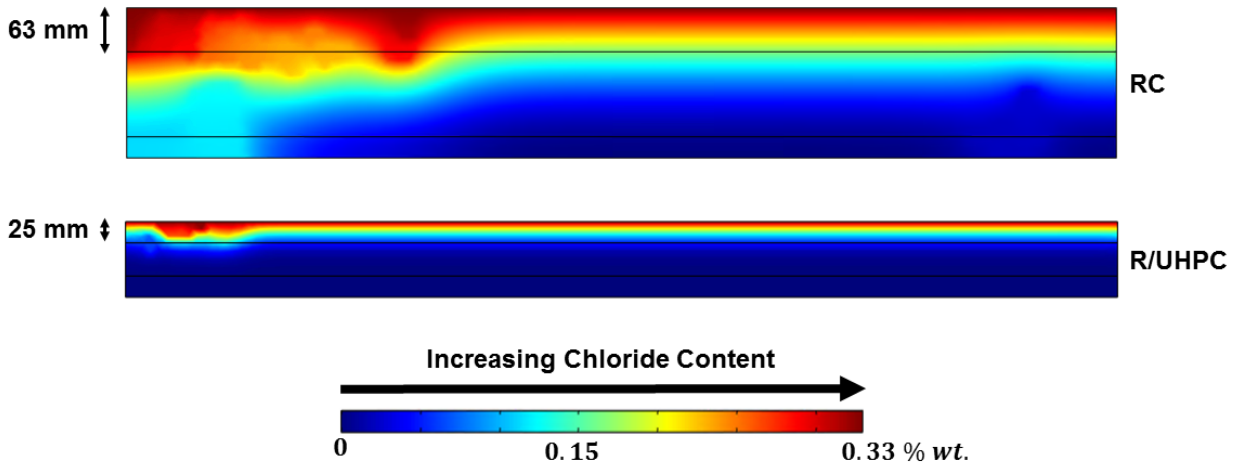

Figure 57. Chloride contour after 30 years of de-icing exposure. The concrete cover was 63 mm, UHPC cover was 25 mm

Deterioration of the Bridge Deck

Figure 58 shows the reference principal tensile strain contours of UHPC and normal strength concrete, which indicates the damage level of the materials. For example, the principal tensile strain level in the range 1 to 2 indicates that the concrete/UHPC were sound because the materials were still in elastic range. Micro cracking in UHPC developed in the range 2 to 3 and was defined as fair condition. Poor condition and severe damage can be assumed in UHPC when the principal tensile strain was in the range 3 to 4, and 4 to 5, respectively. In contrast, normal strength concrete was assumed to experience fair damage from 2 to 3 while 3 to 4 and 4 to 5 were assumed to be in poor and severe damage, respectively.

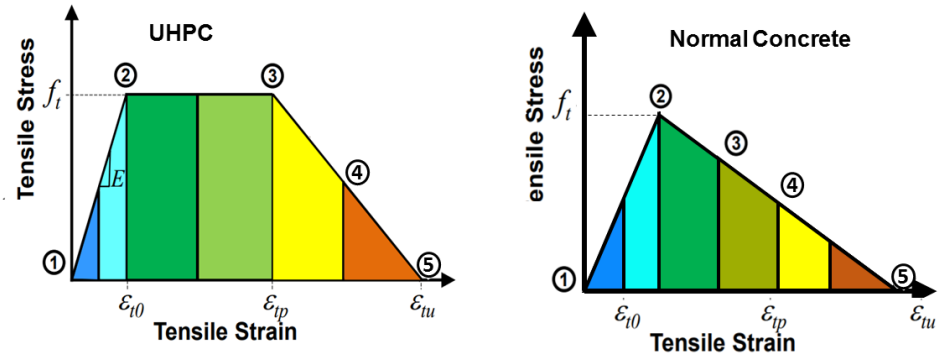

Figure 58. Principal tensile strain contour of UHPC and normal strength concrete

As shown in Figure 59, the normal strength reinforced concrete bridge deck had significant cracking propagation after 30 years of chloride exposure while the reinforced

UHPC bridge deck had relatively low cracking development. In addition, the steel reinforcement bar in the reinforced concrete bridge deck had a maximum cross section loss of 12% after 29 years of corrosion development. In contrast, the steel reinforcement bar cross section loss in the reinforced UHPC bridge deck was only 2.6% after 55 years of corrosion.

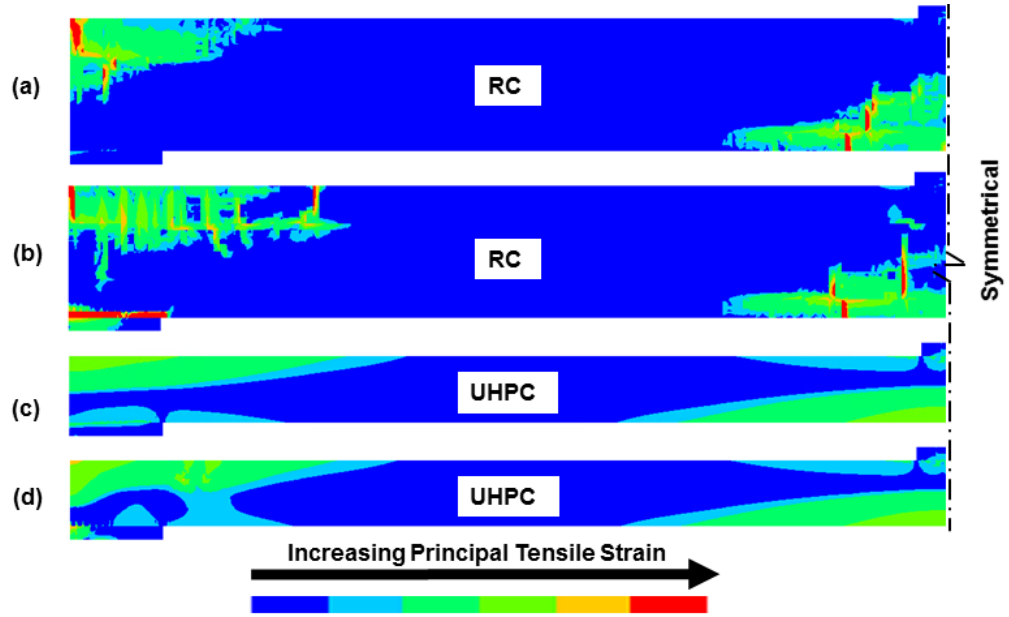

Figure 59. Cracking patterns of reinforced concrete and reinforced UHPC deck (a) and (c) before corrosion, (b) after 29 years of corrosion, (d) after 55 years of corrosion

The delamination rating can be calculated as follows [136]:

$$\text{Delamination rating} = \%\ \text{area in severe} \cdot 0 + \%\ \text{area in poor} \cdot 40 + \%\ \text{area in fair} \cdot 70 + \%\ \text{area in sound} \cdot 100 \quad (16)$$

where 0 indicates worst condition while 100 indicates best condition.

The reinforced concrete bridge deck had a delamination rating of 79.1% after 30 years while the delamination rating of the reinforced UHPC bridge deck was 93.3% after 80 years of chloride exposure. The much higher delamination rating of the reinforced UHPC bridge deck even after a much longer harmful material exposure time showed the superior long-term service life performance of UHPC material. This behavior is ascribed to the combined effect of the dense material property and the ductile material characteristics of UHPC.

Summary

The results and discussion section introduced the comparison study results of the reinforced concrete bridge deck and reinforced UHPC bridge deck in terms of initial damage conditions, chloride profiles, and structural deteriorations. Even though the re-

designed reinforced UHPC bridge deck had a 50% smaller cross section and same amount of reinforcing area compared to the reinforced concrete bridge deck, the reinforced UHPC bridge deck showed significantly slower chloride penetration, which indicated a slower corrosion initiation in the steel reinforcement. Furthermore, the damage propagation, which was measured through delamination rating, was 14.2% less in UHPC material in a much longer time of 80 years of chloride exposure compared to that of normal strength concrete in 30 years of chloride exposure. The excellent long-term durability performance indicates that the required repairment of the reinforced bridge deck would be less. Moreover, the smaller bridge deck cross section could compensate for part of the higher initial construction cost of the reinforced UHPC bridge deck.

Conclusions

This study presents a comparison analysis of reinforced concrete and reinforced UHPC bridge decks through two-dimensional time-dependent multi-physic numerical simulations. Representative local temperature fluctuations and de-icing materials were implemented.

The reinforced UHPC bridge deck exhibited excellent resistance to chloride ingress and corrosion propagation. The simulation results confirmed the great long-term durability performance of reinforced UHPC structures. The reinforced UHPC bridge deck experienced significantly slower structural deterioration under the same traffic loading and environmental conditions. The UHPC material remained intact compared to that normal strength concrete at the end of the selected analysis time duration.

This study provides insights on the further application of UHPC material in structural design by demonstrating the potential of reducing the maintenance cost and helping to achieve a significantly more sustainable infrastructure.

Life-Cycle Cost Analysis of Bridge Decks with Different Technologies

Framework of LCCA

Life cycle cost analysis (LCCA) is a systematic tool used to assess the total cost of infrastructure with flexibility and comprehensiveness. LCCA can be used for bridge decks to calculate all significant and relevant costs over its total life cycle, as shown in Figure 60. The LCCA results can be used to compare the design alternatives of bridge decks with different materials that will fulfill the service life at the lowest overall cost while with satisfied service level and performance. Based on different life-cycle activities of bridge deck, the total cost during its lifetime can be expressed using Equation (17)[137]. It is noted that only agency cost is considered in LCCA due to high uncertainty and large variation of user cost.

$$LCC_{NPV} = C_{ic} + \sum_{i=1}^{n_{ri}} \frac{C_{ri}t_i}{(1+r)^{t_i}} + \sum_{k=1}^{n_{mt}} \frac{C_{mt}t_k}{(1+r)^{t_k}} - \frac{R_v}{(1+r)^T} \quad (17)$$

where, LCC_{NPV} is the total cost represented by Net Present Value (NPV); r is discount rate; C_{ic}, C_{ri}, C_{mt}, , C_d and R_v are costs of initial construction, routine inspection, maintenance, and residual value, respectively; The residual value R_v of the bridge is ascertained by estimating all future costs of the bridge deck till the end of its life and then discounting those costs back to the end of the planning horizon. This cost is further discounted to the net present value in year 0 and subtracted from the life cycle cost. n_{ri} and n_{mt} are the number of corresponding activities during the analysis period; T is analysis period.

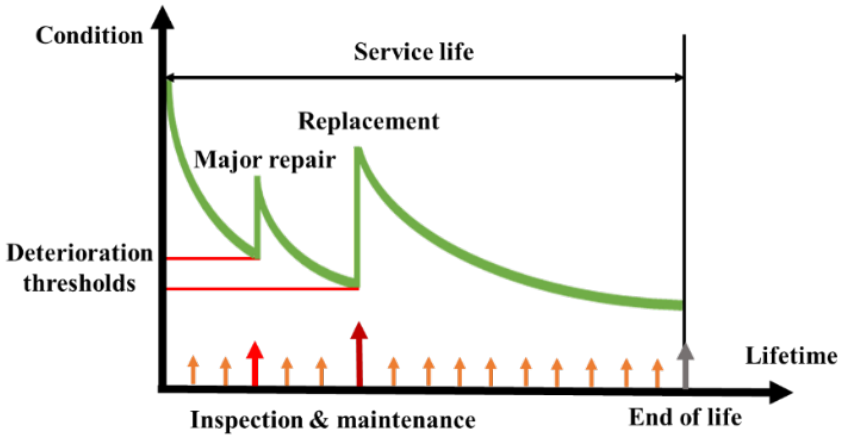

Figure 60. Bridge deck life-cycle with different treatments

The bridge deck made with ultra-high performance concrete usually require high initial cost but need less frequent maintenance and rehabilitation activities and have longer service life, as compared to the bride deck made with conventional concrete with

the shorter lifespan. The equivalent annual cost can be used as an indicator for comparison of bridge decks with different service life. The equivalent annual cost is calculated using Equation 18 [138].

$$LCC_{EAC} = LCC_{NPV} \frac{r}{1-(1+r)^{-T}} \quad (18)$$

Where, LCC_{EAC} is the equivalent annual cost; LCC_{NPV} is the net present value; T is analysis period; and r is the discount rate.

LCCA Inputs and Assumptions

Based on the data from Wisc. DOT and literature, the costs of initial construction, concrete overlay and typical minor maintenance for reinforced concrete (RC) bridge deck are collected for LCCA inputs. Table 17 summarizes the cost data for different construction and maintenance activities of reinforced concrete bridge deck. The initial construction and replacement costs of bridge deck are assumed the same at \$525/m^2, which is the average cost from different bridges. The maintenance types include major maintenance such as deck overlay, and minor maintenance such as patching and crack seal. The maintenance costs are \$40/m^2 to \$110/m^2 for major maintenance and \$4/m^2 to \$25/m^2 for minor maintenance, which varies depending on maintenance activity and application area. The cost of routine inspection is \$2/m^2 at each time obtained from the literature[139]. The routine inspection consists of observations and measurements needed to determine physical and functional condition of bridges.

Table 17. Cost Data for Traditional RC Bridge Decks

Subjects	Cost	References
New deck/Deck replacement	\$525/m^2	
Major maintenance - concrete overlay	\$40~\$110/m^2	Data from Wisc. DOT
Minor Maintenance	\$4~\$25/m^2	
Routine inspection	\$2/m^2	(Cusson, Lounis, & Daigle, 2010)

As for the bridge deck made with UHPC, the related literature has found that the material cost of UHPC is about 4~8 times that of conventional concrete [140,141].

However, the thickness of UHPC deck can be half of the one of conventional concrete deck owing to the advantages of high strength and reliable durability for UHPC[142]. Therefore, the initial unit cost of UHPC bridge deck is set as $1050/m^2 ~ $2100/m^2, which is about 2 to 4 times than that of reinforced concrete. The costs of minor maintenance and routine inspection for UHPC bridge deck are assumed as the same as those of RC bridge deck.

Based on the practice obtained from Wisc. DOT, the maintenance schedules for reinforced concrete bridge deck are summarized, as shown in Table 18. The maintenance interval is the time gap between two consecutive applications of maintenance treatments, which can be 2~4 years for minor maintenance but 20~30 years for major maintenance (deck overlay). Routine inspection is regularly applied every 2 years after initial construction. On the other hand, deck replacement usually happens at 40~50 years after initial construction. Considering the long-lasting life of bridge deck, the analysis period of 100 years is used in LCCA.

Table 18. Bridge Maintenance Schedules for Traditional RC Bridge Decks

Preservation activities	Maintenance Interval, years
Routine inspection	2
Minor maintenance	2~4
Major maintenance - overlay	20~30
Deck replacement	40~50

The performance of RC and UHPC bridge decks are compared using numerical modeling, in which the corrosion process of bridge decks against de-icing materials at the specific loading and climate conditions were simulated based on finite element method (FEM). First, a simplified concentrated load was applied at the mid-span of the bridge deck and then a structural analysis was conducted. The initial damage condition from the structural analysis was adopted and applied to the next step study- chloride penetration analysis. After that, the corrosion simulation was performed, and the corrosion product expansion thickness was calculated. At last, the corrosion product expansion and traffic load was applied together to assess the structural response. The process then be repented until the next time step. At each time step, the corrosion area of the steel reinforcement and the cracking status were updated. The time interval for

reinforced concrete and reinforced UHPC bridge deck were four months and five years, respectively. A larger time step for reinforced UHPC specimen was adopted due to the slower chloride transport in UHPC.

The initial depth of the bridge deck was 250 mm, and the corresponding load capacity of the RC bridge deck and reinforced UHPC deck were 142.3kN and 498.1kN, respectively. However, such reinforced UHPC deck was overdesigned in terms of loading capacity. After re-design, the reinforced UHPC deck depth was reduced to 125 mm that cause the same load capacity between RC and UHPC decks.

According to the simulated corrosion results, the steel reinforcement bar in the RC bridge deck shows maximum cross section loss of 12% after 29 years of corrosion simulation, while the one for the UHPC is only 2.6% after 55 years of corrosion simulation. The reinforced UHPC bridge deck presents negligible damage, while the reinforced concrete bridge deck shows apparent cracks under the same traffic loading.

The main simulation results of crack area density are shown in Figure 61. The crack density was calculated as the total area (length x width) of cracks over the measured area, which was the elevation section area. The crack length increases with the time after chloride exposure. The crack width is 0.05 mm for the RC bridge deck and 0.01 mm for the UHPC bridge deck. A smaller crack width was used for UHPC because of the micro cracking characteristics of the UHPC material. The crack density was found much smaller in the UHPC bridge deck as compared to the RC bridge deck.

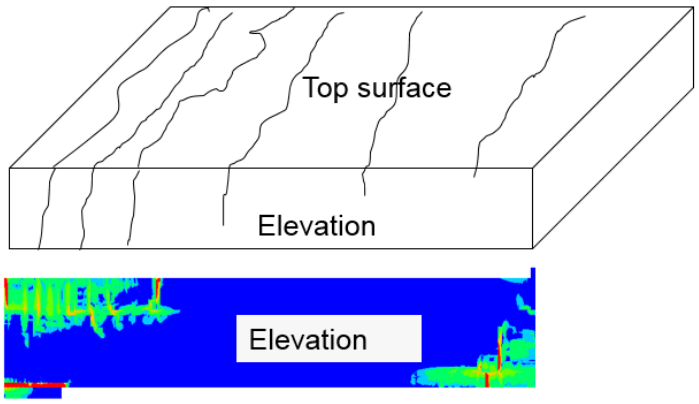

(a)

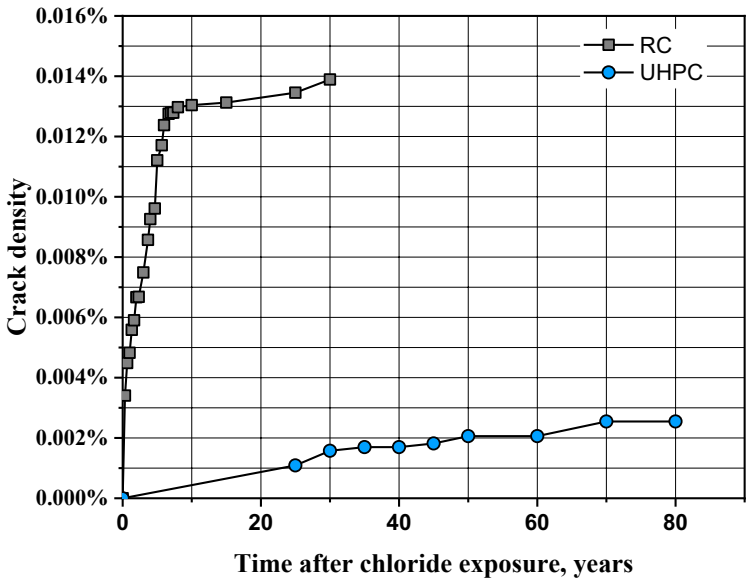

(b)

Figure 61. (a) Illustration of crack simulation results; and (b) Crack area density over time after chloride exposure for RC and UHPC bridge decks

Based on simulation results show in Figure 61, the crack development on the UHPC deck shows a very slow trend under mechanical and environmental loading that will not cause major failure of bridge deck. Therefore, it is assumed that no deck overlay and replacement is needed for the UHPC bridge deck during 100-year service life with less frequent maintenance. The service life of UHPC bridge deck is assumed to be 150 years based on fatigue test results of reinforced concrete (RC) and UHPC[143–145] and the

outstanding mechanical property of UHPC[146]. The interval of minor maintenance for UHPC bridge deck is assumed as 2~6 years in the LCCA.

LCCA Results and Discussion

LCCA is conducted considering the variation of different cost items and maintenance intervals for two different bride decks.

Table 19 lists the analysis scenarios using different maintenance schedules for bridge decks made with reinforced concrete (RC) and UHPC. The discount rate of 0.5% is applied for LCCA based on the 30-year real discount rate presented by Federal Office of Management and Budget (OMB)[147]. The salvage values of RC and UHPC bridge decks are included by considering the residual value before reaching the service life of bridge deck at the end of analysis period.

Table 19. Analysis Scenarios in LCCA

Scenarios	Cost, unit: $/lane_mile			Activity Intervals, year		
	Initial	Overlay	Minor maintenance	Minor maintenance	Overlay	Replacement
RC-1		396K	75K	2	20	40
RC-2		396K	75K	2	30	50
RC-3	2,772K	396K	75K	4	20	40
RC-4		211K	20K	2	20	40
RC-5		581K	130K	2	20	40
UHPC-1	5,544K		75K	2		
UHPC-2	11,088K		75K	2		
UHPC-3	8,316K	-	75K	4	-	-
UHPC-4	8,316K		75K	6		
UHPC-5	8,316K		37K	6		

The life-cycle costs for different analysis scenarios are shown in Figure 62. As for the RC bridge deck, the life-cycle cost can be apparently influenced by either changing the maintenance frequency or the costs of overlay and minor maintenance. When taking the average costs of major and minor maintenance for analysis scenarios of RC-1, RC-

2 and RC-3, the less frequent overlay and replacement (for RC-2) can result in about 6%~30% cost reduction over 100-year service life, compared with baseline scenario of RC-1. Also, the less frequent minor maintenance (4-year interval for RC-3 compared with 2 years for RC-1) can provide about 10%~20% reduction in the life-cycle cost. On the other hand, the analysis results of RC-4 and RC-5 represent the boundaries of life-cycle costs over 100-year service life that generated by the lower and upper limit values of major and minor maintenance costs, respectively.

However, as for the UHPC bridge deck, the life-cycle cost is mainly influenced by its initial construction cost. If compared with the UHPC bridge deck with initial cost of $11,088,000 per lane mile, all analysis scenarios for RC bridge deck remain as cost-effective options during the 100-year analysis period. When the initial cost of UHPC bridge deck is $8316,000 per lane mile, UHPC may become the cost-effective option after 80 years of service as compared to the analysis scenarios of RC-1, RC-3 and RC-5. If the initial cost can be further reduced to $5544,000 per lane mile for UHPC bridge deck, the break point of life-cycle cost can be changed to around 40 years, compared with the analysis scenarios of RC-1 and RC-5.

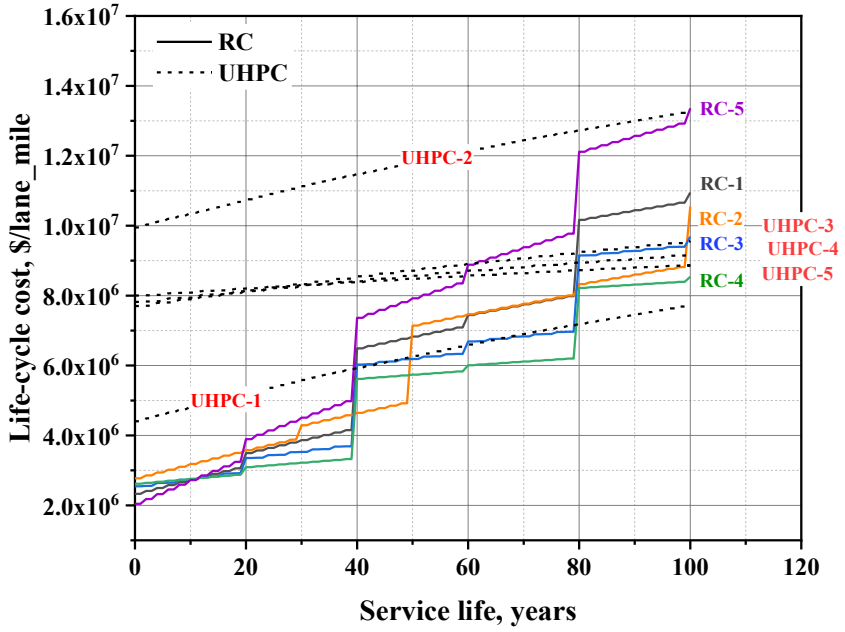

Figure 62. Effect of analysis scenarios on life-cycle cost over 100 years

Figure 63 presents the effect of discount rate on life-cycle cost of RC and UHPC bridge decks. In this case, the calculated total life-cycle costs in 100-year service life for analysis scenarios of RC-1, UHPC-1, UHPC-2, and UHPC-3 are compared using different discount rates. It can be found that the total life-cycle cost for RC-1 shows

remarkable reduction with the increase of discount rate from 0 to 2.5%. This indicates that although the RC bridge deck may need more frequent maintenance during its service life, these maintenance costs is significantly affected by the accumulated discount.

As for the UHPC bridge deck, the reduction of total life-cycle cost in 100-year service life is not significantly affected by the discount rate since the majority of life-cycle cost for the UHPC bridge deck is contributed by initial construction cost. The UHPC bridge decks for analysis scenarios of UHPC-1 and UHPC-3 will be the cost-effective options if the discount rate is below 1.75% or 0.9%, respectively. However, the analysis scenario of UHPC-2 is not cost-effective due to its high initial cost for the analysis period of 100 years.

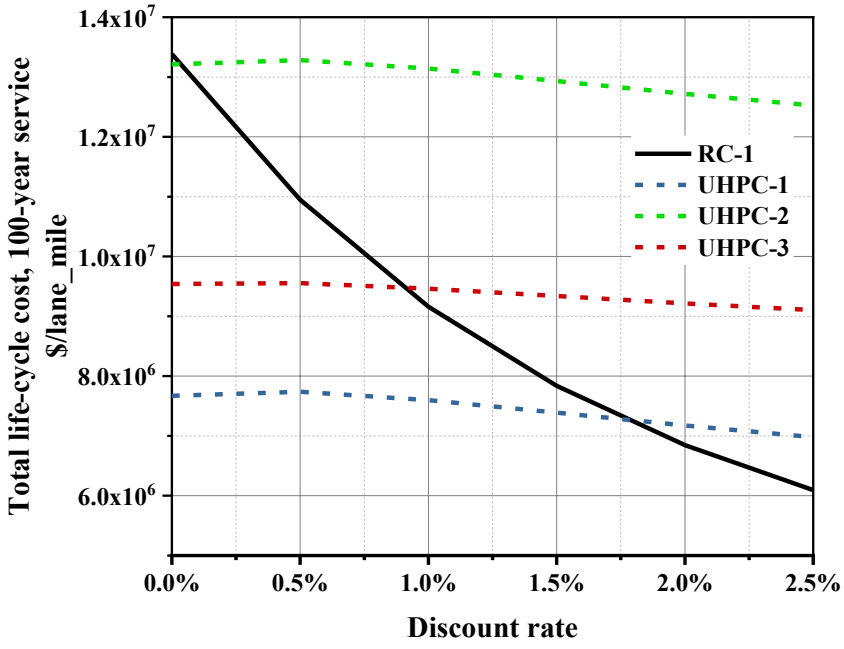

Figure 63. Effect of discount rate on life-cycle cost of RC and UHPC bridge decks

With the discount rate of 0.5%, the equivalent annual costs (EUACs) of bridge decks made with RC and UHPC are calculated, as shown in Figure 64. Given the service life of RC bridge deck is 50 years, its equivalent annual cost is calculated based on the analysis scenario of RC-1, where minor maintenance and overlay are applied every 2 and 30 years, respectively. As indicated in Figure 64, the EUAC of RC bridge deck with 50-year service life is $167,208 per lane mile. Compared with this value, the EUAC of UHPC bridge deck will be lower with 116-year service life, in which the highest

initial cost of UHPC bridge deck is applied ($11,088,000 per lane mile). However, if the initial cost of UHPC bridge deck becomes lower, the break point of EUAC will be shifted to around 70 years (for initial cost of $8,316,000 per lane mile), and less than 50 years (for initial cost of $5,544,000 per lane mile), indicating the increased economic potential of UHPC.

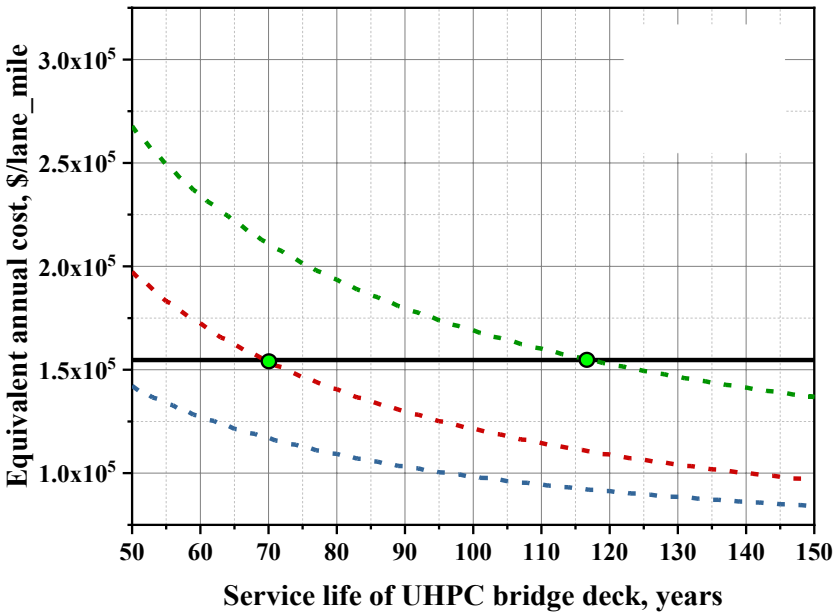

Figure 64. Comparison of equivalent annual cost of bridge decks with different service life of UHPC bridge deck (50-year service life for RC bridge and rate of 0.5%)

Although the construction cost of UHPC is much more expensive than that of conventional reinforced concrete, price reduction of UHPC is expected with improved mixing formula and wider application in the future. The construction cost of UHPC is highly influenced by placement technology[148,149]. On the other hand, considering high durability and corrosion resistance of UHPC, mitigation of deck overlay and replacement can save large amounts of resources and energy consumption in addition to costs, and reduce greenhouse gas emission for sustainability. In addition, less maintenance and repair of UHPC bridge deck brings benefit of reducing work zones and saving user costs. Therefore, the UHPC bridge deck shows high economic potential, although the life-cycle cost varies significantly depending on construction cost.

CONCLUSIONS AND RECOMMENDATIONS

Summary

This research program evaluated the behavior of new and emerging reinforced concrete materials for transportation infrastructure. A series of experimental and numerical research activities were carried out to identify the durability and in-service performance of these systems. A literature review was completed to identify concrete and reinforcing materials of interest for transportation infrastructure applications. An experimental program was then carried out that assessed the corrosion, freeze-thaw, shrinkage, and mechanical behavior of emerging ductile concrete systems. The systems identified include materials that are actively being used by transportation agencies by various state and federal agencies. A numerical modeling program was developed to simulate the long-term durability of a select group of materials under the combined effects of mechanical loading and environmental conditioning. An in-service life cycle analysis model was then applied to compare the long-term durability of a bridge deck made with ductile concrete materials in comparison to normal reinforced concrete systems.

The results of the experimental and numerical research show benefits across a range of durability and mechanical performance metrics. Herein, a summary of major conclusions and recommendations for future research activities are provided.

Conclusions

The following major conclusions can be drawn from this research:

- Corrosion in cracked beams is highly dependent on the crack widths. Small cracks (less than 0.1 mm) have minor or no effects on corrosion performance and can be blocked by corrosion products or self-healing mechanisms.
- High corrosion activity in galvanized reinforcement will be observed in the first several weeks after exposure to chlorides due the high reactivity of zinc coating. This does not influence the long-term corrosion response of galvanized reinforcement.
- UHPC and ECC performed best in terms of freeze-thaw and salt scaling. HPC had a better freeze-thaw and salt scaling resistance than HyFRC and SCC P.
- Different raw materials and fibers in ductile concrete systems cause changes in salt scaling behavior. Rating the scaling in ductile concrete using ASTM C672 can be difficult as no coarse aggregates are used, and fibers help keep loose parts together. A different test method or modifications may be needed to properly rate the salt scaling in ductile concrete systems.
- UHPC Ductal had the lowest drying shrinkage compared to other systems in the test program due to the very low water to cement ratio and dense particle packing. SCC P and HPC mixtures from NJDOT have lower drying shrinkage compared to ECC and HyFRC.
- While the rapid chloride penetration test is a useful tool for assessing the potential corrosion performance of ordinary reinforced concrete materials, it is not well suited for ductile concrete systems. The presence of fibers and different chemistry

of raw materials in ductile concretes may produce result that lack meaning in the rapid chloride penetration test.

- The proposed numerical simulation framework is efficient in predicting chloride profile and corrosion induced damage with reasonable accuracy of normal reinforced concrete system and reinforced HPFRCC system.
- The reinforced UHPC beams and reinforced UHPC bridge decks exhibited excellent resistance to chloride penetration and corrosion propagation according to the modeling results. The structural deteriorations of the reinforced UHPC systems were also significantly slower compared to that of reinforced normal strength concrete systems.
- Chloride induced corrosion performance is affected by the initial damage pattern, which depends on the structure and loading conditions. Therefore, it is important to consider the structural configuration, traffic loading conditions, and local climate characteristics to assess the long-term durability of advanced reinforced concrete system.
- The excellent long-term durability performance of reinforced UHPC systems showed the great potential of further application of advanced reinforced concrete materials in transportation infrastructure. The initial volume of advanced reinforced concrete materials is lower in construction compared to that of normal strength concrete. Moreover, the maintenance frequency in the life cycle can be reduced.

Recommendations

The following major recommendations should be considered for future research based on the findings of this report:

- ASTM G109 is being used to investigate the corrosion performance of chemical admixtures on the corrosion performance. ASTM G109 uses a 280 × 150 × 115 mm (11 × 6 × 4.5 in.) beam. Specimen dimensions can play a role specifically when the cracking effect on the corrosion performance of ductile concrete systems is a matter of discussion. Specimen size can affect the flexural behavior of beams. Short beams mostly fail in shear rather than flexure and making it harder to create flexural cracks in the beams. A modified specimen size with a longer length is recommended for corrosion testing of ductile concrete systems when exposed to cracking.
- Ductile concrete systems have a denser microstructure compared to normal concrete. This dense microstructure increases the time for chloride penetration and limits the access to oxygen in ductile concrete systems. A deeper cover depth can increase the effect of ductile systems' microstructure and results in a much longer corrosion initiation time for ductile systems. ASTM G109 recommends a cover depth as large as twice the maximum aggregate size in the concrete and larger than 0.5 in. Cover depths larger than 1 in are not recommended for corrosion testing of ductile concrete systems as they can result in a very long corrosion initiation time. If only fine materials are used in the concrete system, 0.5 in cover depth is the recommended depth for corrosion testing.

- Higher salt solution concentration and more intensified wetting and drying cycles can accelerate corrosion and decrease the corrosion initiation time in corrosion tests. ASTM G109 recommends 3% salt solution and two weeks of ponding following two weeks of drying. Different salt solutions and wetting and drying cycles can be used depending on the research project goal. Three percent salt solution provides the same saline level as free waters and is more generic in corrosion studies. However, many parameters other than salt solution concentration have been changed in corrosion studies of ductile concrete systems. Generally, higher salt solution concentrations and more intensified wetting drying cycles are recommended for corrosion investigation of ductile concrete systems and alternative reinforcement.
- Rapid chloride penetration testing of ductile concrete systems showed controversial results compared to the literature. The long-term ponding results will provide a better understanding of RCPT test application for ductile concrete systems.
- The simulation input parameters need to be determined experimentally. In particular, the material's transport properties in sound and damaged conditions need to be further verified. The polarization parameters of both normal strength and advanced reinforced concrete materials need to be determined through experiments. As such, further experimental work is necessary before this model framework can be fully validated for all types of advanced reinforced concrete systems.
- The simulation input parameters including mechanical properties, material transport properties, and electrochemical reaction parameters, are in a wide range. A thorough input parameters sensitivity analysis will help determine the dominating factors that influencing the corrosion performance of both reinforced concrete and advanced reinforced concrete systems.
- This study only showed simulation results of two-dimensional models. Three-dimensional models considering the non-uniform rust growth in all reinforcing bar directions could provide more information of corrosion performance of reinforced concrete and advanced reinforced concrete structures.

IMPLEMENTATION AND TRAINING

Based on the findings from the experimental, computational, and cost studies that were performed in this research program, the following recommendations on implementation are suggested.

Training and Implementation of Ductile Concrete in Transportation Infrastructure

The experimental activities showed the promising durability response of ductile concrete systems. The research could be further implemented through the following activities:

- UHPC has been deployed in a number of projects under the supervision of NJDOT. While UHPC's durability performance is excellent, other systems, such as ECC or HyFRC, may be able to provide similar levels of performance with a lower material cost. NJDOT could consider a field study of various ductile systems and monitor the long-term performance to understand life-cycle costs of various systems.
- Since ductile concrete materials have changes in performance compared to normal concrete, understanding how to properly test these materials is critical. For example, the salt-scaling procedure with ductile concretes required a careful wire brushing procedure to complete testing and understand behavior. Proper training on testing procedures when working with these materials will help with field implementation.

Service-Life Modeling Tools

This research used computational tools to predict the durability of representative bridge decks with ductile concrete composites. This could be further implemented through the following activities:

- Conduct numerical simulations to study the impacts of environmental conditions on service life performance of reinforced concrete and reinforced HPFRCCs. This will address the effects of climate change on service life modeling outputs.
- Run parametric studies to evaluate uncertainty in service life prediction.
- Compare service life performance of transportation infrastructure elements with various ductile concrete materials in terms of corrosion, delamination, and other deterioration metrics.
- Develop an application programming interface (API) of the service life simulation framework that can integrate mechanical degradation, chloride transport, and data processing tools. This will help NJDOT and future researchers evaluate deterioration of novel materials in transportation infrastructure application.
- Develop Microsoft Excel spreadsheet tools that can estimate chloride and oxygen transport properties. This would be based on concrete and ductile concrete mixture constituents.
- Develop Microsoft Excel spreadsheet tools that can estimate life-cycle costs of reinforced concrete and ductile concrete systems in transportation infrastructure applications. The development of this spreadsheet would be based on parametric study results.

REFERENCES

1. Popovics, S. *Concrete-making materials*. (Hemisphere Pub. Corp., 1979).

2. Bandelt, M. J. & Billington, S. L. Bond behavior of steel reinforcement in high-performance fiber-reinforced cementitious composite flexural members. *Mater Struct* **49**, 71–86 (2016).

3. Moreno, D. M., Trono, W., Jen, G., Ostertag, C. & Billington, S. L. Tension stiffening in reinforced high performance fiber reinforced cement-based composites. *Cem Concr Compos* **50**, 36–46 (2014).

4. Wille, K. & Naaman, A. E. Fracture energy of UHP-FRC under direct tensile loading. in *FraMCoS-7 international conference* 65–72 (2010).

5. Cornelia Magureanu Camelia Negrutiu, and Bogdan Heghes, I. S. Mechanical Properties and Durability of Ultra-High-Performance Concrete. *ACI Mater J* **109**,.

6. Wang, Y. B., Liew, J. Y. R., Lee, S. C. & Xiong, D. X. Experimental study of ultra-high-strength concrete under triaxial compression. *ACI Mater J* **113**, 105–112 (2016).

7. Ibrahim, M. A., Farhat, M., Issa, M. A. & Hasse, J. A. Effect of material constituents on mechanical & fracture mechanics properties of ultra-high-performance concrete. *ACI Struct J* **114**, 453–465 (2017).

8. Dawood, M. *et al.* Advancements in Concrete Mix Designs: High-Performance and Ultrahigh-Performance Concretes from 1970 to 2016. *Journal of Materials in Civil Engineering* **30**, 04017310 (2017).

9. Graybeal, B. & Tanesi, J. Durability of an Ultrahigh-Performance Concrete. *Journal of Materials in Civil Engineering* **19**, 848–854 (2007).

10. Recommendations, I. Association Française de Génie Civil. Preprint at (2002).

11. Bărbos, G. – A. Long-term Behavior of Ultra – High Performance Concrete (UHPC) Bended Beams. *Procedia Technology* **22**, 203–210 (2016).

12. Ma, J., Orgass, M., Dehn, F., Schmidt, D. & Tue, N. v. Comparative investigations on ultra-high performance concrete with and without coarse aggregates. in *International Symposium on Ultra High Performance Concrete, Kassel, Germany* 205–212 (2004).

13. Azmee, N. M. & Shafiq, N. Ultra-high performance concrete: From fundamental to applications. *Case Studies in Construction Materials* **9**, (2018).

14. Shafieifar, M., Farzad, M. & Azizinamini, A. Experimental and numerical study on

mechanical properties of Ultra High Performance Concrete (UHPC). *Constr Build Mater* **156**, 402–411 (2017).

15. Shi, C. *et al.* A review on ultra high performance concrete: Part I. Raw materials and mixture design. *Constr Build Mater* **101**, 741–751 (2015).

16. Spasojevic, A. *Structural implications of ultra-high performance fibre-reinforced concrete in bridge design*. (2008).

17. Richard, P. & Cheyrezy, M. Composition of reactive powder concretes. *Cem Concr Res* **25**, 1501–1511 (1995).

18. Perry, V. H. Ultra-High-Performance-Concrete Advancements and Industrialization—The Need for Standard Testing. *Adv Civ Eng Mater* **4**, 20140028 (2015).

19. Wu, Z., Shi, C., He, W. & Wang, D. Uniaxial compression behavior of ultra-high performance concrete with hybrid steel fiber. *Journal of Materials in Civil Engineering* **28**, 06016017 (2016).

20. Zhou, M., Lu, W., Song, J. & Lee, G. C. Application of Ultra-High Performance Concrete in bridge engineering. *Constr Build Mater* **186**, 1256–1267 (2018).

21. Graybeal, B. A. *Material property characterization of ultra-high performance concrete*. (2006).

22. Khaloo, A. R., Karimi, H., Asadollahi, S. & Dehestani, M. A New Mixture Design Method for Ultra-High-Strength Concrete. *ACI Mater J* **114**, 215–224 (2017).

23. Saleem, M. A., Mirmiran, A., Xia, J. & Mackie, K. Ultra-high-performance concrete bridge deck reinforced with high-strength steel. *ACI Struct J* **108**, 601–609 (2011).

24. Fládr, J., Bílý, P. & Vodička, J. Experimental Testing of Resistance of Ultra-high Performance Concrete to Environmental Loads. *Procedia Eng* **151**, 170–176 (2016).

25. Gao, R., Liu, Z. M., Zhang, L. Q. & Stroeven, P. Static properties of plain reactive powder concrete beams. in *Key Engineering Materials* vol. 302 521–527 (Trans Tech Publ, 2006).

26. Habel, K. & Gauvreau, P. Response of ultra-high performance fiber reinforced concrete (UHPFRC) to impact and static loading. *Cem Concr Compos* **30**, 938–946 (2008).

27. Su, Y., Wu, C., Li, J., Li, Z. X. & Li, W. Development of novel ultra-high performance concrete: From material to structure. *Constr Build Mater* **135**, 517–528 (2017).

28. Chandrangsu, A. E. N. and K. Innovative Bridge Deck System Using High-Performance Fiber-Reinforced Cement Composites. *ACI Struct J* **101**,.

29. Tang, M.-C. High performance concrete—past, present and future. in *Proceedings of the international symposium on UHPC, Kassel, Germany* 3–9 (2004).

30. Tanaka, Y. *et al.* The innovation and application of UHPFRC bridges in Japan. *Designing and Building with UHPFRC* 149–188 (2011).

31. Denarié, E., Jacomo, D., Fady, N. & Corvez, D. *Rejuvenation of maritime signalisation structures with UHPFRC*. (2013).

32. Mazzacane, P., Ricciotti, R., Teply, F., Tollini, E. & Corvez, D. MUCEM: The builder's perspective. *Proceedings UHPFRC* 3–16 (2013).

33. Chasioti, S. G. & Vecchio, F. J. Effect of fiber hybridization on basic mechanical properties of concrete. *ACI Struct J* **114**, 375–384 (2017).

34. Chasioti, S. G. & Vecchio, F. J. Shear behavior and crack control characteristics of hybrid steel fiber-reinforced concrete panels. *ACI Struct J* **114**, 209–220 (2017).

35. Qian, C. X. & Stroeven, P. Development of hybrid polypropylene-steel fibre-reinforced concrete. **30**, 63–69 (2000).

36. Banthia, N. & Sappakittipakorn, M. Toughness enhancement in steel fiber reinforced concrete through fiber hybridization. *Cem Concr Res* **37**, 1366–1372 (2007).

37. Shah, S. P. Do Fibers Increase the Tensile Strength of Cement-Based Matrix? *ACI Mater J* **88**,.

38. Lawler, J. S., Zampini, D. & Shah, S. P. Microfiber and macrofiber hybrid fiber-reinforced concrete. *Journal of Materials in Civil Engineering* **17**, 595–604 (2005).

39. Ganesan, N., Indira, P. v. & Sabeena, M. v. Tension stiffening and cracking of hybrid fiber-reinforced concrete. *ACI Mater J* **110**, 715–721 (2013).

40. Sivakumar, A. & Santhanam, M. Mechanical properties of high strength concrete reinforced with metallic and non-metallic fibres. *Cem Concr Compos* **29**, 603–608 (2007).

41. Yang, K. H. Tests on concrete reinforced with hybrid or monolithic steel and polyvinyl alcohol fibers. *ACI Mater J* **108**, 664–672 (2011).

42. Chi, Y., Xu, L. & Zhang, Y. Experimental study on hybrid fiber–reinforced concrete subjected to uniaxial compression. *Journal of Materials in Civil Engineering* **26**,

211–218 (2014).

43. Dawood, E. T. & Ramli, M. Contribution of hybrid fibers on the hybrid fibers on the properties of high strength concrete having high workability. *Procedia Eng* **14**, 814–820 (2011).

44. Pakravan, H. R., Latifi, M. & Jamshidi, M. Hybrid short fiber reinforcement system in concrete: A review. *Constr Build Mater* **142**, 280–294 (2017).

45. Ma, H., Qian, S., Zhang, Z., Lin, Z. & Li, V. C. Tailoring Engineered Cementitious Composites with local ingredients. *Constr Build Mater* **101**, 584–595 (2015).

46. Sahmaran, M., Lachemi, M., Hossain, K. M. A., Ranade, R. & Li, V. C. Influence of aggregate type and size on ductility and mechanical properties of engineered cementitious composites. *ACI Mater J* **106**, 308–316 (2009).

47. Zhu, Y., Yang, Y. & Yao, Y. Use of slag to improve mechanical properties of engineered cementitious composites (ECCs) with high volumes of fly ash. *Construction and Building Materials* vol. 36 1076–1081 Preprint at https://doi.org/10.1016/j.conbuildmat.2012.04.031 (2012).

48. Soe, K. T., Zhang, Y. X. & Zhang, L. C. Material properties of a new hybrid fibre-reinforced engineered cementitious composite. *Constr Build Mater* **43**, 399–407 (2013).

49. Ahmed, S. F. U. & Mihashi, H. Corrosion durability of strain hardening fibre-reinforced cementitious composites. *Australian Journal of Civil Engineering* **8**, 13–26 (2010).

50. Li, V. C. On Engineered Cementitious Composites (ECC). *Journal of Advanced Concrete Technology* **1**, 215–230 (2003).

51. Lepech, M. D. & Li, V. C. Water permeability of engineered cementitious composites. *Cem Concr Compos* **31**, 744–753 (2009).

52. Ke-Quan, Y., Jian-Guo, D., Zhou-Dao, L. & Y., L. C. K. Mechanical Properties of Engineered Cementitious Composites Subjected to Elevated Temperatures. *Journal of Materials in Civil Engineering* **27**, 4014268 (2015).

53. Li, V. C. Advances in ECC research. *ACI Special Publications* **206**, 373–400 (2002).

54. Said, S. H. & Razak, H. A. The effect of synthetic polyethylene fiber on the strain hardening behavior of engineered cementitious composite (ECC). *Mater Des* **86**, 447–457 (2015).

55. Li, V. C. Engineered cementitious composites (ECC)-tailored composites through

micromechanical modeling. in (1998).

56. Mohammed, B. S., Khed, V. C. & Liew, M. S. Optimization of hybrid fibres in engineered cementitious composites. *Constr Build Mater* **190**, 24–37 (2018).

57. Moreno, D. M., Trono, W., Jen, G., Ostertag, C. & Billington, S. L. Tension-stiffening in reinforced high performance fiber-reinforced cement-based composites under direct tension. in *High Performance Fiber Reinforced Cement Composites 6* 263–270 (Springer, 2012).

58. Douglas, K. S. & Billington, S. L. Strain rate dependence of HPFRCC cylinders in monotonic tension. *Mater Struct* **44**, 391–404 (2011).

59. Li, V. C. & Kanda, T. Engineered cementitious composites for structural applications. *Journal of Materials in Civil Engineering* **10**, 66–69 (1998).

60. Li, V. C., Wang, S. & Wu, C. Tensile strain-hardening behavior or polyvinyl alcohol engineered cementitious composite (PVA-ECC). *ACI Mater J* **98**, 483–492 (2001).

61. Li, V. C. *Applications of engineered cementitious composites (ecc)*. *Engineered Cementitious Composites (ECC)* (Springer, 2019). doi:10.1007/978-3-662-58438-5_9.

62. Yildirim, G. *et al.* Effects of compressive strength, autogenous shrinkage, and testing methods on bond behavior of high-early- strength engineered cementitious composites. *ACI Mater J* **112**, 409–418 (2015).

63. Kai, M. F., Xiao, Y., Shuai, X. L. & Ye, G. Compressive behavior of engineered cementitious composites under high strain-rate loading. *Journal of Materials in Civil Engineering* **29**, 1–8 (2017).

64. Liu, H., Zhang, Q., Li, V., Su, H. & Gu, C. Durability study on engineered cementitious composites (ECC) under sulfate and chloride environment. *Constr Build Mater* **133**, 171–181 (2017).

65. Li, V. C., Horikoshi, T., Ogawa, A., Torigoe, S. & Saito, T. Micromechanics-based durability study of polyvinyl alcohol-engineered cementitious composite. *Materials Journal* **101**, 242–248 (2004).

66. Şahmaran, M. & Li, V. C. Durability of mechanically loaded engineered cementitious composites under highly alkaline environments. *Cem Concr Compos* **30**, 72–81 (2008).

67. Qian, S., Li, V. C., Zhang, H. & Keoleian, G. A. Durable and sustainable overlay with ECC. *9th International Conference on Concrete Pavements: The Golden Gate to Tomorrow's Concrete Pavements* **2**, 918–933 (2008).

68. Poursaee, A. *Corrosion of Steel in Concrete Structures*. *Corrosion of Steel in Concrete Structures* (2016). doi:10.1016/C2014-0-01384-6.

69. Berrocal, C. G., Lundgren, K. & Löfgren, I. Corrosion of steel bars embedded in fibre reinforced concrete under chloride attack: state of the art. *Cem Concr Res* **80**, 69–85 (2016).

70. Montemor, M. F., Simoes, A. M. P. & Ferreira, M. G. S. Chloride-induced corrosion on reinforcing steel: from the fundamentals to the monitoring techniques. *Cem Concr Compos* **25**, 491–502 (2003).

71. Angst, U. M., Elsener, B., Larsen, C. K. & Vennesland, Ø. Chloride induced reinforcement corrosion: Electrochemical monitoring of initiation stage and chloride threshold values. *Corros Sci* **53**, 1451–1464 (2011).

72. Ann, K. Y. & Song, H. W. Chloride threshold level for corrosion of steel in concrete. *Corros Sci* **49**, 4113–4133 (2007).

73. Ahmad, S. Reinforcement corrosion in concrete structures, its monitoring and service life prediction—a review. *Cem Concr Compos* **25**, 459–471 (2003).

74. Bertolini, L., Elsener, B., Pedeferri, P., Redaelli, E. & Polder, R. Corrosion of steel in concrete: prevention, diagnosis, repair. 2013.

75. C39/C39M-20, A. *ASTM C39 / C39M - 20 Standard Test Method for Compressive Strength of Cylindrical Concrete Specimens*. (2020).

76. Ismail, M. K., Hassan, A. A. A. A. & Lachemi, M. Effect of Fiber Type on Impact and Abrasion Resistance of Engineered Cementitious Composite. *ACI Mater J* **115**, 957–968 (2018).

77. Shaikh, F. U. A. Effect of cracking on corrosion of steel in concrete. *Int J Concr Struct Mater* **12**, 3 (2018).

78. Toufigh, V., Hosseinali, M. & Shirkhorshidi, S. M. Experimental study and constitutive modeling of polymer concrete's behavior in compression. *Constr Build Mater* **112**, (2016).

79. Broomfield, J. P. *Corrosion of steel in concrete: understanding, investigation and repair*. (CRC Press, 2003).

80. Bertolini, L., Elsener, B., Pedeferri, P. & Polder, R. Corrosion of Steel in Concrete–Prevention, Diagnosis and Repair. Wieley–VCH. Preprint at (2004).

81. Angst, U., Elsener, B., Larsen, C. K. & Vennesland, Ø. Critical chloride content in reinforced concrete - A review. *Cem Concr Res* **39**, 1122–1138 (2009).

82. Li, M., Lin, V., Lynch, J. & Li, V. C. Multifunctional carbon black engineered cementitious composites for the protection of critical infrastructure. in *High Performance Fiber Reinforced Cement Composites 6* 99–106 (Springer, 2012).

83. Andrade, C. & Buják, R. Effects of some mineral additions to Portland cement on reinforcement corrosion. *Cem Concr Res* **53**, 59–67 (2013).

84. ASTM G 109-13. Standard Test Method for Determining the Effects of Chemical Admixtures on the Corrosion of Embedded Steel Reinforcement in Concrete. *Annual Book of ASTM Standards* **07**, 1–5 (2013).

85. Standard Test Method for Acid-Soluble Chloride in Mortar and Concrete. doi:10.1520/C1152_C1152M-20.

86. Designation: C1556 − 11a Standard Test Method for Determining the Apparent Chloride Diffusion Coefficient of Cementitious Mixtures by Bulk Diffusion 1. doi:10.1520/C1556-11AR16.

87. Mehta, P. K. Concrete durability-fifty years progress. in *Proceedings of the 2nd International Conference on Concrete Durability, Montreal, QC, Canada* vol. 49 132 (1991).

88. Ma, W. Simulate initiation and formation of cracks and potholes. *Maste r Report, Northeastern University, Boston, Massachusetts, USA* (2016).

89. Xie, C., Cao, M., Yin, H., Guan, J. & Wang, L. Effects of freeze-thaw damage on fracture properties and microstructure of hybrid fibers reinforced cementitious composites containing calcium carbonate whisker. *Constr Build Mater* **300**, 123872 (2021).

90. Wang, R., Hu, Z., Li, Y., Wang, K. & Zhang, H. Review on the deterioration and approaches to enhance the durability of concrete in the freeze–thaw environment. *Constr Build Mater* **321**, 126371 (2022).

91. Tanesi, J., Graybeal, B. & Simon, M. *EFFECTS OF CURING PROCEDURE ON FREEZE-THAW DURABILITY OF ULTRA-HIGH PERFORMANCE CONCRETE*.

92. Zhou, Z. & Qiao, P. Durability of ultra-high performance concrete in tension under cold weather conditions. *Cem Concr Compos* **94**, 94–106 (2018).

93. Gu, C. *et al.* Investigation of Microstructural Damage in Ultrahigh-Performance Concrete under Freezing-Thawing Action. *Advances in Materials Science and Engineering* **2018**, (2018).

94. Acker, P. & Behloul, M. Ductal® technology: A large spectrum of properties, a wide range of applications. in *Proc. of the Int. Symp. on UHPC Kassel, Germany* 11–23 (2004).

95. Lepech, M. & Li, V. C. *DURABILITY AND LONG TERM PERFORMANCE OF ENGINEERED CEMENTITIOUS COMPOSITES*.

96. Hammer, T. A. & Sellevoid, E. J. Frost resistance of high-strength concrete. *Special Publication* **121**, 457–488 (1990).

97. Gagne, R. & Pigeon, M. Deicer salt scaling resistance of high-performance concrete. *Special Publication* **122**, 29–44 (1990).

98. Jacobsen, S. & Sellevold, E. J. Frost/salt scaling and ice formation of concrete: effect of curing temperature and silica fume on normal and high strength concrete. *RILEM PROCEEDINGS 30. FREEZE-THAW DURABILITY OF CONCRETE* (1997).

99. Nam, J., Kim, G., Lee, B., Hasegawa, R. & Hama, Y. Frost resistance of polyvinyl alcohol fiber and polypropylene fiber reinforced cementitious composites under freeze thaw cycling. *Compos B Eng* **90**, 241–250 (2016).

100. Dong, F. *et al.* Effect of freeze–thaw cycling on mechanical properties of polyethylene fiber and steel fiber reinforced concrete. *Constr Build Mater* **295**, (2021).

101. Astm C666/C666M. Standard Test Method for Resistance of Concrete to Rapid Freezing and Thawing. *ASTM International, West Conshohocken, PA* **03**, 1–6 (2003).

102. C672C672M.18012.

103. Naaman, A. E. & Reinhardt, H. W. Characterization of high performance fiber reinforced cement composites—HPFRCC. in *High performance fiber reinforced cement composites* vol. 2 1–24 (1996).

104. Silva, R. v, de Brito, J. & Dhir, R. K. Prediction of the shrinkage behavior of recycled aggregate concrete: A review. *Constr Build Mater* **77**, 327–339 (2015).

105. Zhang, H., Wang, Y., Lehman, D. E., Geng, Y. & Kuder, K. Time-dependent drying shrinkage model for concrete with coarse and fine recycled aggregate. *Cem Concr Compos* **105**, 103426 (2020).

106. Medjigbodo, S., Bendimerad, A. Z., Rozière, E. & Loukili, A. How do recycled concrete aggregates modify the shrinkage and self-healing properties? *Cem Concr Compos* **86**, 72–86 (2018).

107. Zhang, J., Gong, C., Guo, Z. & Zhang, M. Engineered cementitious composite with characteristic of low drying shrinkage. *Cem Concr Res* **39**, 303–312 (2009).

108. Hsie, M., Tu, C. & Song, P. S. Mechanical properties of polypropylene hybrid

fiber-reinforced concrete. *Materials Science and Engineering A* **494**, 153–157 (2008).

109. Yao, Y., Zhu, Y. & Yang, Y. Incorporation superabsorbent polymer (SAP) particles as controlling pre-existing flaws to improve the performance of engineered cementitious composites (ECC). *Constr Build Mater* **28**, 139–145 (2012).

110. Zhu, Y., Yang, Y. Z. & Yao, Y. Effect of high volumes of fly ash on flowability and drying shrinkage of engineered cementitious composites. in *Materials Science Forum* vol. 675 677 61–64 (Trans Tech Publications Ltd, 2011).

111. ASTM C157. StandardTest Method for Length Change of Hardened Hydraulic-Cement Mortar and. *Annual Book of ASTM Standards* **08**, 1–7 (2016).

112. Koh, K., Ryu, G., Kang, S., Park, J. & Kim, S. Shrinkage properties of ultra-high performance concrete (UHPC). *Adv Sci Lett* **4**, 948–952 (2011).

113. Naaman, A. E. & Reinhardt, H. W. Proposed classification of HPFRC composites based on their tensile response. *Materials and Structures/Materiaux et Constructions* **39**, 547–555 (2006).

114. Sohail, M. G., Kahraman, R., Al Nuaimi, N., Gencturk, B. & Alnahhal, W. Durability characteristics of high and ultra-high performance concretes. *Journal of Building Engineering* **33**, 101669 (2021).

115. Ghafari, E., Arezoumandi, M., Costa, H. & Júlio, E. Influence of nano-silica addition in the durability of UHPC. *Constr Build Mater* **94**, 181–188 (2015).

116. Cheung, M. M., Zhao, J. & Chan, Y. B. Service Life Prediction of RC Bridge Structures Exposed to Chloride Environments. *Journal of Bridge Engineering* **14**, 164–178 (2009).

117. Nokken, M., Boddy, A., Hooton, R. D. & Thomas, M. D. A. Time dependent diffusion in concrete—three laboratory studies. *Cem Concr Res* **36**, 200–207 (2006).

118. Ožbolt, J., Balabanić, G. & Kušter, M. 3D Numerical modelling of steel corrosion in concrete structures. *Corros Sci* **53**, 4166–4177 (2011).

119. Isgor, O. B. & Razaqpur, A. G. Modelling steel corrosion in concrete structures. *Materials and Structures/Materiaux et Constructions* **39**, 291–302 (2006).

120. Saetta, A. V., Scotta, R. V. & Vitaliani, R. V. Analysis of chloride diffusion into partially saturated concrete. *ACI Mater J* **90**, 441–451 (1993).

121. Broomfield & Moncayo, G. *Corrosion of steel in concrete: understanding, investigation and repair*.

122. Bohni, H. *Corrosion in reinforced concrete structures*. (2005).

123. Michel, A. *et al.* Penetration of corrosion products and corrosion-induced cracking in reinforced cementitious materials: Experimental investigations and numerical simulations. *Cem Concr Compos* **47**, 75–86 (2014).

124. Cao, C., Cheung, M. M. S. & Chan, B. Y. B. Modelling of interaction between corrosion-induced concrete cover crack and steel corrosion rate. *Corros Sci* **69**, 97–109 (2013).

125. Zhao, Y. & Jin, W. *Steel Corrosion-Induced Concrete Cracking*. (Joe Hayton, 2016).

126. Fan, J., Shirkhorshidi, S. M., Adams, M. P. & Bandelt, M. J. Predicting corrosion in reinforced UHPC members through time-dependent multi-physics numerical simulation. *Constr Build Mater* **340**, 127805 (2022).

127. DIANA FEA. *DIANA User's Manual*. (DIANA FEA BV, 2021).

128. Pokhrel, M. & Bandelt, M. J. Material properties and structural characteristics influencing deformation capacity and plasticity in reinforced ductile cement-based composite structural components. *Compos Struct* **224**, 111013 (2019).

129. COMSOL. *COMSOL Multiphysics Reference Manual*. (COMSOL, Inc., 2018).

130. Djerbi, A., Bonnet, S., Khelidj, A. & Baroghel-bouny, V. Influence of traversing crack on chloride diffusion into concrete. *Cem Concr Res* **38**, 877–883 (2008).

131. Shao, Y. & Billington, S. L. Impact of UHPC Tensile Behavior on Steel Reinforced UHPC Flexural Behavior. *Journal of Structural Engineering* **148**, 1–17 (2022).

132. Bandelt, M. J. & Billington, S. L. Impact of reinforcement ratio on on deformation capacity of reinforced high-performance fiber-reinforced cementitious composites. *Journal of Structural Engineering* 457–463 (2015).

133. Rafiee, A. Computer Modeling and Investigation on the Steel Corrosion in Cracked Ultra High Performance Concrete. (Kassel University, 2012).

134. Cao, C. 3D simulation of localized steel corrosion in chloride contaminated reinforced concrete. *Constr Build Mater* **72**, 434–443 (2014).

135. ACI Committee 224. *Control of Cracking in Concrete Structures Reported by ACI Committee 224. ACI 224R-01*. *ACI Committee 224R-01* (2001).

136. Szary, P. & Roda, A. M. *Bridge Resource Program*. (2014).

137. Frangopol, D. M., Dong, Y. & Sabatino, S. Bridge life-cycle performance and cost:

analysis, prediction, optimisation and decision-making. *Structures and Infrastructure Systems* 66–84 Preprint at (2019).

138. Jones, T. W. & Smith, J. D. An historical perspective of net present value and equivalent annual cost. *Account Hist J* 103–110 (1982).

139. Cusson, D., Lounis, Z. & Daigle, L. Benefits of internal curing on service life and life-cycle cost of high-performance concrete bridge decks–A case study. *Cem Concr Compos* **32**, 339–350 (2010).

140. Dong, Y. Performance assessment and design of ultra-high performance concrete (UHPC) structures incorporating life-cycle cost and environmental impacts. *Constr Build Mater* **167**, 414–425 (2018).

141. Ngo, T. Application of UHPC in Long Span Bridge Design. (2016).

142. Cao, J., Shao, X., Deng, L. & Gan, Y. Static and fatigue behavior of short-headed studs embedded in a thin ultrahigh-performance concrete layer. *Journal of Bridge Engineering* **22**, 4017005 (2017).

143. Hu, R., Fang, Z., Jiang, R., Xiang, Y. & Liu, C. Fatigue prediction model of ultra-high-performance concrete beams prestressed with CFRP tendons. *Advances in Structural Engineering* **25**, 611–624 (2022).

144. Katakalos, K. & Papakonstantinou, C. G. Fatigue of reinforced concrete beams strengthened with steel-reinforced inorganic polymers. *Journal of Composites for Construction* **13**, 103–112 (2009).

145. Feng, Z. *et al.* Static and fatigue test on lightweight UHPC-OSD composite bridge deck system subjected to hogging moment. *Eng Struct* **241**, 112459 (2021).

146. Zhu, Y., Zhang, Y., Hussein, H. H. & Chen, G. Flexural strengthening of reinforced concrete beams or slabs using ultra-high performance concrete (UHPC): A state of the art review. *Eng Struct* **205**, 110035 (2020).

147. OMB, U. Discount rates for cost-effectiveness, lease purchase, and related analyses. *Washington, DC: US Office of Management and Budget* **OMB Circul**, (2022).

148. Shah, H. A., Yuan, Q. & Photwichai, N. Use of materials to lower the cost of ultra-high-performance concrete–A review. *Constr Build Mater* **327**, 127045 (2022).

149. Alkaysi, M. & El-Tawil, S. Effects of variations in the mix constituents of ultra high performance concrete (UHPC) on cost and performance. *Mater Struct* **49**, 4185–4200 (2016).